



FLUORESCENCE
FOUNDATION

Principles of Fluorescence Techniques

Urbana-Champaign, Illinois

April 15-18, 2024

Basic Fluorescence Principles III: David Jameson
Förster Resonance Energy Transfer (FRET):
In Vitro and *In Vivo* Fluorescence Probes

Förster Resonance Energy Transfer

FRET

I should note before we start that the Merriam-Webster online dictionary defines “FRET” as:
“to cause to suffer emotional strain”

Milestones in the Theory of Resonance Energy Transfer

1922 G. Cario and J. Franck demonstrate that excitation of a mixture of mercury and thallium atomic vapors with 254nm (the mercury resonance line) also displayed thallium (sensitized) emission at 535nm.

1924 E. Gaviola and P. Pringsham observed that an increase in the concentration of fluorescein in viscous solvent was accompanied by a progressive depolarization of the emission.

1925 J. Perrin proposed the mechanism of resonance energy transfer

1928 H. Kallmann and F. London developed the quantum theory of resonance energy transfer between various atoms in the gas phase. The dipole-dipole interaction and the parameter R_0 are used for the first time

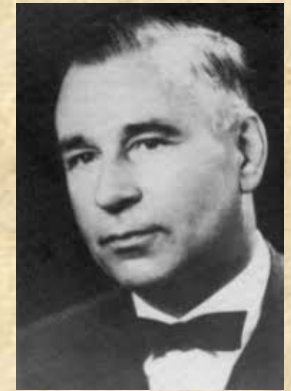
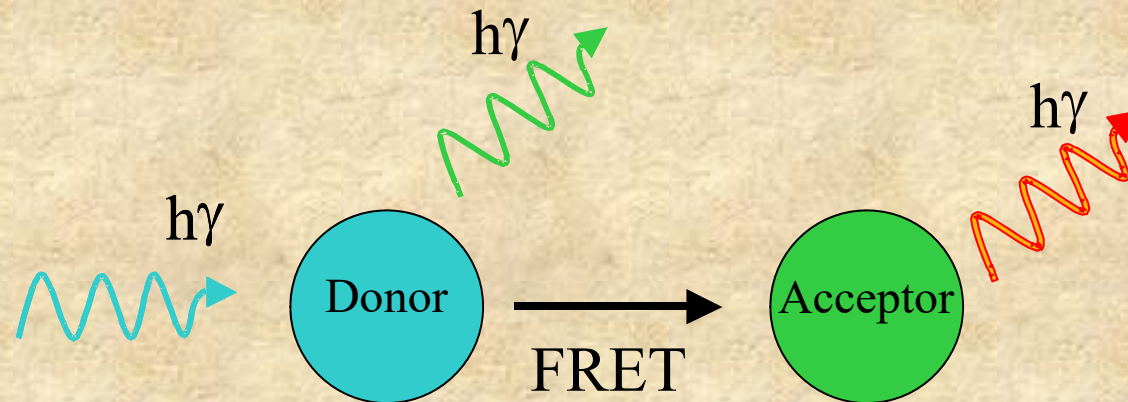
1932 F. Perrin published a quantum mechanical theory of energy transfer between molecules of the same specie in solution. Qualitative discussion of the effect of the spectral overlap between the emission spectrum of the donor and the absorption spectrum of the acceptor

1946-1949 T. Förster develop the first complete quantitative theory of molecular resonance energy transfer

Förster Resonance Energy Transfer

FRET

What is FRET ?

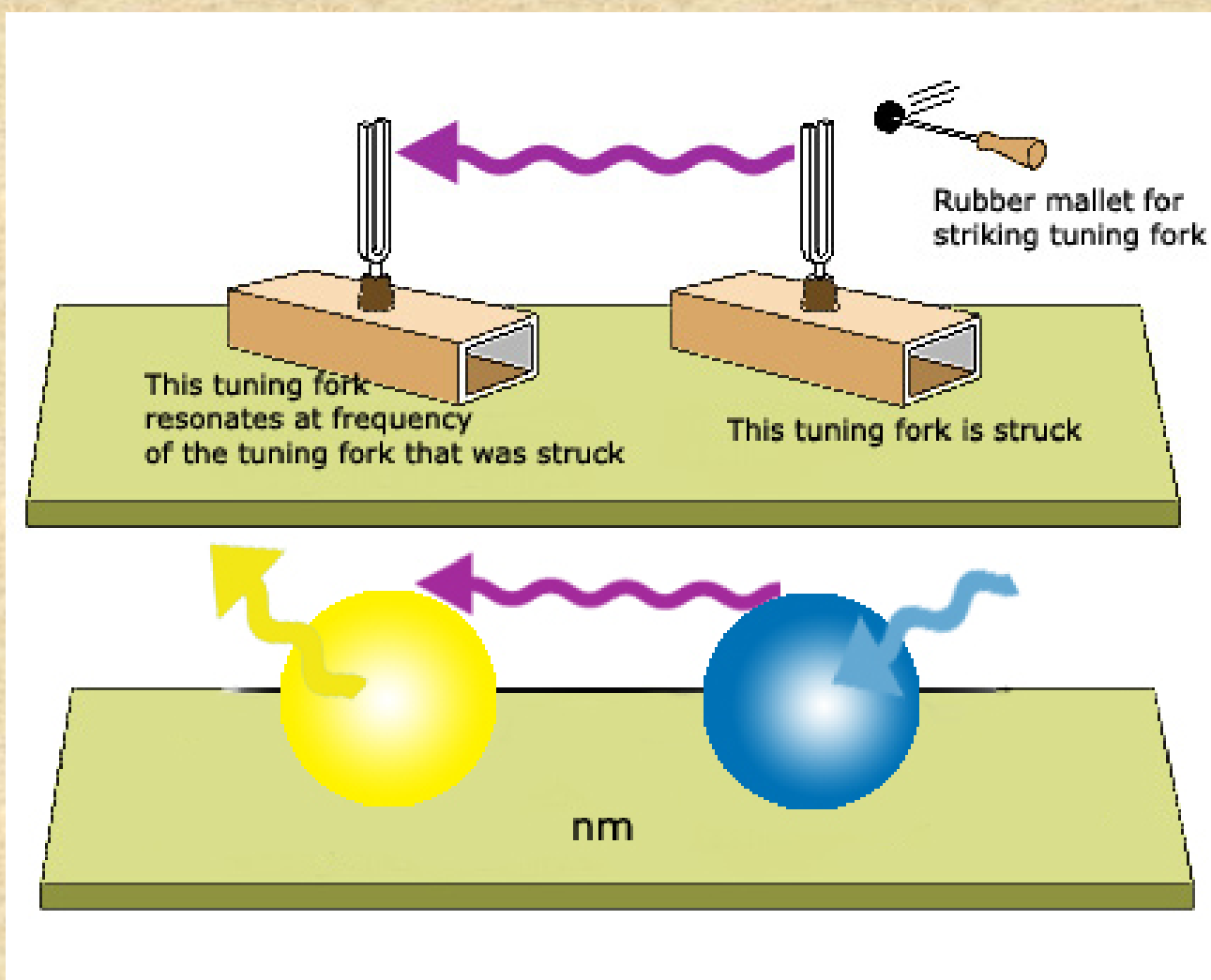


Theodore Förster

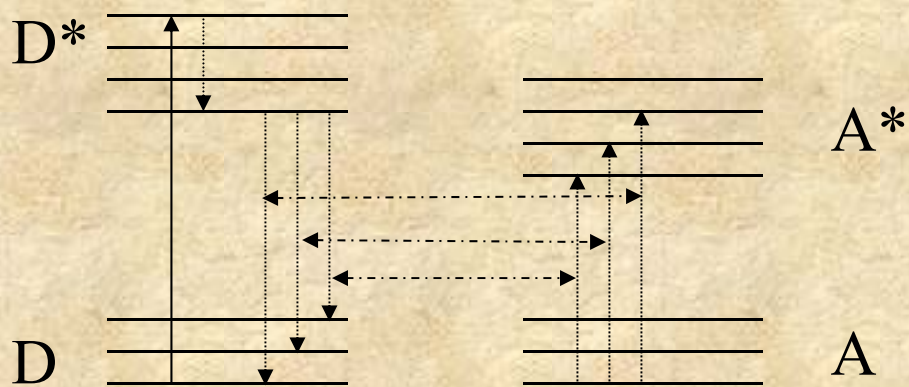
When the donor molecule absorbs a photon, and there is an acceptor molecule close to the donor molecule, radiationless energy transfer can occur from the donor to the acceptor.

FRET results in a decrease of the fluorescence intensity and lifetime of the donor probe, It enhance the fluorescence of the acceptor probe when the acceptor is fluorescent.

Tuning fork analogy for resonance energy transfer



Simplified FRET Energy Diagram



Coupled transitions

Suppose that the energy difference for one of these possible deactivation processes in the donor molecule matches that for a possible absorption transition in a nearby acceptor molecule. Then, with sufficient energetic coupling between these molecules (overlap of the emission spectrum of the donor and absorption spectrum of the acceptor), both processes may occur simultaneously, resulting in a transfer of excitation from the donor to the acceptor molecule



The interaction energy is of a dipole-dipole nature and depends on the distance between the molecules as well as the relative orientation of the dipoles

Dipole-dipole interaction



The rate of transfer (k_T) of excitation energy is given by:

$$k_T = (1/\tau_d)(R_0/r)^6$$

Where τ_d is the fluorescence lifetime of the donor in the absence of acceptor, r the distance between the centers of the donor and acceptor molecules and R_0 the Förster critical distance at which 50% of the excitation energy is transferred to the acceptor and can be approximated from experiments independent of energy transfer.

Förster critical distance

$$R_0 = 0.2108 (n^{-4} Q_d \kappa^2 J)^{1/6} \text{ \AA}$$

↑ ↑ ↑ ↑

n is the refractive index of the medium in the wavelength range where spectral overlap is significant (usually between 1.2-1.4 for biological samples)

Q_d is the fluorescence quantum yield of the donor in absence of acceptor (i.e. number of quanta emitted / number of quanta absorbed)

κ^2 (pronounced “kappa squared”) is the orientation factor for the dipole-dipole interaction

J is the normalized spectral overlap integral [$\epsilon(\lambda)$ is in $M^{-1} \text{ cm}^{-1}$, λ is in nm and J units are $M^{-1} \text{ cm}^{-1} (\text{nm})^4$]

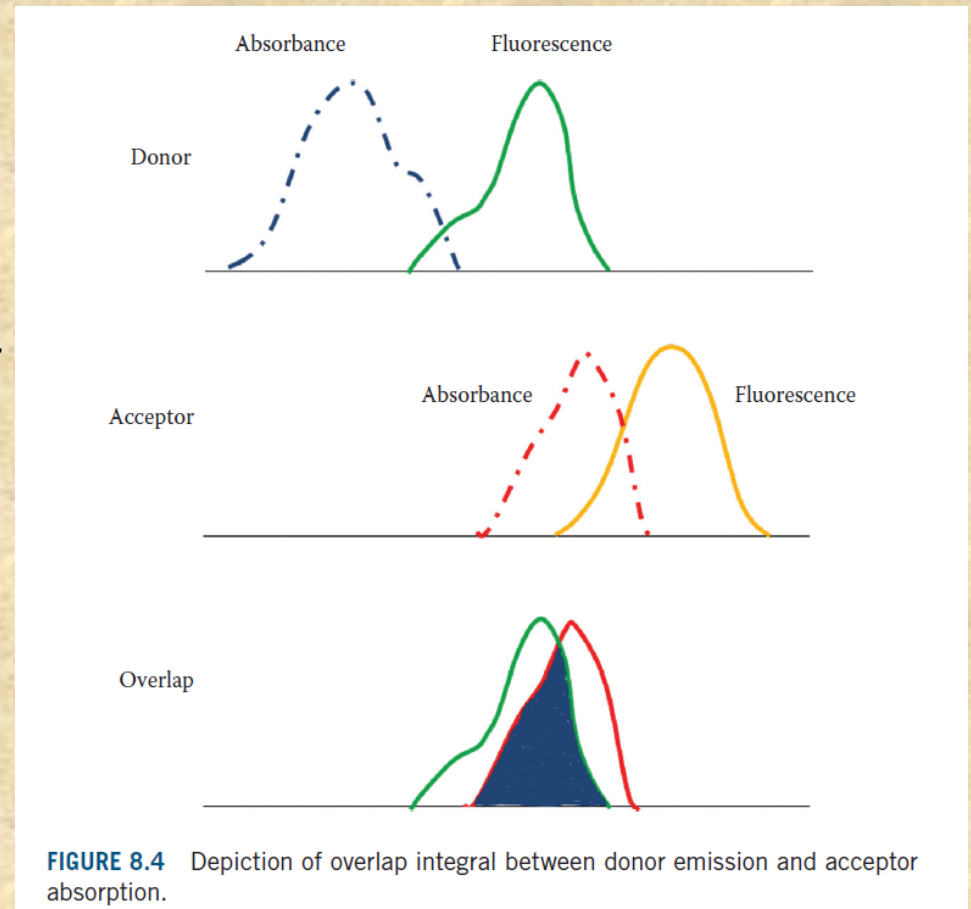
The overlap integral J is defined by:

$$J = \int_0^{\infty} I_D(\lambda) \varepsilon_A(\lambda) \lambda^4 d\lambda$$

Where λ is the wavelength of the light, $\varepsilon_A(\lambda)$ is the molar absorption coefficient at that wavelength and $I_D(\lambda)$ is the fluorescence spectrum of the donor normalized on the wavelength scale:

$$I_D(\lambda) = \frac{F_{D\lambda}(\lambda)}{\int_0^{\infty} F_{D\lambda}(\lambda) d\lambda}$$

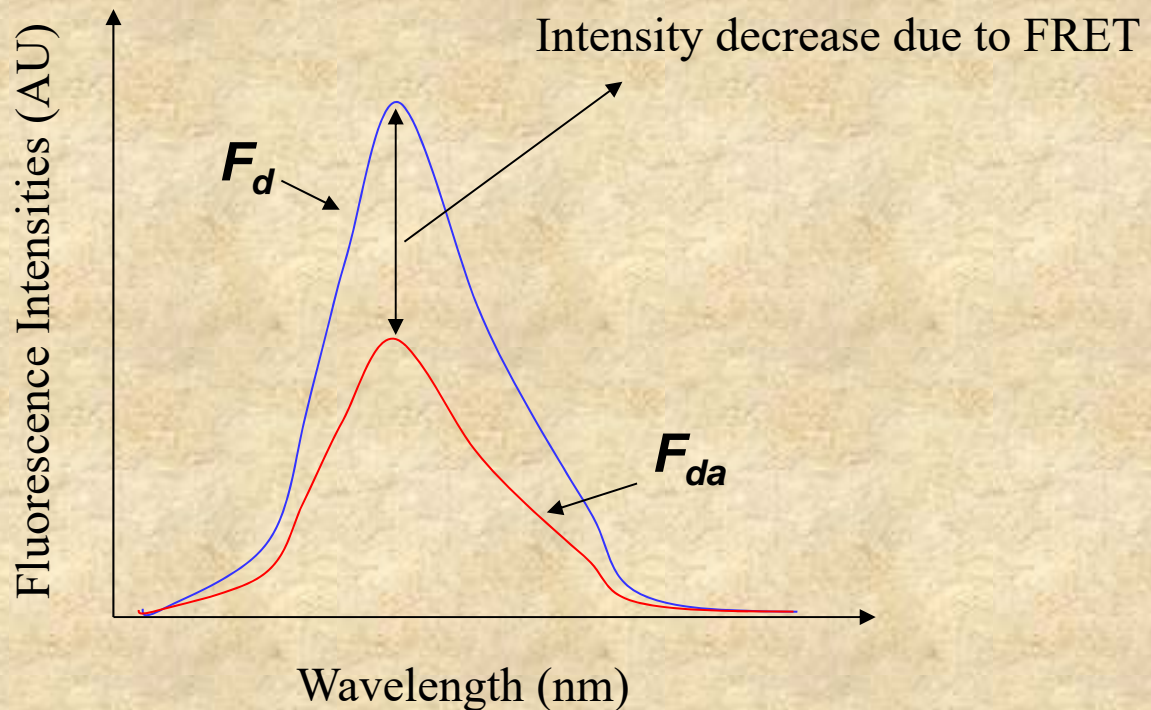
Where $F_{D\lambda}(\lambda)$ is the donor fluorescence per unit wavelength interval



Determination of the efficiency of energy transfer (E)

Steady state method: *Decrease in donor fluorescence.* the fluorescence intensity of the donor is determined in absence and presence of the acceptor.

$$E = 1 - \frac{F_{da}}{F_d}$$



Determination of the efficiency of energy transfer (E)

Time-resolved method: Decrease in the lifetime of the donor

If the fluorescence decay of the donor is a single exponential then:

$$E = 1 - \frac{\tau_D}{\tau_D^0}$$

Where τ_D and τ_D^0 are the lifetime of the donor in the presence and absence of acceptor, respectively

Determination of the efficiency of energy transfer (E)

If the donor fluorescence decay in absence of acceptor is not a single exponential (probably resulting from heterogeneity of the probe's microenvironment) , then it may be modeled as a sum of exponential and the transfer efficiency can be calculated using the average decay times of the donor in absence and presence of acceptor:

$$E = 1 - \frac{\langle \tau_D \rangle}{\langle \tau_D^0 \rangle}$$

Where $\langle \tau \rangle$ is the amplitude-average decay time and is defined as:

$$\langle \tau \rangle = \frac{\sum_i \alpha_i \tau_i}{\sum_i \alpha_i}$$

The distance dependence of the energy transfer efficiency (E)



The efficiency of transfer varies with the inverse sixth power of the distance.

R_0 in this example was set to 40 Å. When the E is 50%, $R=R_0$

Distances can usually be measured between $0.5 R_0$ and $\sim 1.5R_0$. Beyond these limits, we can often only say that the distance is smaller than $0.5 R_0$ or greater than $1.5R_0$. If accurate distance measurement is required then a probe pair with a different R_0 is necessary.

The distance dependence of the energy transfer efficiency (E)

$$r = \left(\frac{1}{E} - 1 \right)^{1/6} R_0$$

Where r is the distance separating the donor and acceptor fluorophores, R_0 is the Förster distance.

Many equivalent forms of this equation is found in the literature, such as:

$$E = R_0^6 / (R_0^6 + r^6) \quad \text{or} \quad E = 1 / \left[1 + (r/R_0)^6 \right]$$

Distributions

Proc. Nat. Acad. Sci. USA
Vol. 68, No. 9, pp. 2099–2101, September 1971

Determination of Distance Distribution Functions by Singlet-Singlet Energy Transfer

(flexibility/Förster theory/fluorescence/molecular structure)

CHARLES R. CANTOR AND PHILIP PECHUKAS

Proc. Nat. Acad. Sci. USA
Vol. 69, No. 8, pp. 2273–2277, August 1972

Evaluation of the Distribution of Distances Between Energy Donors and Acceptors by Fluorescence Decay

(energy transfer/fluorescence/decay/conformation/polymers)

A. GRINVALD, E. HAAS, AND I. Z. STEINBERG

$$E(R_0) = \int_0^{\infty} dR f(R) \frac{R_0^6}{R_0^6 + R^6}$$

Distributions

Proc. Nat. Acad. Sci. USA
Vol. 72, No. 5, pp. 1807-1811, May 1975

Distribution of End-to-End Distances of Oligopeptides in Solution as Estimated by Energy Transfer

(fluorescence decay/conformation)

ELISHA HAAS, MEIR WILCHEK, EPHRAIM KATCHALSKI-KATZIR, AND IZCHAK Z. STEINBERG

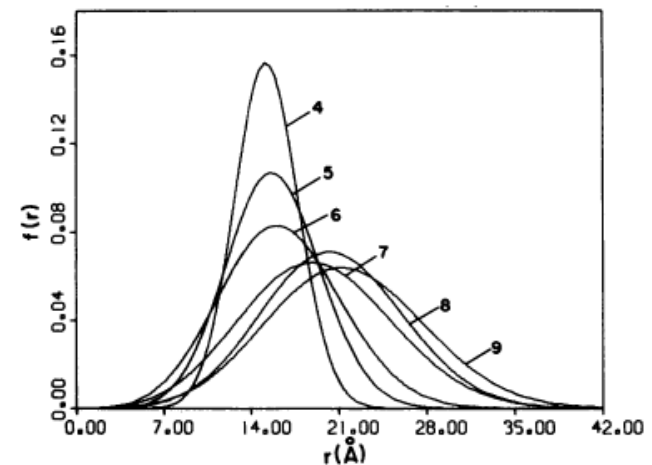
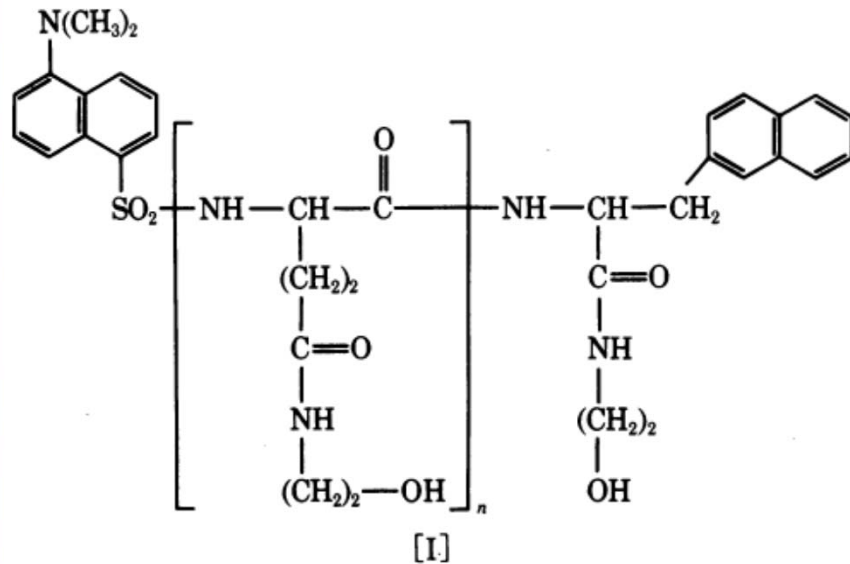


FIG. 4. The distribution function of the distances between donor and acceptor for the series of oligopeptides I, $n = 4, 5, 6, 7, 8$, and 9. The numbers in the figure refer to the values of n .

Distributions

Biochemistry 1988, 27, 9149–9160

9149

Distance Distributions in Proteins Recovered by Using Frequency-Domain Fluorometry. Applications to Troponin I and Its Complex with Troponin C†

Joseph R. Lakowicz,^{*,†} Ignacy Gryczynski,^{‡,§} Herbert C. Cheung,^{||} Chien-Kao Wang,^{||} Michael L. Johnson,[⊥] and Nanda Joshi[‡]

5238

Biochemistry 1991, 30, 5238–5247

Distance Distributions and Anisotropy Decays of Troponin C and Its Complex with Troponin I†

Herbert C. Cheung,^{*,†} Chien-Kao Wang,^{‡,§} Ignacy Gryczynski,^{||} Wieslaw Wiczak,^{||} Gabor Laczko,^{||} Michael L. Johnson,[⊥] and Joseph R. Lakowicz^{||}

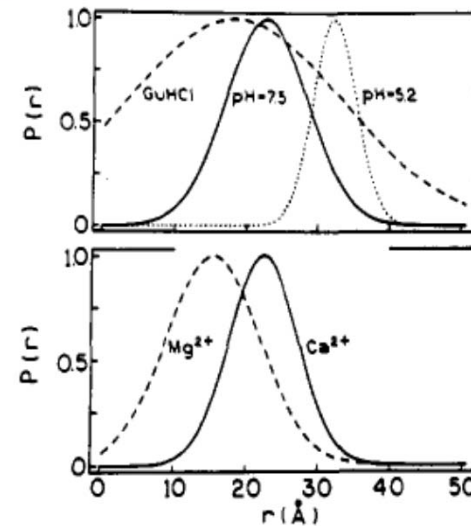
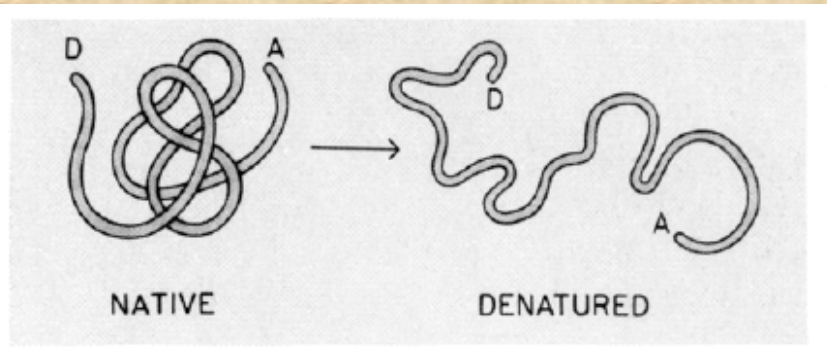


FIGURE 4: Distance distributions for TnC-DNZ-IAE in the absence of cations (top) and in the presence of Mg²⁺ and Ca²⁺ (pH 7.5, bottom). The pH for guanidine hydrochloride (GuHCl) was 7.5.

An impressive example of the use of FRET methodologies to study protein systems is given by the work of Lillo et al. (“Design and characterization of a multisite fluorescence energy-transfer system for protein folding studies: a steady-state and time-resolved study of yeast phosphoglycerate kinase” *Biochemistry*. 1997 Sep 16;36(37):11261-72 and “Real-time measurement of multiple intramolecular distances during protein folding reactions: a multisite stopped-flow fluorescence energy-transfer study of yeast phosphoglycerate kinase” *Biochemistry*. 1997 Sep 16;36(37):11273-81)

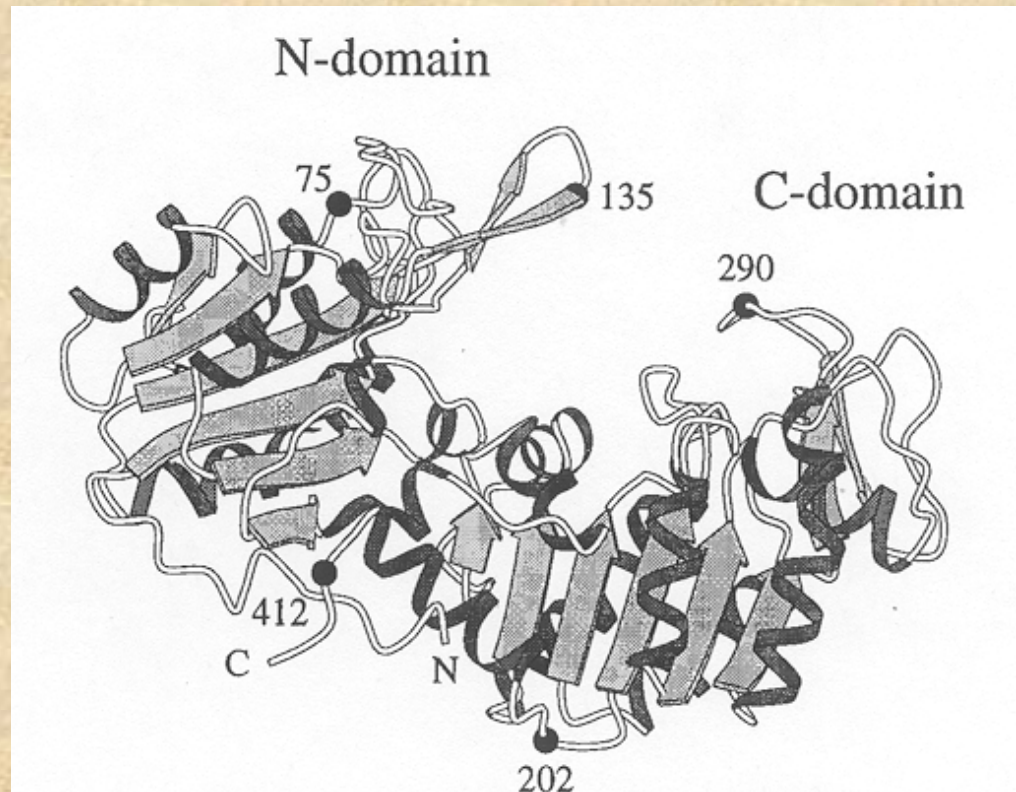
Site-directed mutagenesis was used to introduce pairs of cysteine residues in the protein at the positions shown

The pairs studied were:

135 – 290; 75 – 290

290 – 412; 412 – 202

135 – 412; 412 - 75



The donor was IAEDANS and the acceptor was IAF (iodoacetamindo-fluorescein). The various labeled protein products were separated by chromatography!

Table 1: Summary of the Labeled Proteins Examined for the Photophysical Characterization of Each Energy-Transfer Pair Cys_i → Cys_j

sample	name	Cys _i → Cys _j	no. of cysteines	fluorophore
donor only (D-PGK)	<i>i</i> -single cysteine	D - -	1 (<i>i</i>)	AEDANS (<i>i</i>)
	<i>j</i> -single cysteine	- - D	1 (<i>j</i>)	AEDANS (<i>j</i>)
	<i>i</i> -two cysteines	D - - Cys	2 (<i>i, j</i>)	AEDANS (<i>i</i>)
	<i>j</i> -two cysteines	Cys - - D	2 (<i>i, j</i>)	AEDANS (<i>j</i>)
	(<i>i, j</i>)-two cysteine average	D - - Cys + Cys - - D	2 (<i>i, j</i>)	AEDANS (<i>i</i>) + AEDANS (<i>j</i>)
	(<i>i, j</i>)-two cysteine "double donor"	D - - D	2 (<i>i, j</i>)	AEDANS (<i>i, j</i>)
acceptor only	<i>i</i> -single cysteine	A - -	1 (<i>i</i>)	AF (<i>i</i>)
	<i>j</i> -single cysteine	- - A	1 (<i>j</i>)	AF (<i>j</i>)
donor-acceptor (D-PGK-A)	<i>i, j</i> specific label	D → A	2 (<i>i, j</i>)	AEDANS (<i>i</i>) and AF (<i>j</i>)
	<i>j, i</i> specific label	A ← D	2 (<i>i, j</i>)	AEDANS (<i>j</i>) and AF (<i>i</i>)
	<i>i, j</i> average label	D → A + A ← D	2 (<i>i, j</i>)	AEDANS (<i>i</i>) and AF (<i>j</i>) and + AEDANS (<i>i</i>) and AF (<i>i</i>)

Table 5: Comparison of the Measured FRET Distances with That Predicted from the Crystal Structure^e

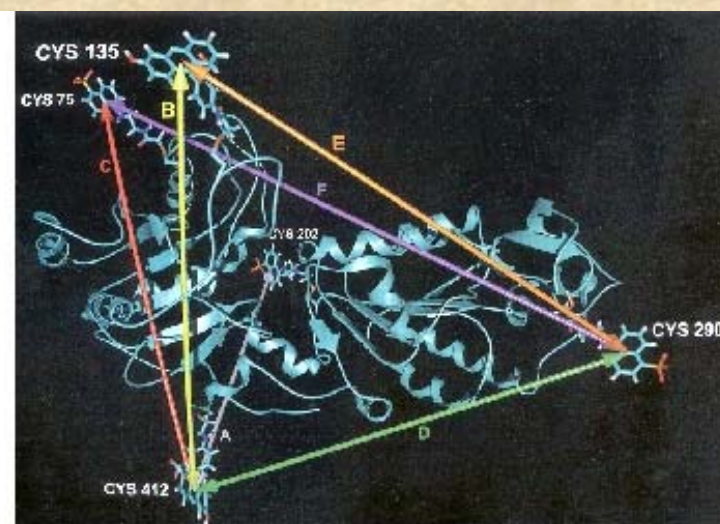
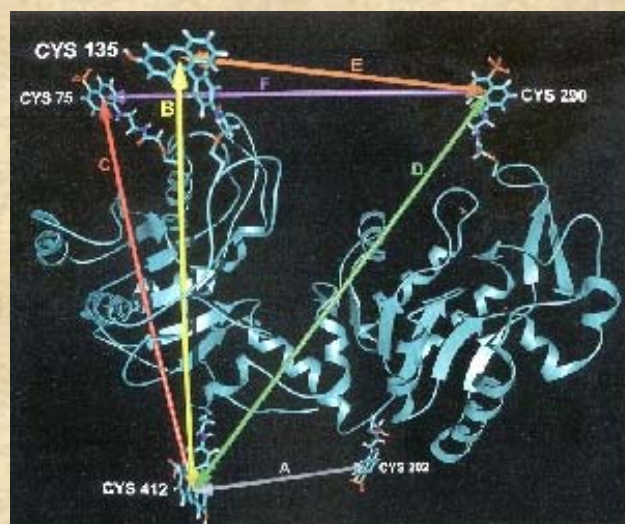
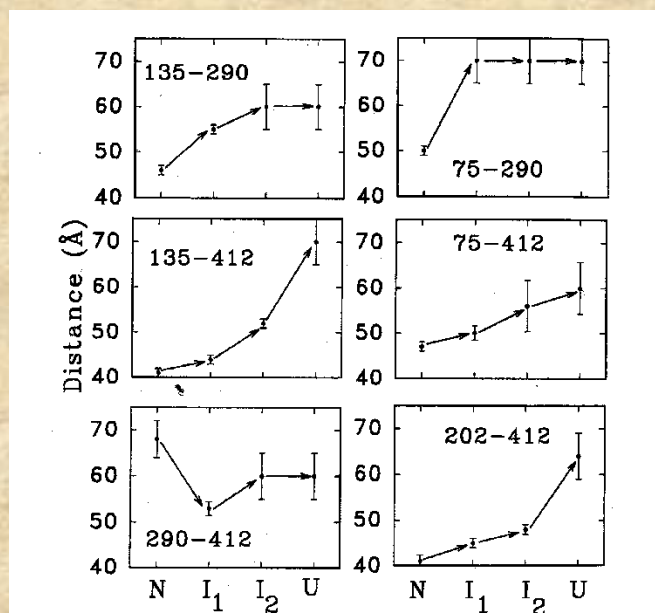
energy-transfer pair	measured steady-state distance (Å)	measured time-resolved discrete distance		measured time-resolved distance distribution			crystal structure C _α → C _α (Å) ^a	estimated dye-to-dye distances (Å) ^b
		<i>R</i> (Å)	χ ²	<i>R_c</i> (Å) [±2]	σ (Å)	χ ²		
135 ↔ 290	43	43.3	2.7	39.4	7.3	1.3	39	39
		40.3 ^c	1.6	38.8 ^c	6.1	1.2		
135 ↔ 412	40	40.4	2.7	39.5	3.8	1.3	40	46
		39.5	2.1	38.0	3.9	1.2		
412 → 135	40	38.7	1.4	38.1 ^c	3.4	1.3	48	56
		63.6	1.4	64.8	13.5	1.3		
290 ↔ 412	69	56.6 ^c	1.8	58.6 ^c	13.2	1.4	40	46
		51.7	4.3	46.6	13.5	1.2		
75 ↔ 290	50	41.7	1.5	37.8	6.6	1.1	26	34
202 ↔ 412	39	48.2	3.1	44.8	13.5	1.4	32	46
412 → 75	47	60-70	1.1	60-80	15-30	1.1	-	-
all ^d	-							

^a Watson et al. (1982). ^b Donor-to-acceptor distance from MD simulations based on Watson et al. (1982) crystal structure. ^c Acceptor-side FRET measurements. ^d Unfolded samples (MOPS buffer at pH 7.5 and 25 °C and 2 M GuHCl). ^e MOPS buffer at pH 7.5 and 25 °C. D ↔ A: average labeled samples (donor distributed between the two Cys sites). D → A: specific labeled samples. Unless otherwise indicated, distance determinations are from donor-side experiments. The errors on the recovered distances are dominated by "nonfitting" sources and are estimated to be ±3 Å (see the text).

Lifetime measurements were carried out on all samples

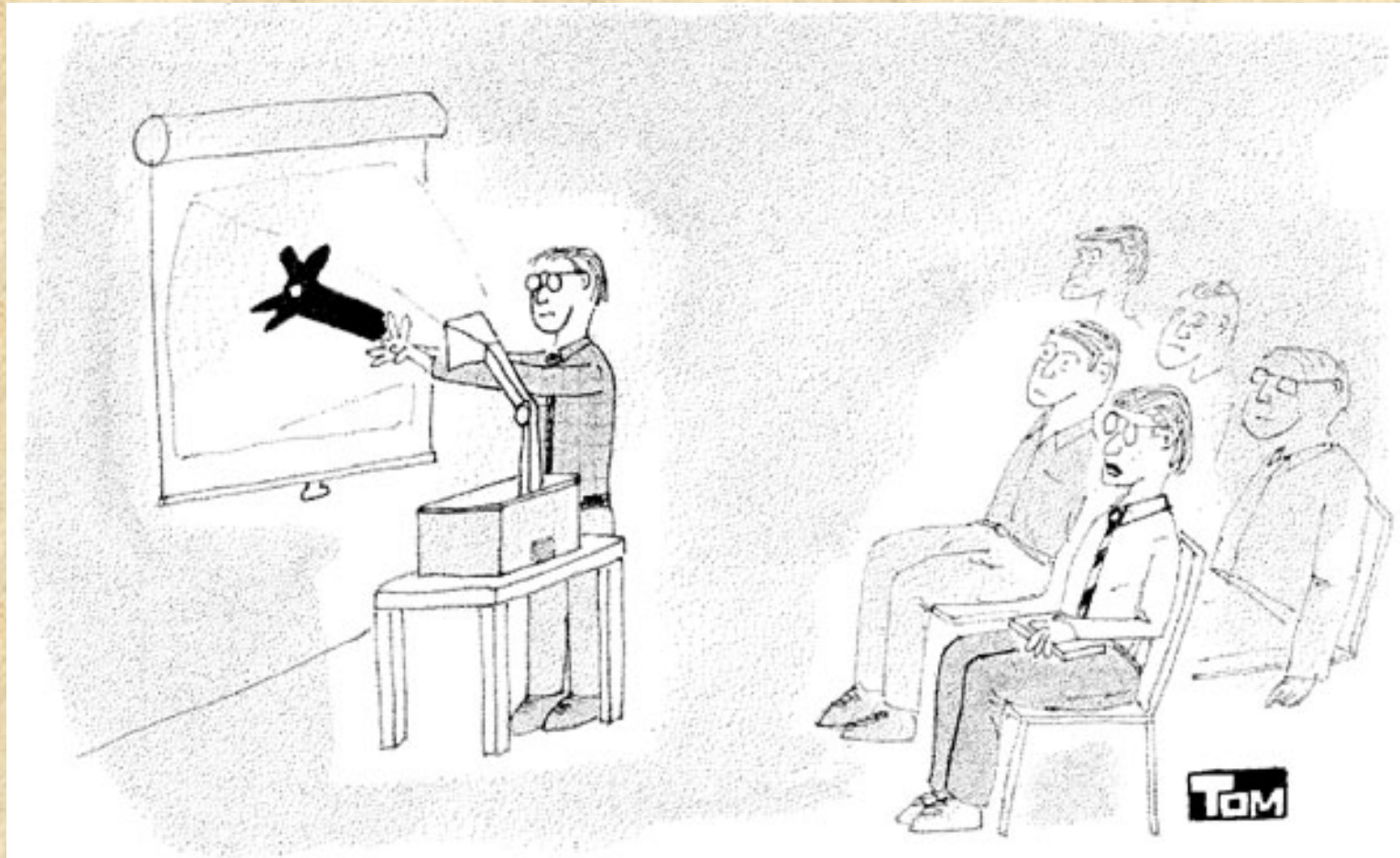
The intramolecular distances for the six energy transfer pairs are recovered for the each intermediate formed during the GuHCL induced unfolding of PGK

The authors proposed a specific structural transition associated with the unfolding of PGK from the native state (left) to the first unfolded state (right).



The C terminal domain (on the right of the monomer) is twisted by approximately 90° relative to the N-terminal domain resulting in an increase in the distances A, E and F and a shortening of the distance D.

The orientation factor κ^2



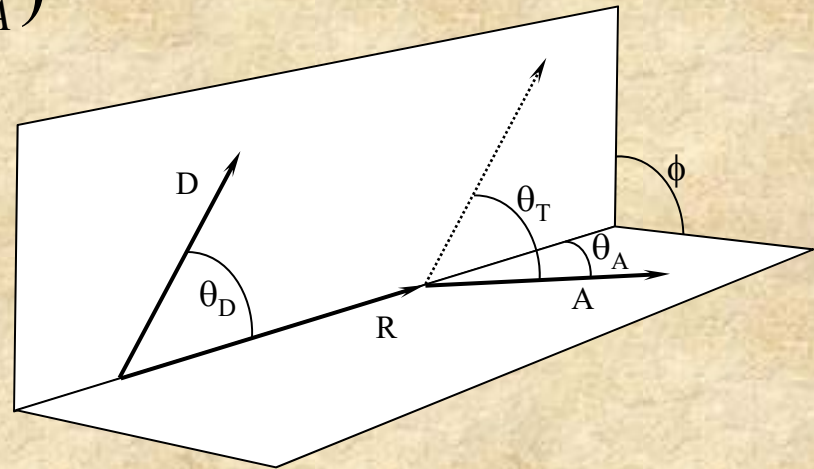
"I WAS HOPING TO SEE MORE EVIDENCE
for the choice of $2/3$ for κ^2

©1995 Tom Swanson

The orientation factor κ^2

$$\kappa^2 = (\cos \theta_T - 3 \cos \theta_D \cos \theta_A)^2$$

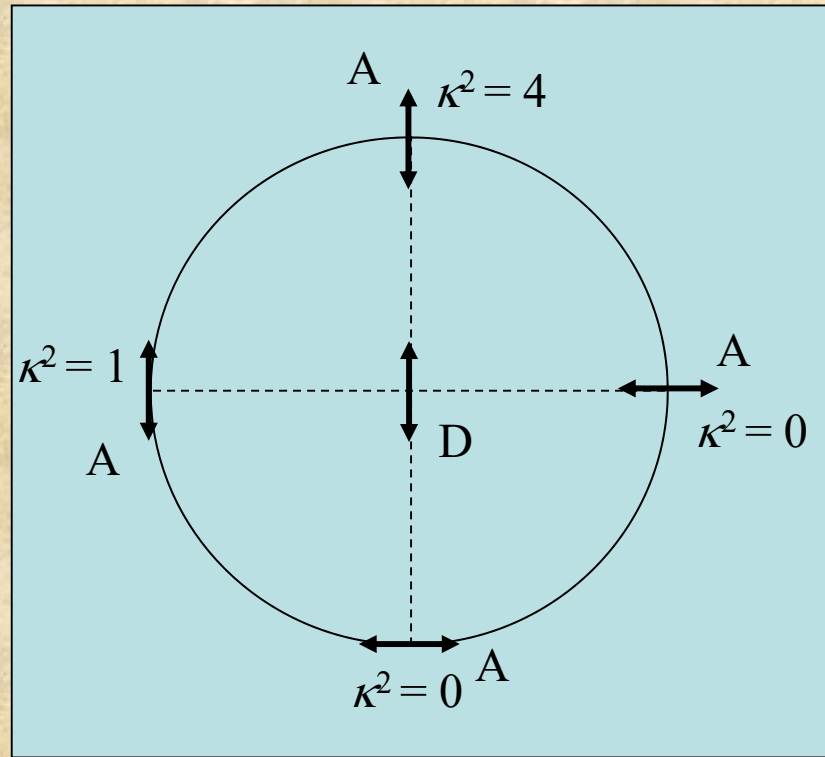
Where θ_T is the angle between the D and A moments, given by



$$\cos \theta_T = \sin \theta_D \sin \theta_A \cos \phi + \cos \theta_D \cos \theta_A$$

In which θ_D , θ_A are the angles between the separation vector R, and the D and A moment, respectively, and ϕ is the azimuth between the planes (D,R) and (A,R)

The orientation factor κ^2



The limits for κ^2 are 0 to 4, The value of 4 is only obtained when both transitions moments are in line with the vector R . The value of 0 can be achieved in many different ways.

If the molecules undergo fast isotropic motions (dynamic averaging) then $\kappa^2 = 2/3$

From Eisinger and Dale in: "Excited States of Biological Molecules" Edited by John Birks (1976)

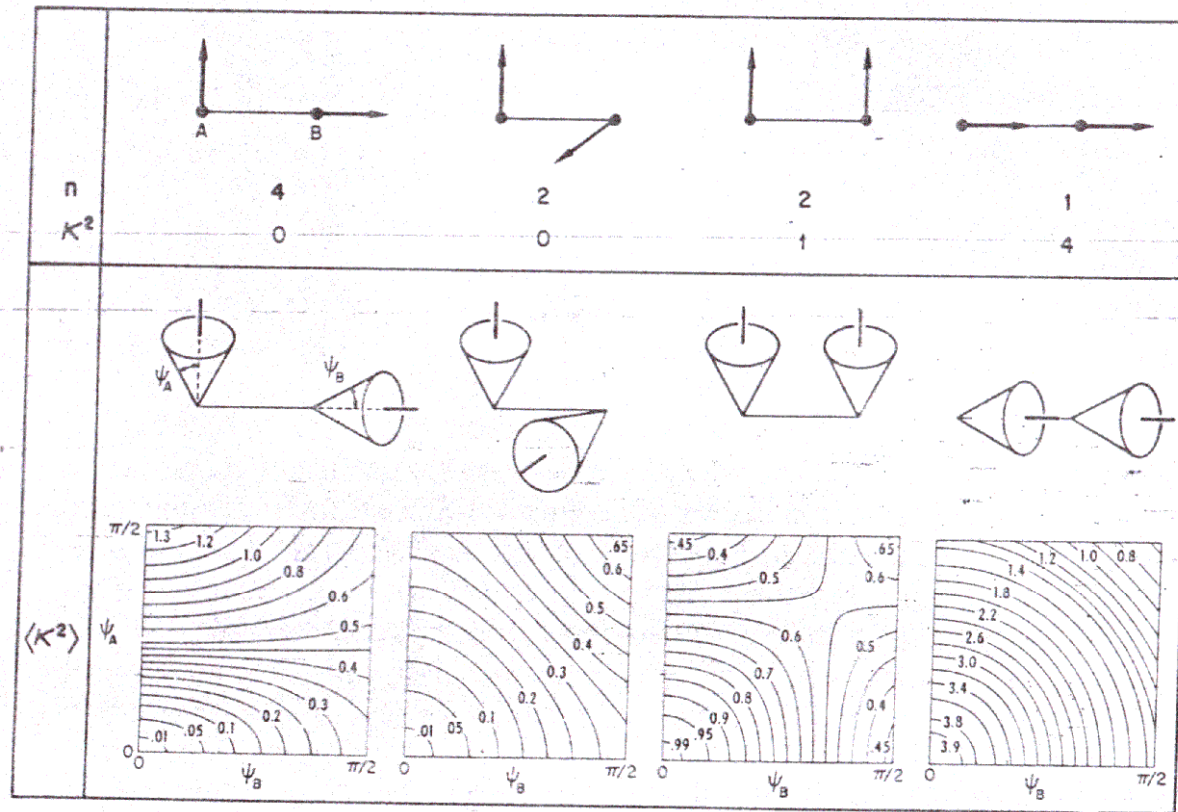


Figure 1 The upper part of the diagram illustrates the nine possible relative orientations of two transition dipoles each of which is fixed and can lie along either the x , y or z axis of a Cartesian triad. The corresponding κ^2 values are shown along with their statistical weights (n) and they are seen to lead to an average for κ^2 of $2/3$, the same as for isotropically random orientations of the transition dipole moments. The lower part of the figure illustrates how these $\langle \kappa^2 \rangle$ values change as the transition dipole directions are permitted orientational freedom within cones of half-angles ψ_A and ψ_B . Note that $\langle \kappa^2 \rangle$ departs quite slowly from its fixed minimum and maximum values (0 and 4) as the two cones open up and that when each cone half-angle is $\pi/2$, corresponding to an isotropic distribution of the transition dipole directions, $\langle \kappa^2 \rangle$ is equal to $2/3$ for each of the cases considered

What if the system is static but randomly oriented?

For example for a system in a highly viscous solvent or in general if the fluorescence lifetimes are very short relative to any rotational motions (as happens in many cases of fluorescent proteins conjugated to other proteins).

$$\text{Then } \kappa^2 = 0.476$$

THE JOURNAL OF CHEMICAL PHYSICS

VOLUME 48, NUMBER 6

15 MARCH 1968

Nonradiative Energy Transfer in Systems in which Rotatory Brownian Motion is Frozen

IZCHAK Z. STEINBERG

The Weizmann Institute of Science, Rehovoth, Israel

(Received 28 August 1967)

The effect of the complete restriction of rotatory Brownian motion of donor and acceptor molecules on the extent of nonradiative energy transfer in systems containing many donors and acceptors has been investigated. It is assumed that the molecules under discussion are randomly distributed and randomly oriented in space at the moment of excitation. The number of donor molecules which retain their excitation energy at time t after excitation is found to decrease exponentially with the sum of two terms: one proportional to t and the other proportional to $t^{1/2}$. This time dependence is similar in form to that found by Förster for systems in which donor and acceptor molecules undergo rapid rotatory diffusion. While the coefficient of $-t$ in the exponent is the same in both cases, the coefficient of $-t^{1/2}$ is smaller for systems in which molecular rotation is frozen than for systems in which rotatory Brownian motion is rapid.



So how do we determine κ^2 ?

Except in very rare cases, κ^2 can not be uniquely determined in solution.

What value of κ^2 should be used ?

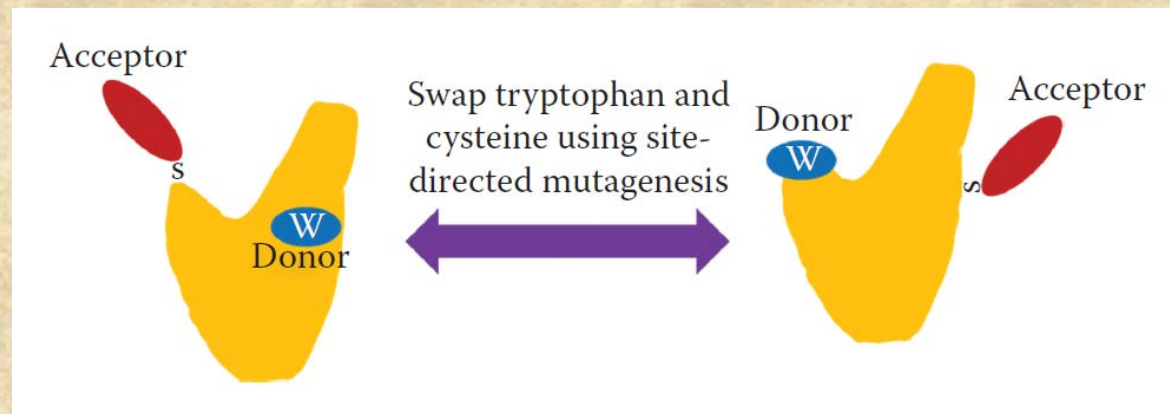
We can **assume** fast isotropic motions of the probes and value of $\kappa^2 = 2/3$, and verify experimentally that it is indeed the case.

We can **calculate** the lower and upper limit of κ^2 using polarization spectroscopy (Dale, Eisinger and Blumberg 1979).

Assuming $\kappa^2 = 2/3$

We can test this assumption experimentally:

By swapping probes: The micro-environment of the probes will be different. Therefore, if the micro-environment affects the probes' mobility and κ^2 is not equal to $2/3$, once swapped, the value of κ^2 will change and hence the distance measured by FRET.



By using different probes: If the distance measured using different probe pairs are similar (taking into account the size of the probes) then the assumption that κ^2 is equal to $2/3$ is probably valid.

Lower and upper limit of κ^2

We can calculate the lower and upper limit of κ^2 using polarization (Dale, Eisinger and Blumberg 1979).

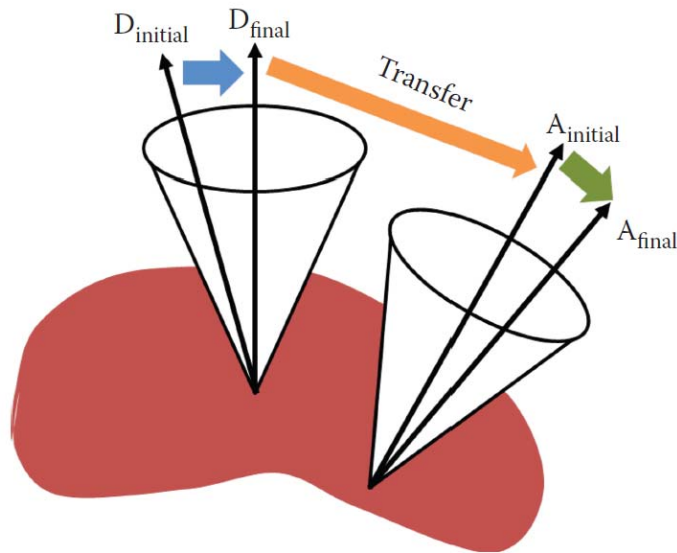
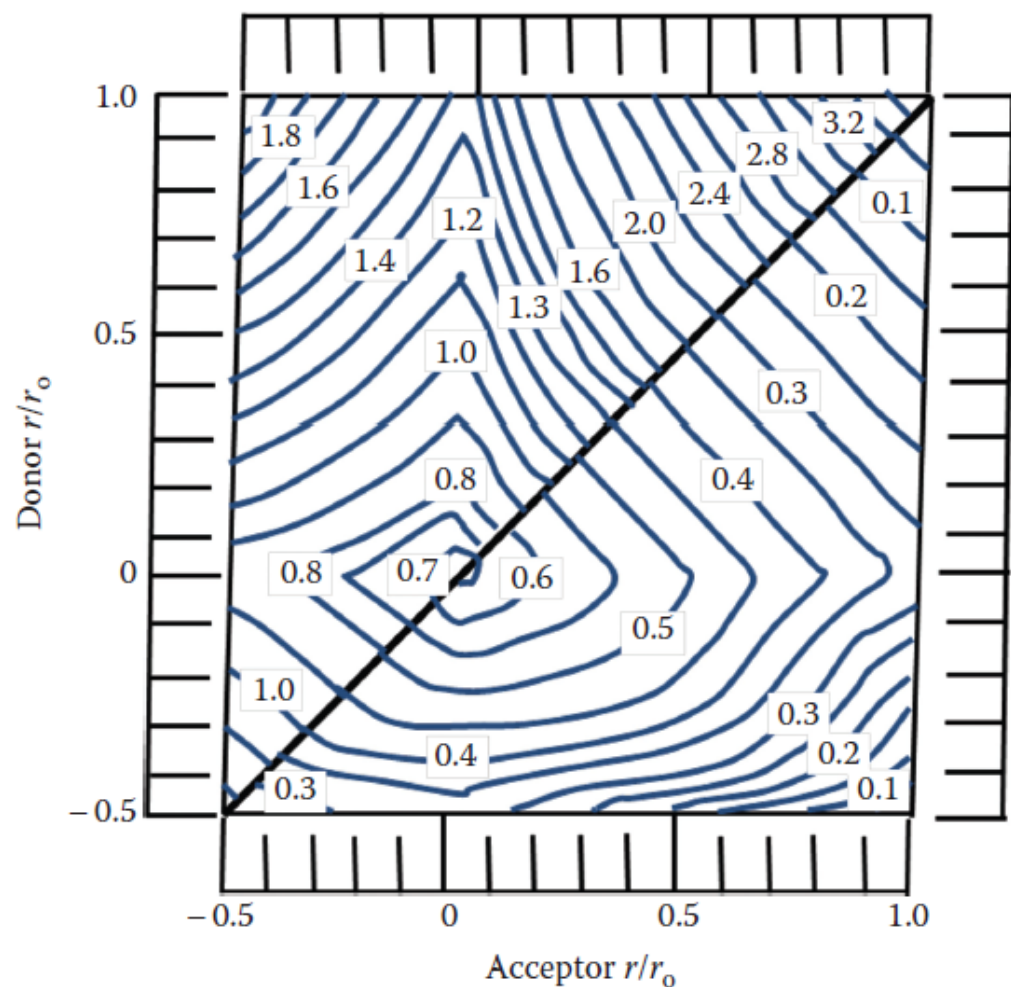


FIGURE 8.10 Illustration of mobilities of both donor and acceptor dipoles, which lead to depolarization.

Lets consider that each probe is rotating within a cone of axes D and A for the donor and acceptor, respectively, then 3 depolarization steps occur after the absorption of the excitation energy by the donor: An axial depolarization of the donor, a depolarization due to transfer and an axial depolarization of the acceptor

In the Dale-Eisinger-Blumberg approach, one measures the ratio of the observed polarizations of donors and acceptors to their limiting polarizations and then uses the calculated contour plots to put limits on κ^2



This approach was used in:

Arbildua et al.,

Fluorescence resonance energy transfer and molecular modeling studies on 4',6-diamidino-2-phenylindole (DAPI) complexes with tubulin.

Protein Sci. (2006) 15(3):410-9.

FRET occurs between DAPI
and TNP-GTP bound to tubulin
– a heterodimer protein

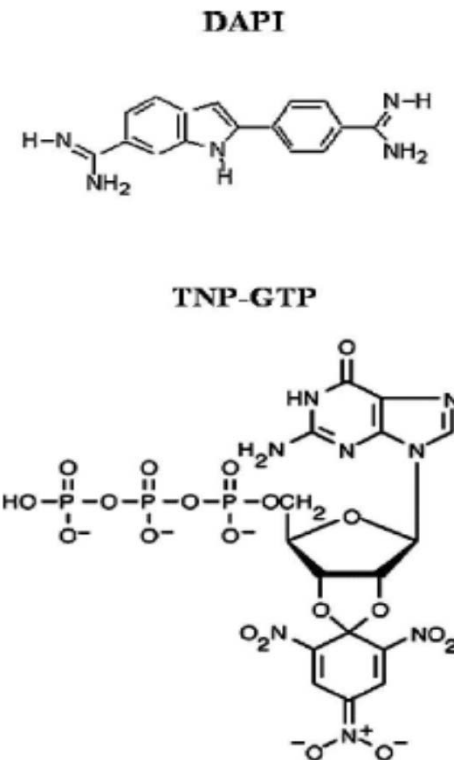


Figure 1. Structures of 4'-6-diamidino-2-phenylindole (DAPI) and 2',3'-O-(2,4,6-trinitrophenylidene)-GTP (TNP-GTP) at neutral or basic pH.

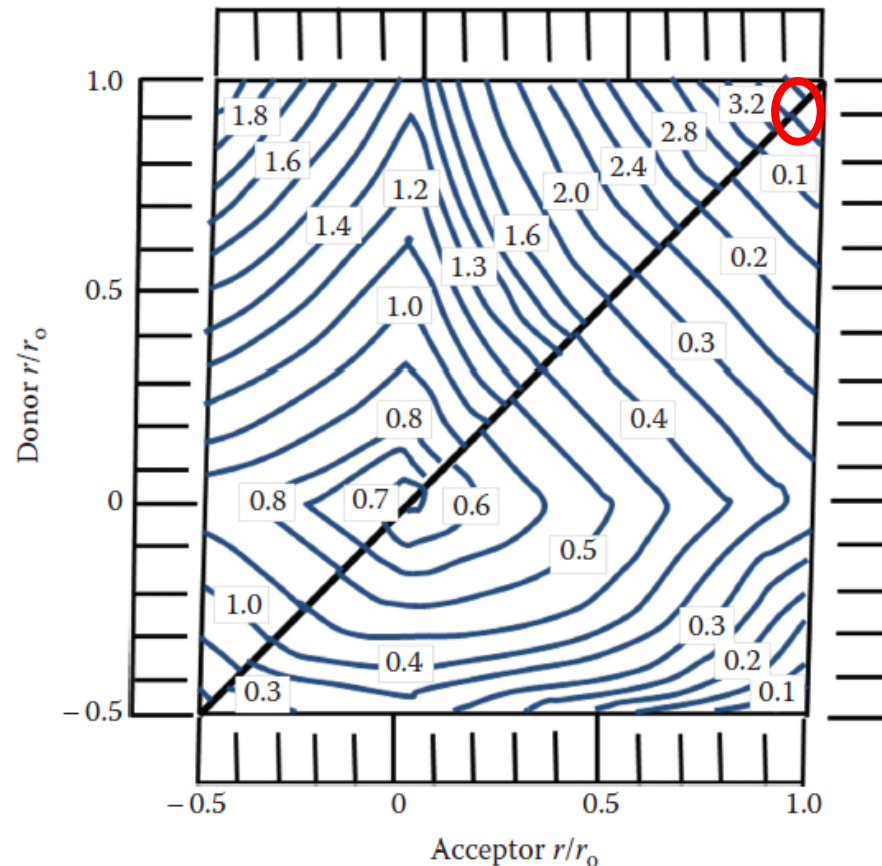
Assuming a κ^2 value of 2/3, one would calculate the DAPI-TNP-GTP distance to be ~43 Angstroms

But DAPI is bound non-covalently - hence has no local motion so its polarization is high (~0.42)

And, TNP-GTP is also non-covalently bound and has a short lifetime and hence a high polarization (~0.48)

These observed polarization values are close to the limiting polarization values for these probes: 93% and 100% respectively, for DAPI and TNP-GTP

Using the Dale-Eisenger-Blumberg plot one can then estimate that κ^2 can be anywhere between 0.02 and 3.7!



In fact the authors concluded, based on other information, that the distance between DAPI and TNP-GTP bound to tubulin was likely to ~ 30 Angstroms.

Quantitative distance determinations using FRET – i.e., as a true “spectroscopic ruler” - remain **difficult at best**

But FRET can be very powerful when used to detect changes in a system, such as alterations in distance and or orientation between donor and acceptor attached to biomolecules, i.e., due to ligand binding or protein-protein interactions

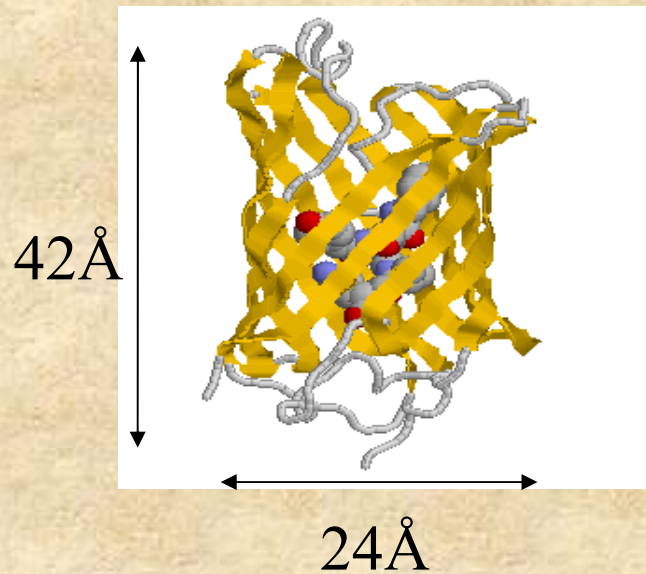
The renaissance of fluorescence resonance energy transfer

Paul R. Selvin

Recent advances in fluorescence resonance energy transfer have led to qualitative and quantitative improvements in the technique, including increased spatial resolution, distance range, and sensitivity. These advances, due largely to new fluorescent dyes, but also to new optical methods and instrumentation, have opened up new biological applications.

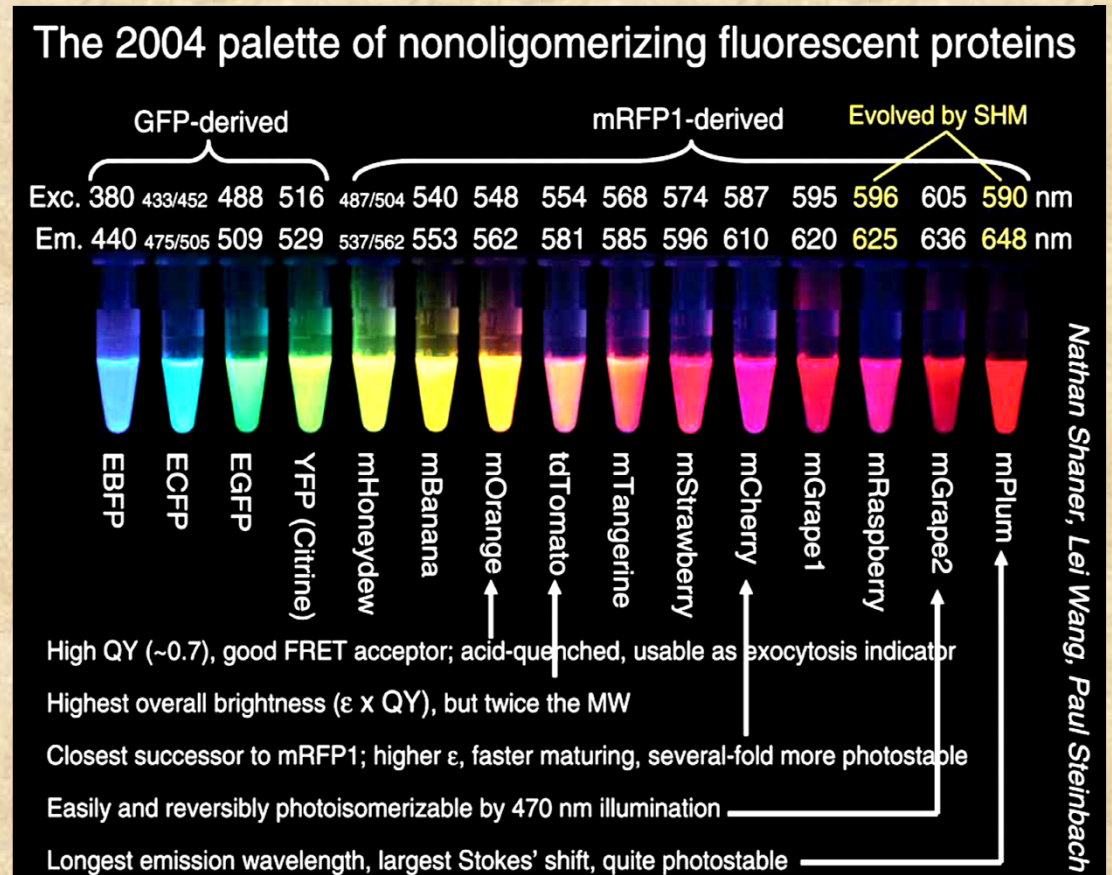
nature structural biology • volume 7 number 9 • september 2000

The development of Fluorescent Proteins has led to a significant increase in FRET studies



The GFP is fused to the protein of interest and expressed in the organism under study.

Fluorescent proteins with the appropriate absorption and emission properties are chosen as donors and acceptors. Such systems can be used in vitro as well as in vivo



Homo-transfer of electronic excitation energy

So far, we considered the donor and acceptor molecules to be different. However, if the probe excitation spectrum overlaps its emission spectrum, FRET can occur between identical molecules.

« Il suffit qu'un transfert d'activation puisse se produire entre deux molécules voisines d'orientation différentes, c'est à dire portant des oscillateurs non parallèles, pour qu'il en résulte en moyenne une diminution de l'anisotropie de distribution des oscillateurs excités et par suite de la polarisation de la lumière émise. »

(F. Perrin *Ann de Phys.* 1929)

It suffices that a transfer of activation can occur between two neighboring molecules with different orientations, that is with non-parallel oscillators, in order to have, on average, a decrease in the anisotropy of the distribution of excited oscillators, and therefore a decrease of the polarization of the emitted light.

« ...L'existence de transferts d'activation est expérimentalement prouvée pour de telles molécules par la décroissance de la polarisation de la lumière de fluorescence quand la concentration croît... »

(F. Perrin *Ann de Phys.* 1932)

...The existence of transfer of activation is proven experimentally for such molecules by the decrease in polarization of the fluorescent light when the concentration is increased...

Homo-transfer of electronic excitation energy

“...Excitation transfer between alike molecules can occur in repeated steps. So the excitation may *migrate* from the absorbing molecule over a considerable number of other ones before deactivation occurs by fluorescence or other process. Though this kind of transfer cannot be recognized from fluorescence spectra, it may be observed by the decrease of fluorescence polarization...” (Förster, 1959)

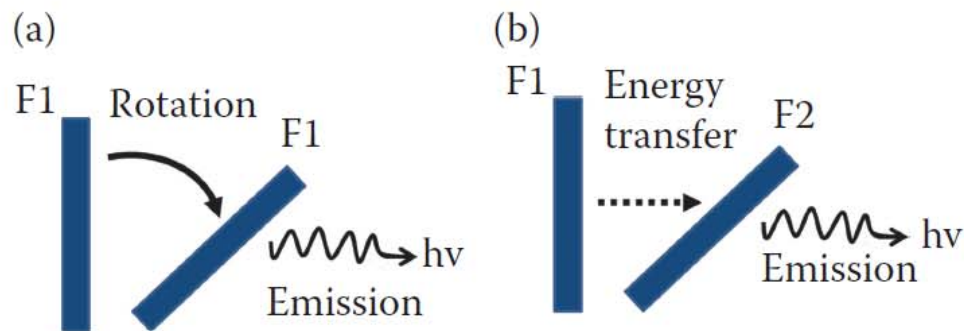


FIGURE 5.29 Depiction of depolarization due to (a) rotational diffusion and (b) energy transfer.

A. Depolarization resulting from rotational diffusion of the fluorophore. The excited fluorophore ($F1^*$) rotates then emits light. **B.** The excited fluorophore ($F1^*$) transfer energy to another fluorophore $F2$ which in turn emits light.

Electronic energy transfer between identical fluorophores was originally observed by Gaviola and Pringsheim in 1924.

Über den Einfluß der Konzentration auf die Polarisation der Fluoreszenz von Farbstofflösungen.

Von **E. Gaviola** und **Peter Pringsheim** in Berlin.

Mit zwei Abbildungen. (Eingegangen am 24. März 1924.)

Tabelle 2. Uranin in ganz wasserfreiem Glycerin.

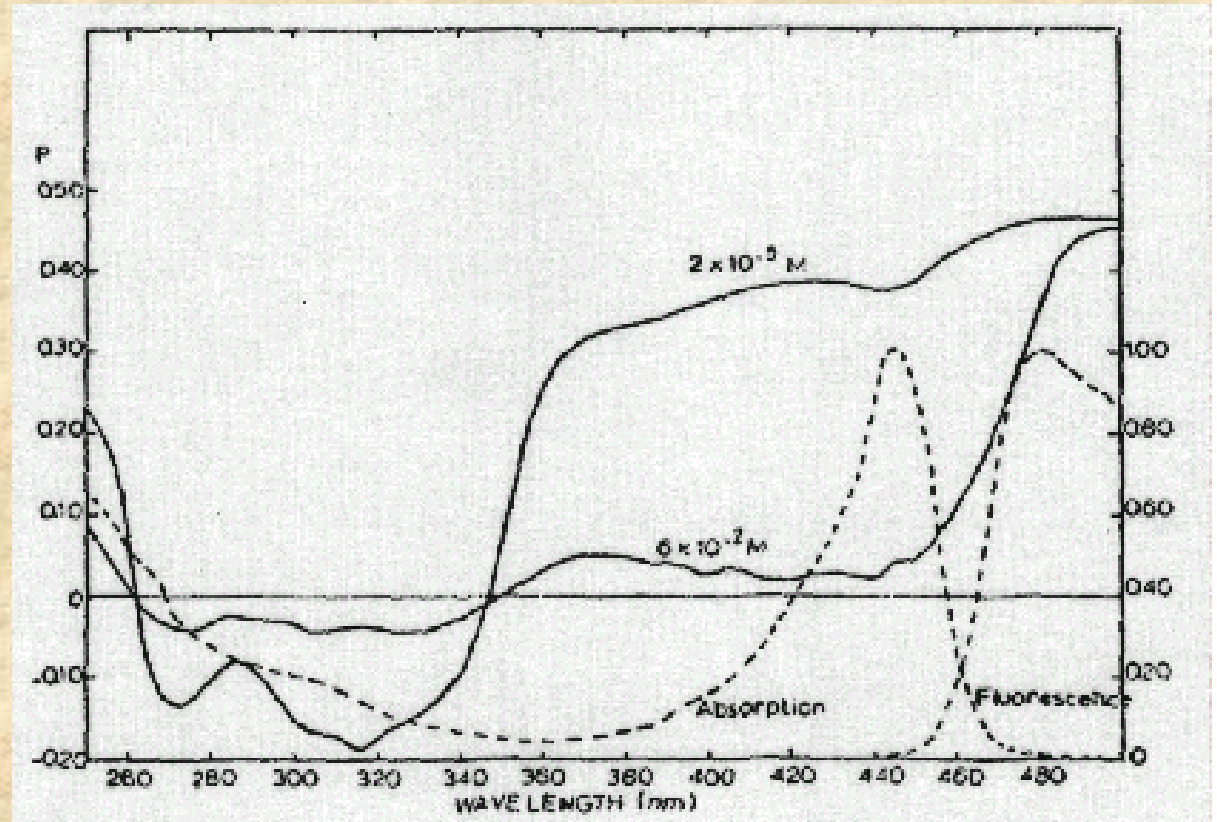
C	p	C	p	C	p	C	p
$\frac{1}{4}$	0	$\frac{1}{32}$	6,5	$\frac{1}{256}$	15	$\frac{1}{2048}$	39,2
$\frac{1}{8}$?	$\frac{1}{64}$	8,1	$\frac{1}{512}$	19,5	$\frac{1}{4100}$	43,5
$\frac{1}{16}$	3,2	$\frac{1}{128}$	11,1	$\frac{1}{1024}$	30,7	etwa $\frac{1}{20000}$	45

(note: uranin is the sodium salt of fluorescein)

Weber's Red-Edge Effect

In 1960 Weber was the first to report that homotransfer among indole molecules disappeared upon excitation at the red-edge of the absorption band - this phenomenon is now known as the "Weber red-edge effect".

In 1970 Weber and Shinitzky published a more detailed examination of this phenomenon. They reported that in the many aromatic residues examined, transfer is much decreased or undetectable on excitation at the red edge of the absorption spectrum.



Distance determination using homotransfer

The efficiency of transfer can be calculated from a knowledge of the polarization in the absence and presence of energy transfer.

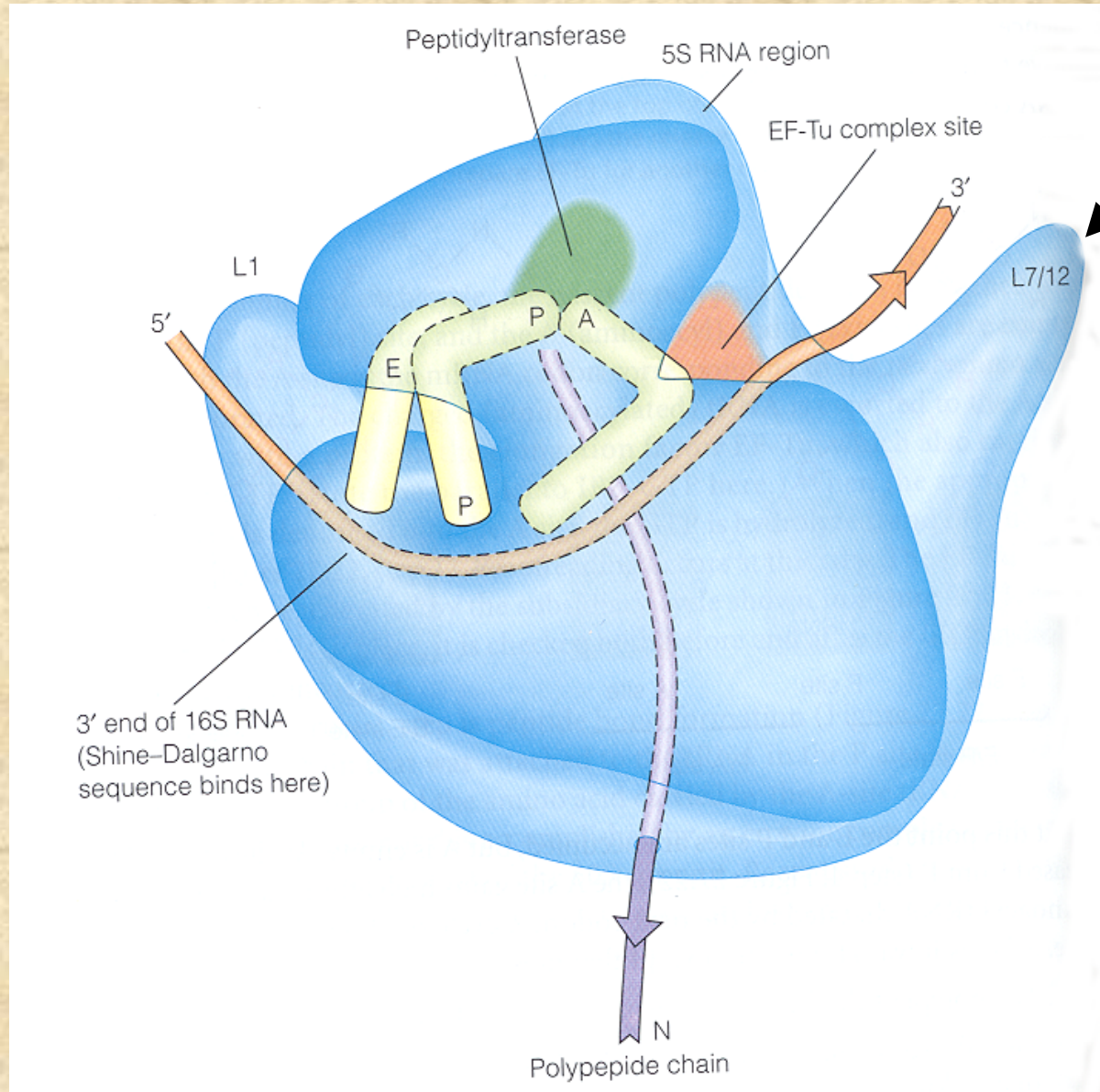
The steady state expression for the efficiency of energy transfer (E) as a function of the anisotropy is given by

$$E = 2(r_d - \langle r \rangle) / (r_d - r_a)$$

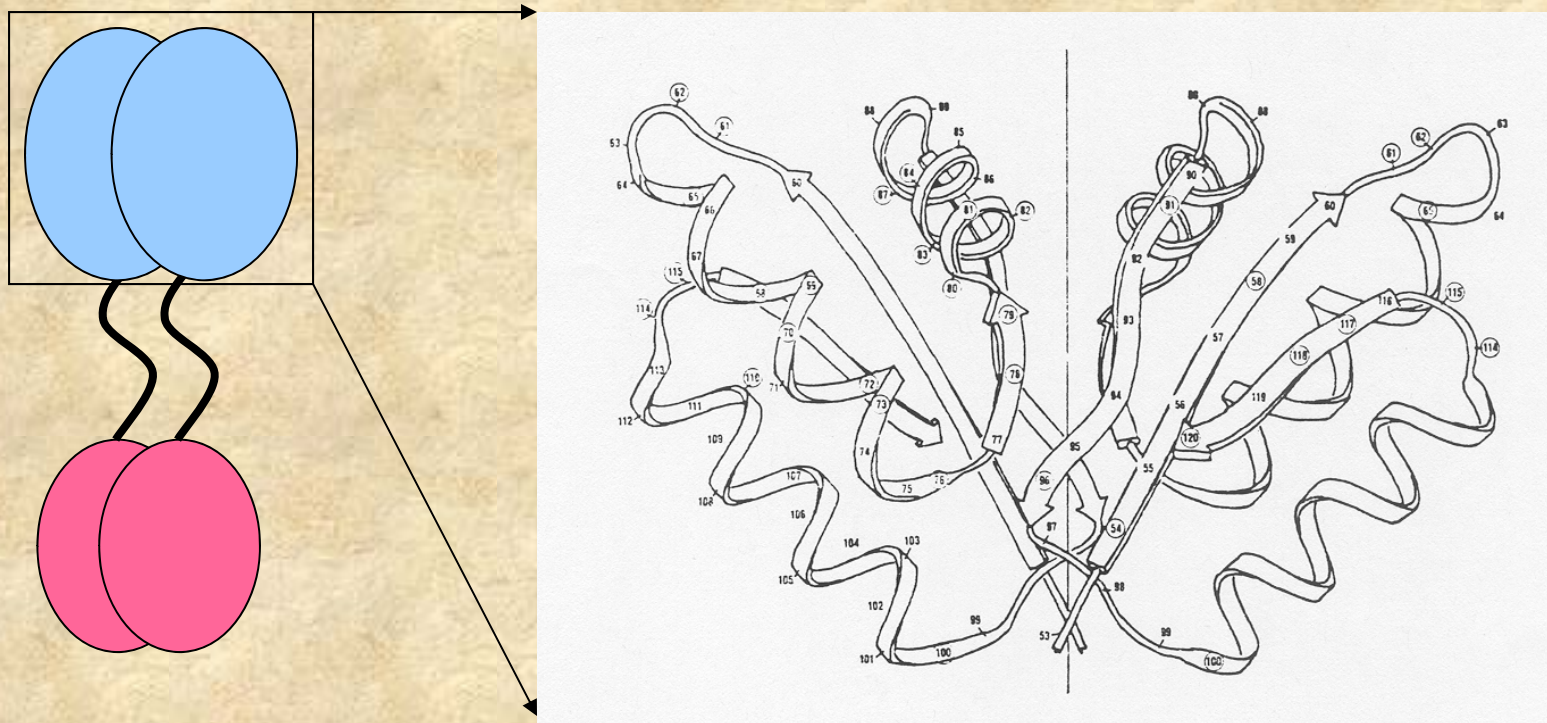
Where r_d and r_a are the anisotropy decay of the donor and acceptor only, respectively and $\langle r \rangle$ is the observed anisotropy in presence of both donor and acceptor. If $\kappa^2 = 2/3$ then $r_a = 0$ and

$$E = 2(r_d - \langle r \rangle) / r_d$$

An example of homo-FRET used to study protein interactions is the work by Hamman et al (Biochemistry 35:16680) on a prokaryotic ribosomal protein



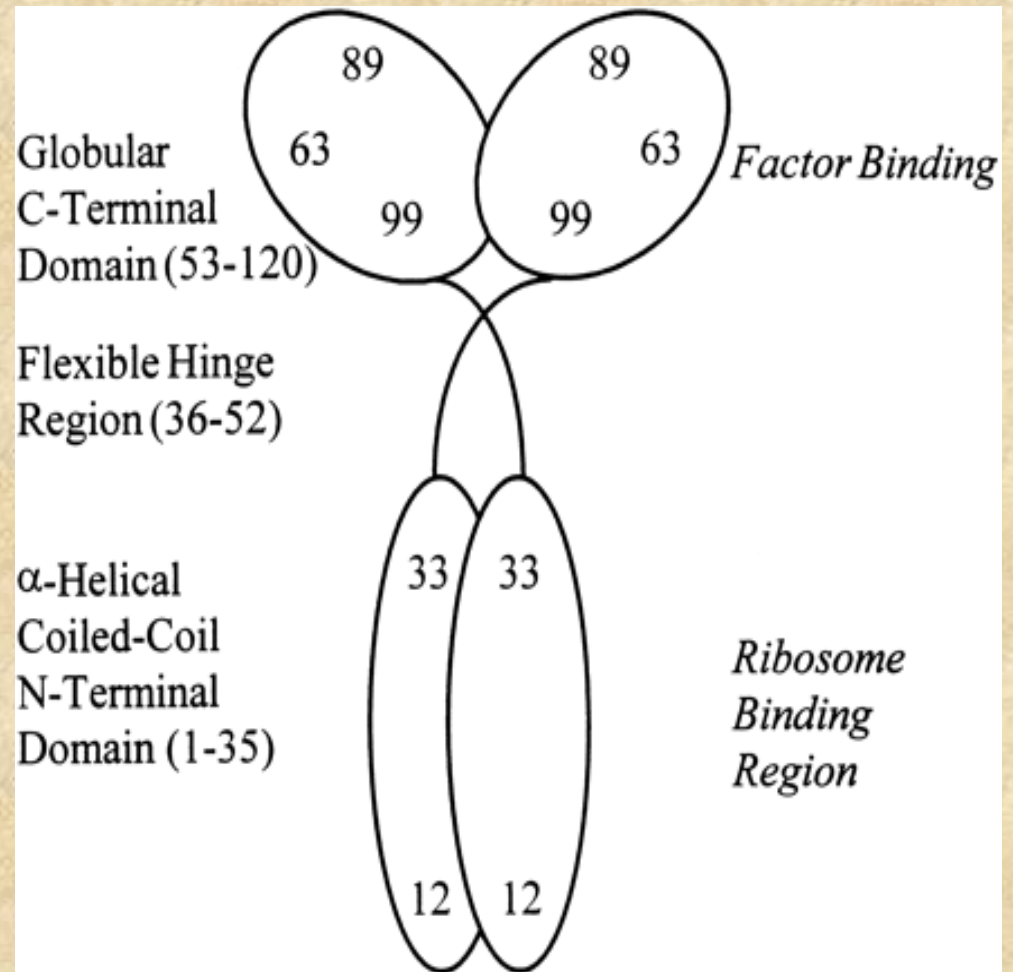
L7/L12 is present as two dimers in the ribosome. An X-ray structure of monomeric C-terminal domains led to the speculation that the C-terminal domains of L7/L12 interacted through hydrophobic surfaces as shown below



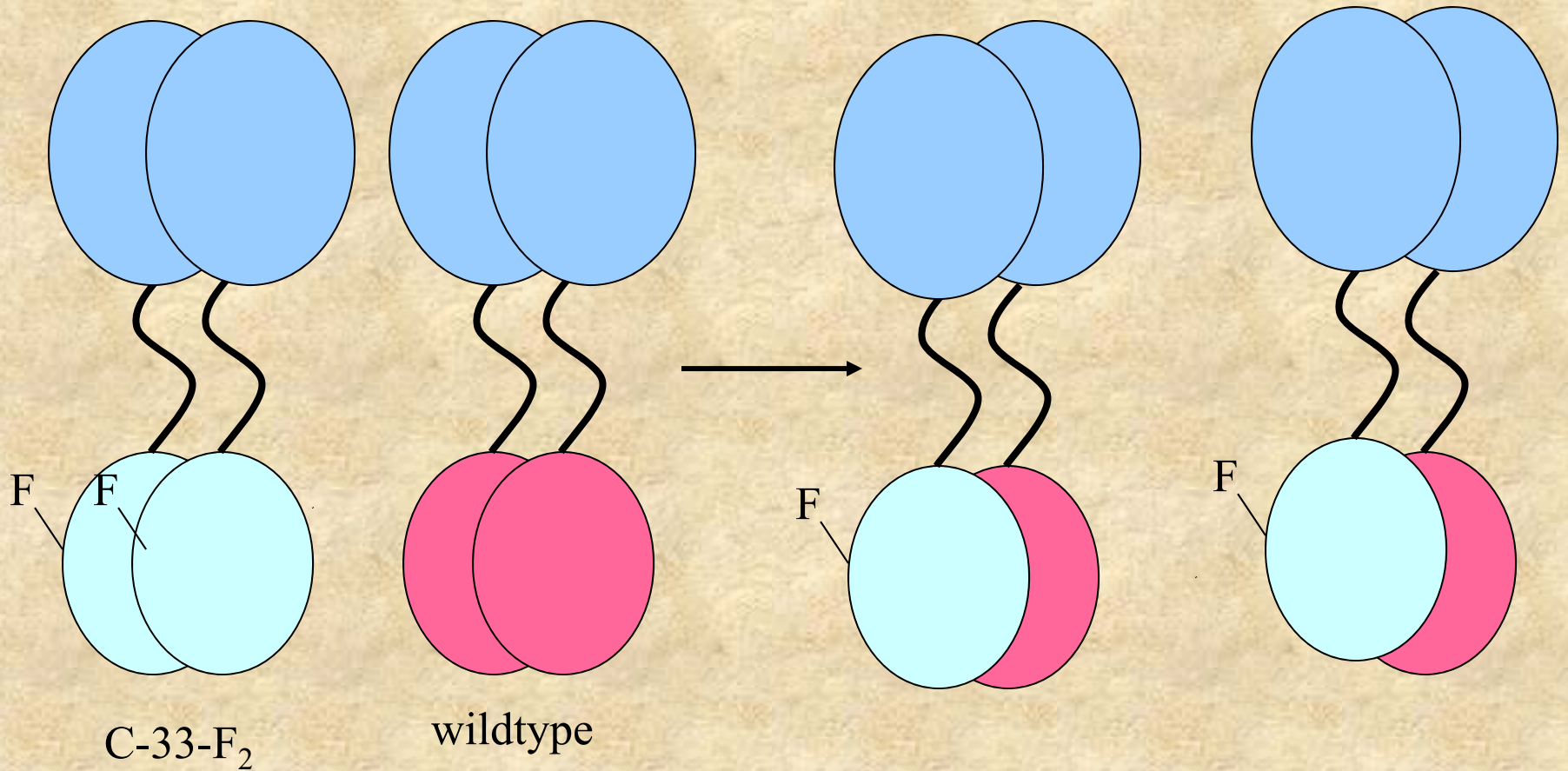
To study this protein fluorescence probes were introduced at specific locations along the L7/L12 peptide backbone.

To introduce these probes at specific locations site-directed mutagenesis was used to place cysteine residues in different locations

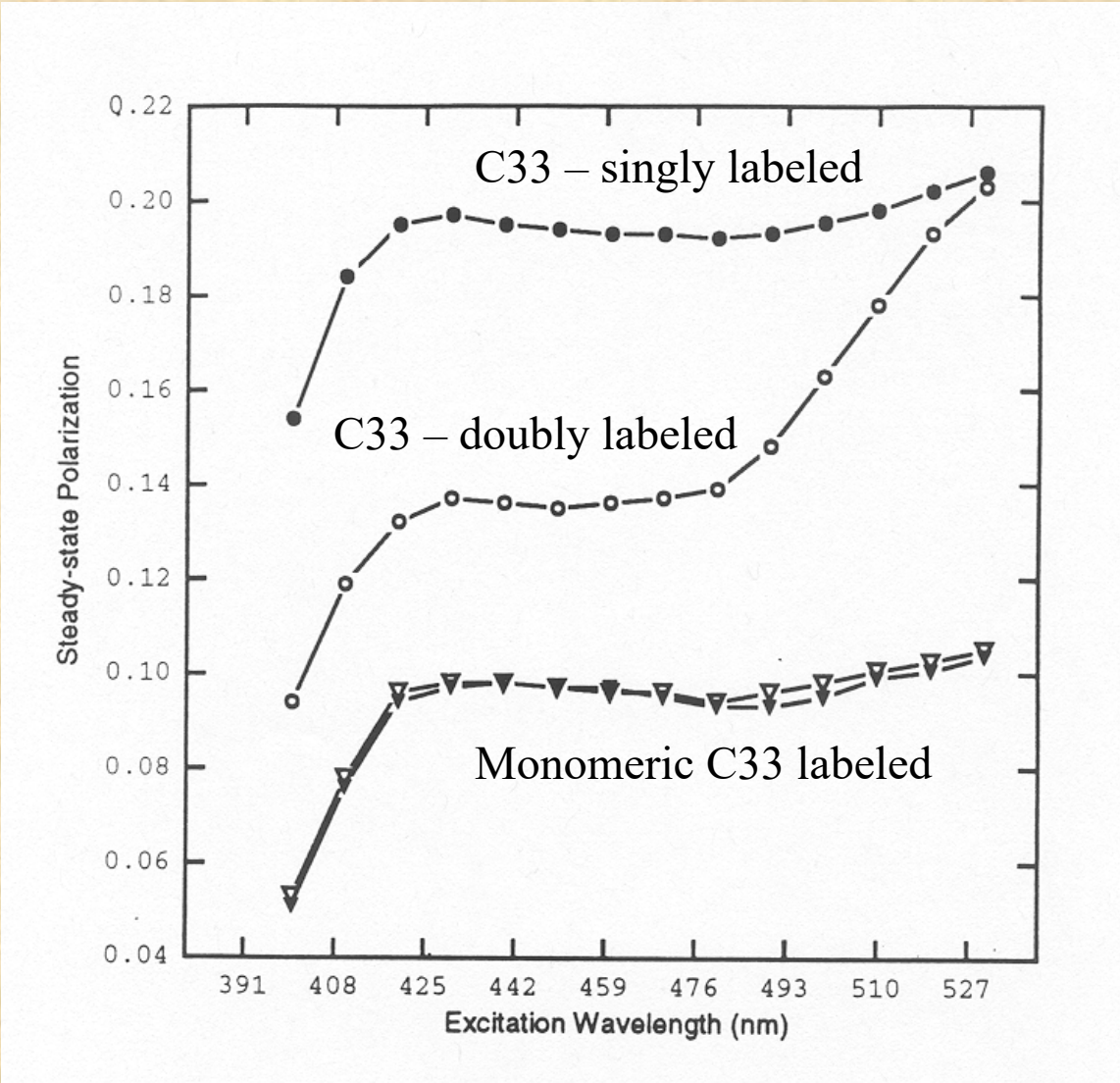
Sulfhydryl-reactive fluorescence probes were then covalently attached to these cysteine residues



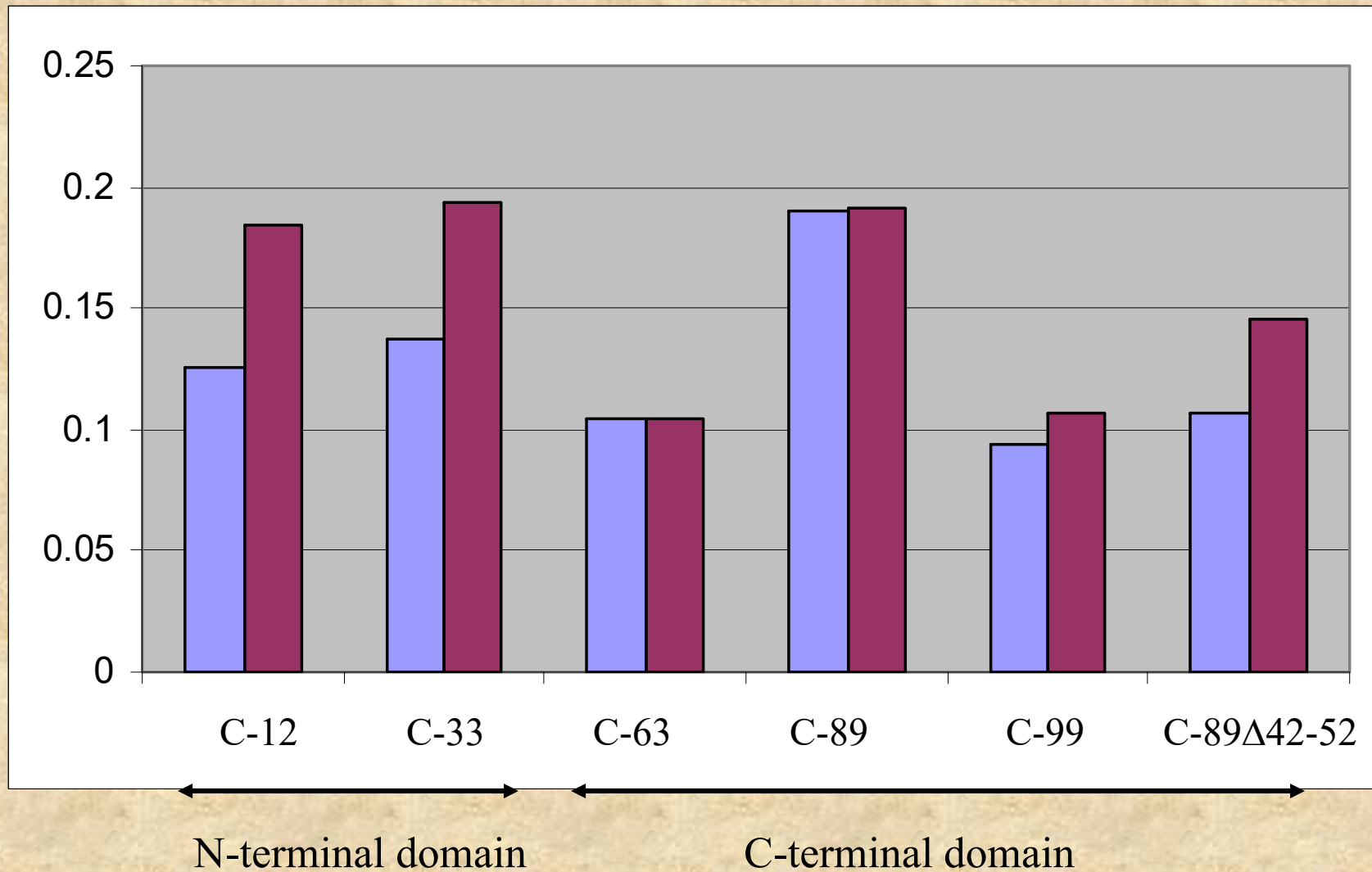
Subunit exchange experiments allowed the preparation of singly labeled dimers



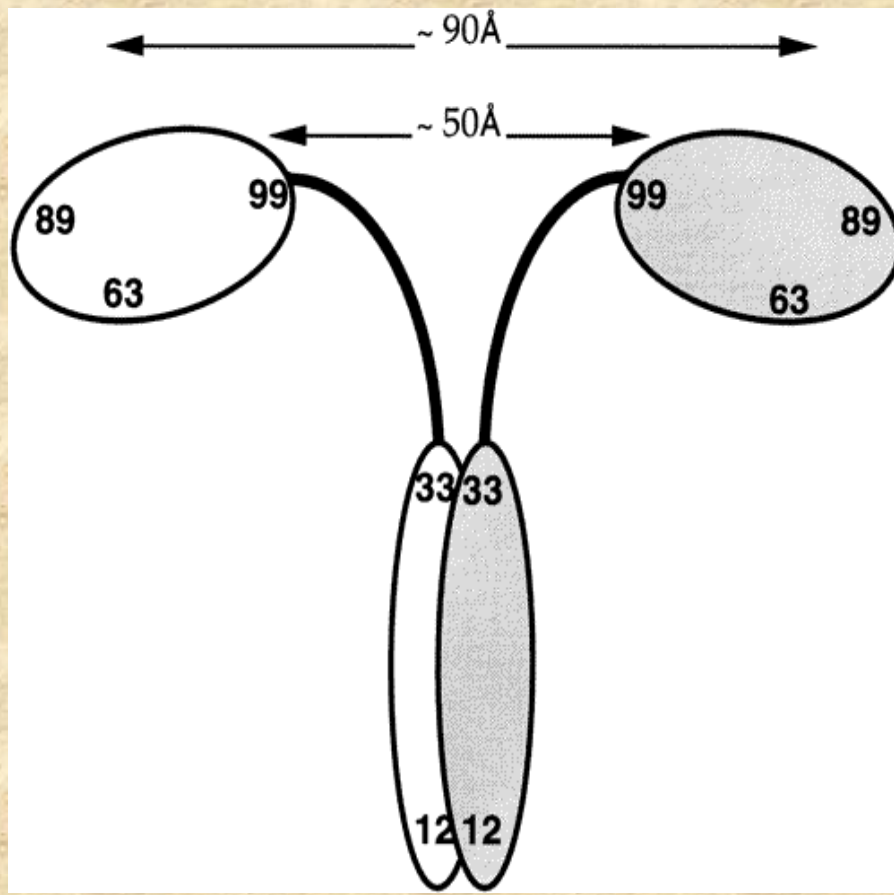
The presence of homoFRET was evident in the excitation polarization spectrum as shown by the Weber Red-Edge Effect.



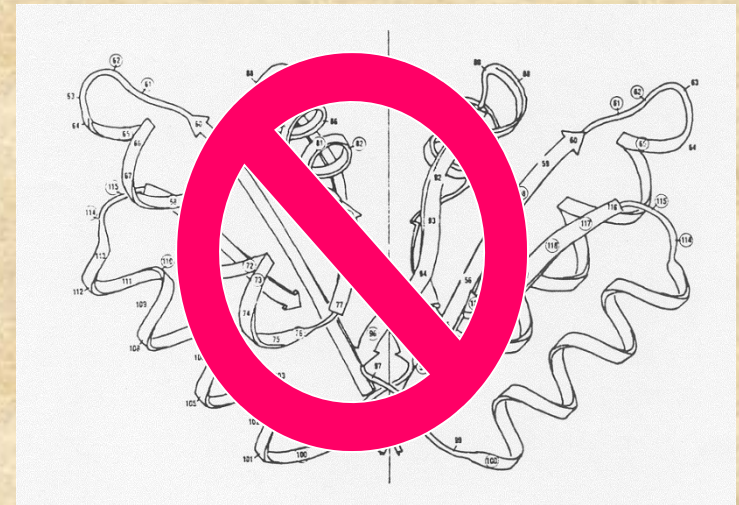
The polarization values, before and after subunit exchange, indicate which residues undergo homoFRET. The polarization data below are for fluorescein labeled constructs before (violet) and after (magenta) subunit exchange



These changes in polarization due to homoFRET allow us to assign maximum proximity values for the C-terminal domains.



The conclusion is that the C-terminal domains are well-separated – contrary to the original model from the X-ray studies and the usual depictions in the literature



Homo-FRET Microscopy in Living Cells to Measure Monomer-Dimer Transition of GFP-Tagged Proteins

I. Gautier,* M. Tramier,* C. Durieux,* J. Coppey,* R. B. Pansu,† J-C. Nicolas,‡ K. Kemnitz,§ and M. Coppey-Moisan*

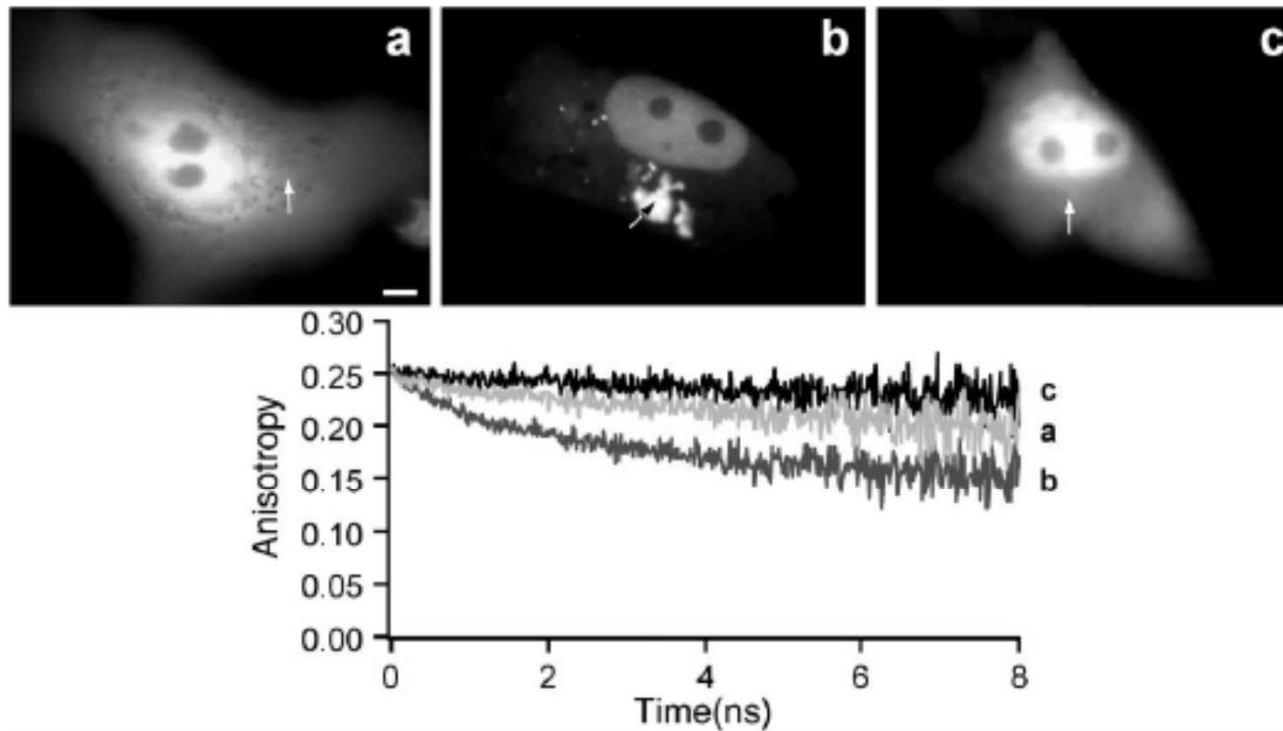


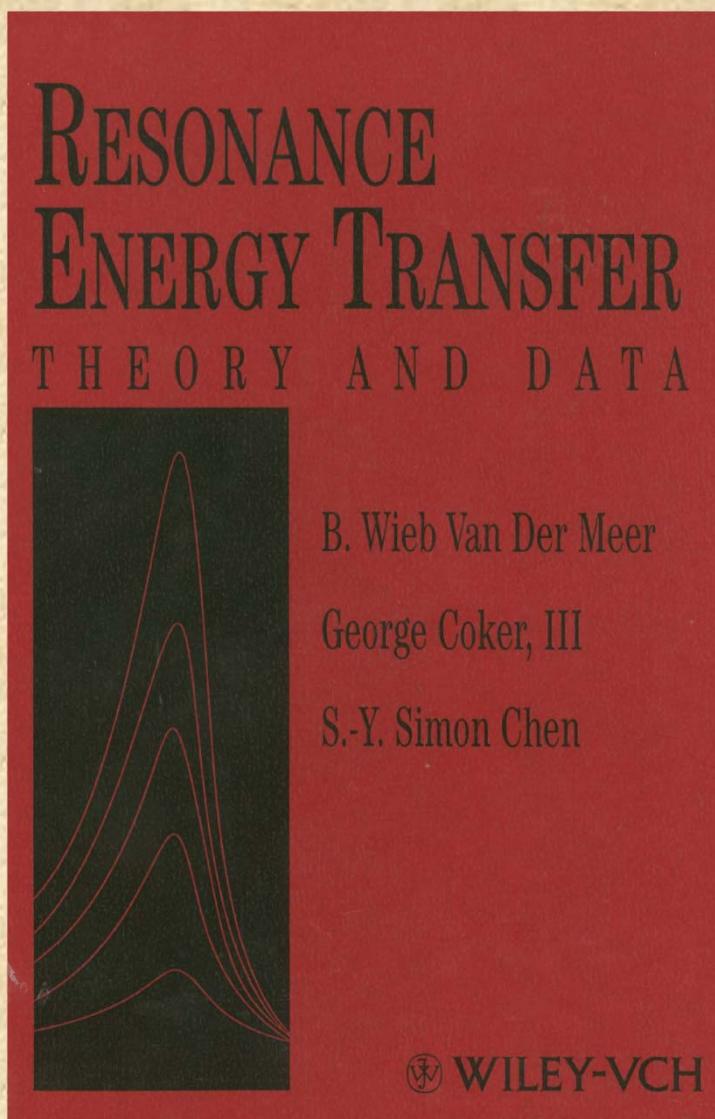
FIGURE 1 Subcellular fluorescence anisotropy decays of TK₂₇-GFP and TK₃₆₆-GFP proteins. (Top) Steady-state fluorescence images of Vero cells expressing TK₂₇-GFP (a) and TK₃₆₆-GFP (b and c). (a and c) Cells presenting only a diffuse cytoplasmic and nuclear fluorescence pattern; (b) Cells containing fluorescent aggregates. (Bottom) Time-resolved fluorescence depolarization from a cytoplasmic area of diffuse fluorescence (a and c) and from an area inside an aggregate (b). The subcellular location of the illuminated volume ($\sim 1 \mu\text{m}^3$) from which the anisotropy decay was performed is indicated by an arrow. For cells containing aggregates, anisotropy decays from nuclear or cytoplasmic area of diffuse fluorescence were similar to that obtained from aggregates (b). Bar in a, 5 μm .

Biophys J, June 2001, p. 3000-3008, Vol. 80, No. 6

Other examples of homo-FRET *in vivo* can be found in: Tramier et al., 2003 “Homo-FRET versus hetero-FRET to probe homodimers in living cells” *Methods Enzymol.* 360:580-97.

To summarize this lecture is not intended to prepare you to start FRET measurements immediately but rather to make you aware of the salient principles and pitfalls

Several books on this topic are available as well as MANY articles in the primary literature



Fluorescence Probes

Where Do Fluorophores Come From?

Some fluorophores occur naturally in the plant or animal world, such as quinine, which has played an important role in the development of the fluorescence field. Many such natural fluorophores, or “intrinsic fluorophores,” including the aromatic amino acids, are very useful in modern research.

Yet, most modern fluorescence studies would not be possible without fluorescent molecules designed and synthesized in a laboratory. Indeed, the rapid development of the biological fluorescence field owes much to synthetic organic chemistry, as well as to modern molecular biology and the commercialization of instrumentation.

Most beginning fluorescence practitioners do not have to synthesize their own fluorophores, since literally thousands are now available. Yet, even as late as the 1970s - when I was a graduate student with Gregorio Weber at the University of Illinois - only a handful of fluorescence probes were commercially available.

Consequently, for some of my studies, I had to synthesize the probe, build the instrument, and walk 5 miles uphill each day through the snow to the lab



OK - maybe I didn't actually have to walk 5 miles uphill through the snow - but the rest is true!

Fluorescence Probes

In vitro (or *In Silico*)

In vivo (or more accurately in cells)

Classification of probes

Intrinsic Fluorophores

Fluorophores that are naturally part of the system being studied

Extrinsic Fluorophores

Synthetic dyes or modified biochemicals that are added to a specimen to produce fluorescence with specific spectral properties.

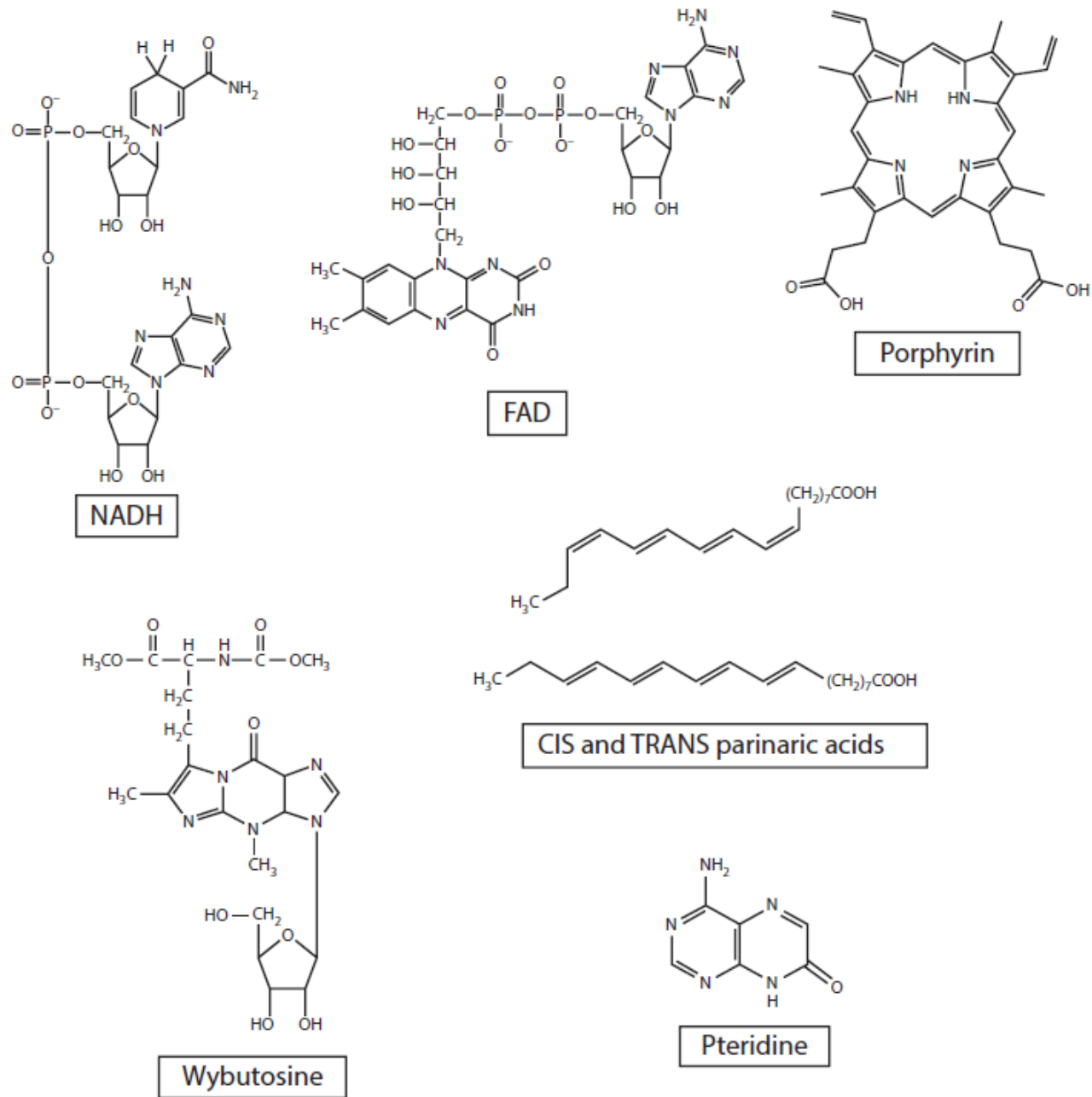
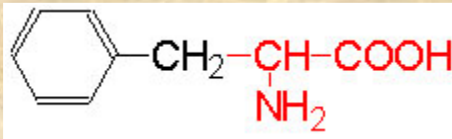


FIGURE 10.2 Structures of several intrinsically fluorescent biomolecules.

Fluorophores

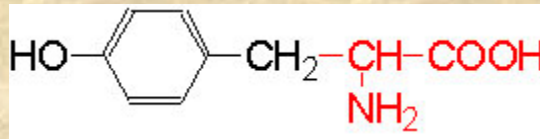
Proteins: Naturally Occurring Fluorophores

Aromatic amino acids



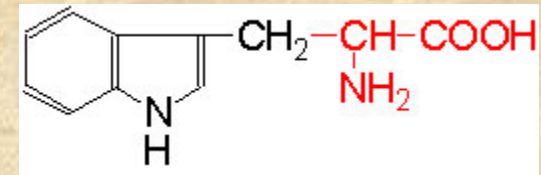
Phenylalanine (Phe – F)

Ex/Em 260 nm/282 nm



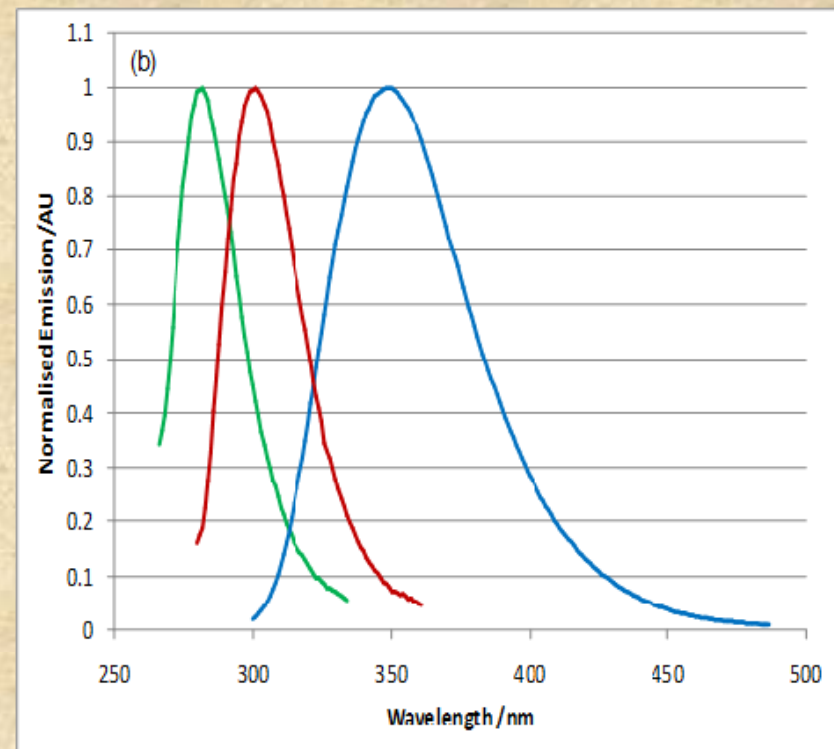
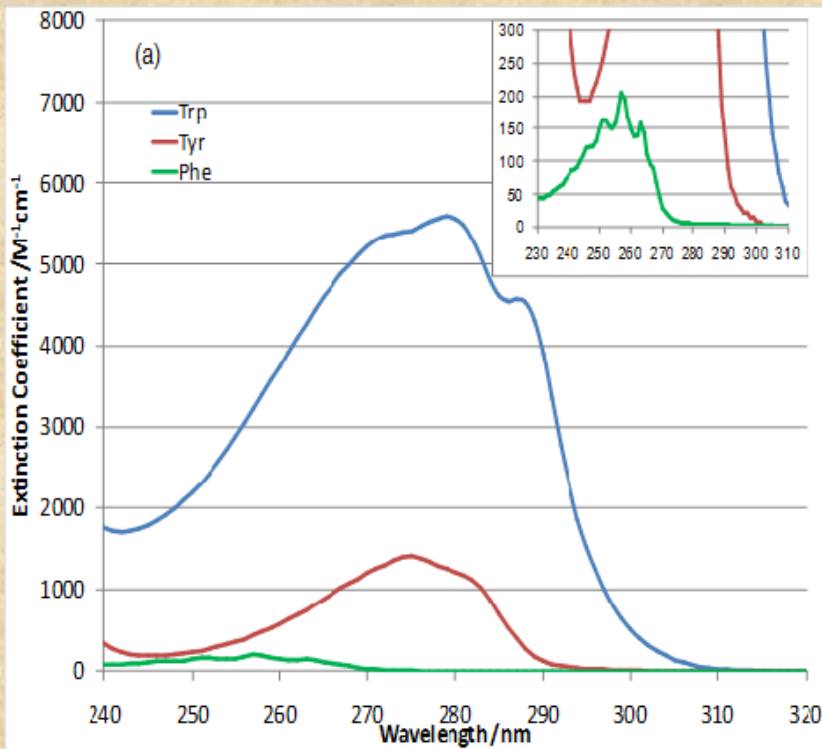
Tyrosine (Tyr – Y)

Ex/Em 280 nm/303 nm



Tryptophan (Trp-W)

Ex/Em 280, 295nm/ 305-350 nm



Fluorescent Probes

- Non covalent interactions

A non-covalent fluorescent probe is designed to localize within a specific region of a biological specimen or to respond to a specific analyte.

- Covalent interactions

A covalent fluorescent probe is designed to react with and make covalent attachments to specific chemical residues

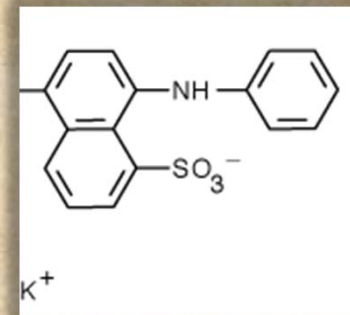
Extrinsic probes

(not present in the natural molecule/macromolecule)

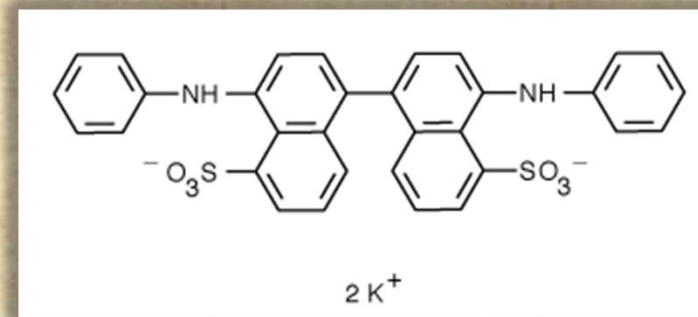
Non-covalent Attachment

Barely fluorescent in pure water but their fluorescence can be strongly enhanced if the environment becomes hydrophobic (hydrophobic patches on proteins)

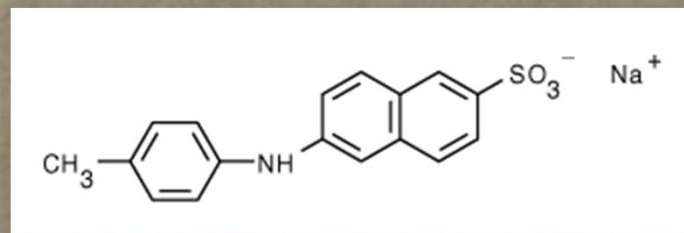
1,8-ANS



bis-ANS



2,6-TNS



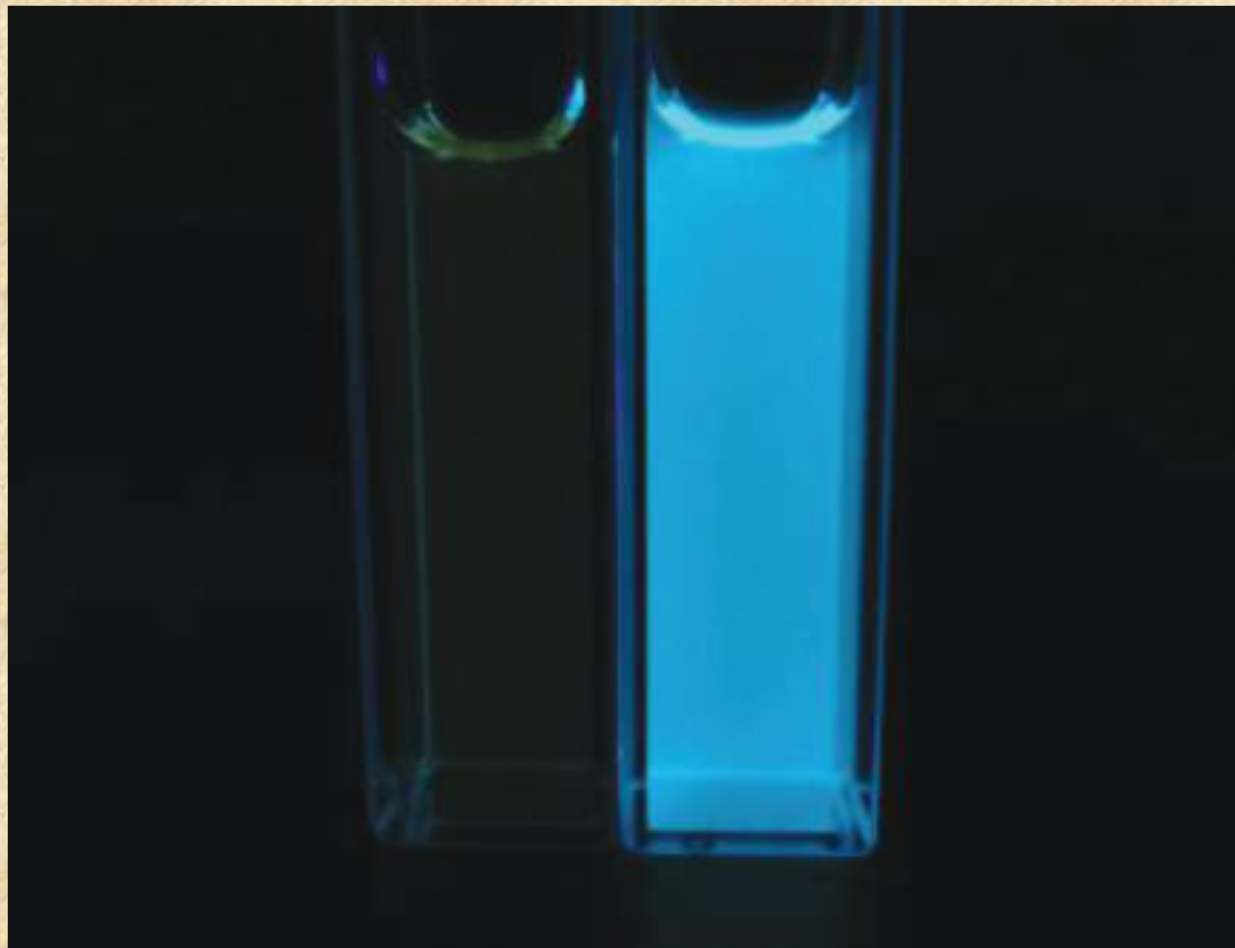
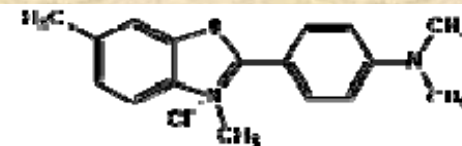


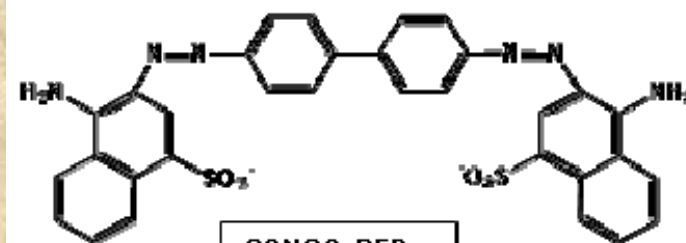
FIGURE 10.14 Solution of ANS in PBS (left) and the same concentration of ANS in PBS after addition of bovine serum albumin (right). Solutions are illuminated using a UV handlamp set for the long wavelength (366 nm).

Other probes, which bind to some proteins noncovalently, include thioflavin T and Congo Red, dyes, which have become extremely popular for following amyloid fiber formation. Thioflavin T exhibits shifts in its excitation and emission spectra and a significant increase in its quantum yield upon binding to amyloid-type protein. When Congo Red interacts with amyloid fibrils, its absorption maximum shifts from about 490 nm to 540 nm.

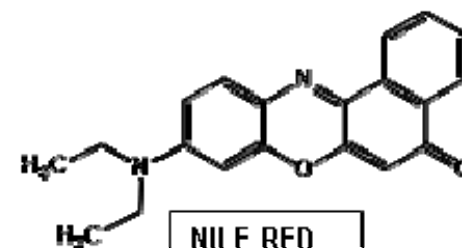
Nile Red, although primarily known as a lipid probe, also binds to hydrophobic regions of some proteins and has been used to study protein aggregation and denaturation.



THIOFLAVIN T

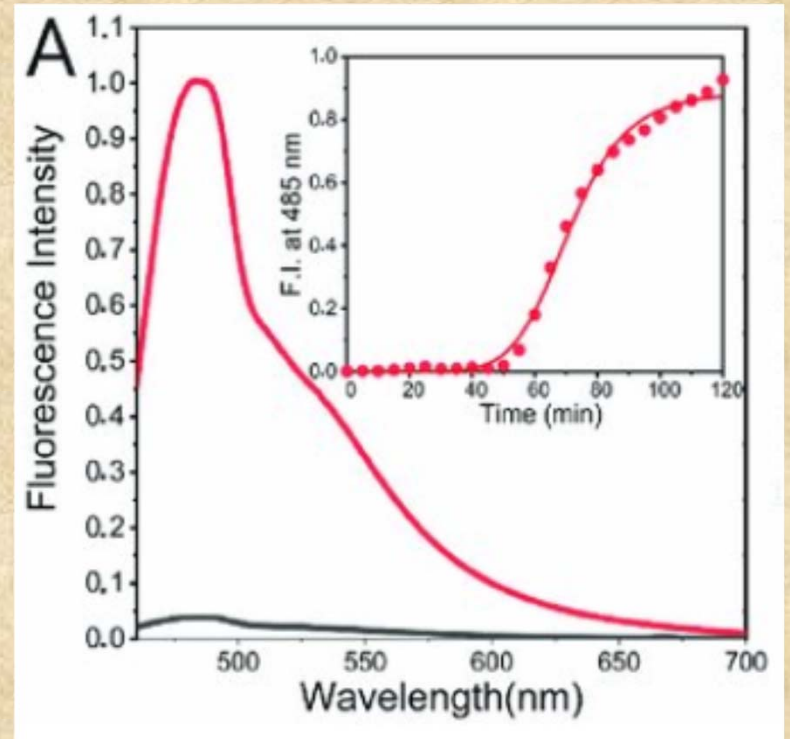
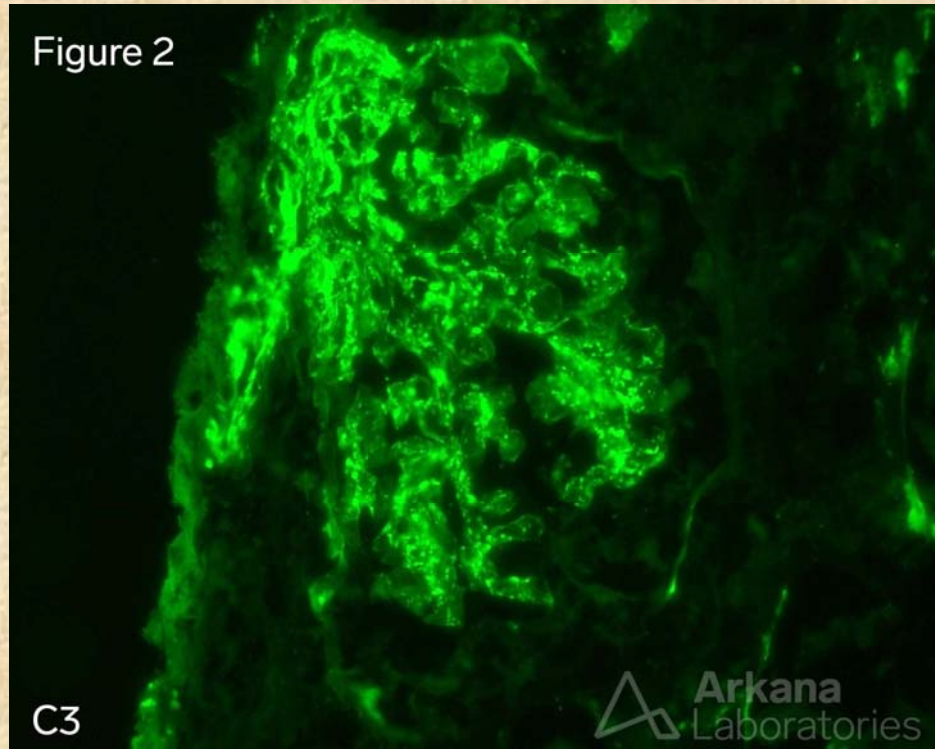


CONGO RED



NILE RED

Thioflavin T



Covalent Attachments

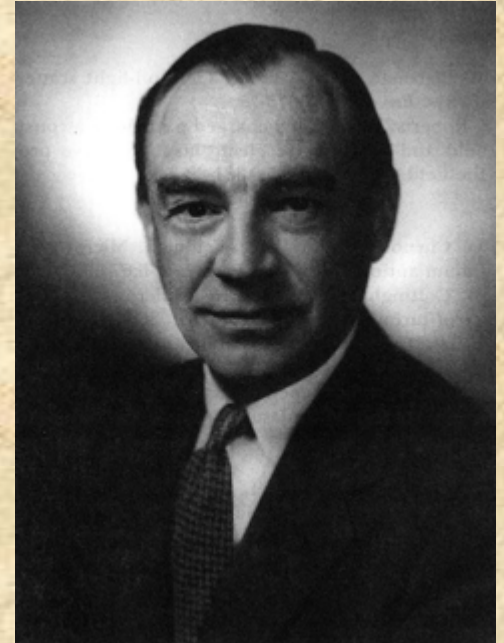
Albert Coons (1941) labeled antibodies with Fluorescein Isocyanate, thus giving birth to the field of immunofluorescence.

Coons, A. H.; Creech, H. J.; Jones, R. N. *Proc. Soc. Exp. Biol. Med.* . 1941, 47, 200.

Riggs et al. first reported FITC, in 1958, which they synthesized to circumvent problems inherent in the isocyanate derivative, including the difficulty of its synthesis and its instability.

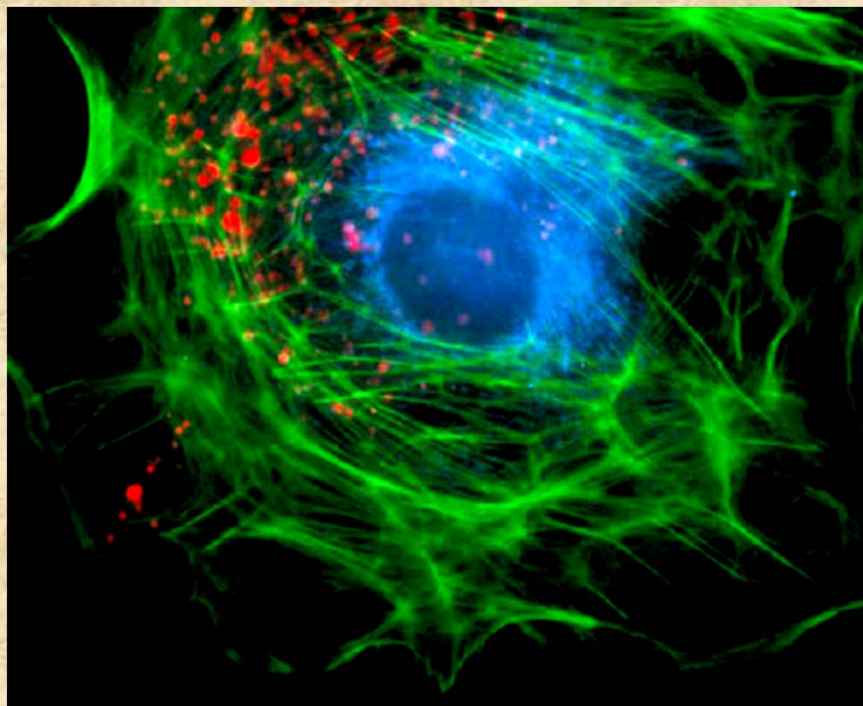
Riggs, J. L.; Seiwald, R. J.; Burckhalter, J. H.; Downs, C. M.; Metcalf, T. G. *Am J Pathol* 1958, 34, 1081-97.

Gregorio Weber (1952) synthesized dansyl chloride for attachment to proteins and used polarization to study protein hydrodynamics - these studies initiated the field of quantitative biological fluorescence.



Covalent Attachments

The Alexa-Fluor series



1999

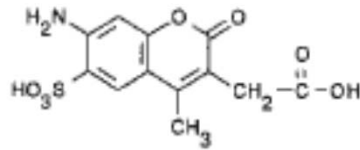
“there is a need for probes with high fluorescence quantum yield and high photostability to allow detection of low-abundance biological structures with great sensitivity and **selectivity**”

The Journal of Histochemistry & Cytochemistry Volume 47(9): 1179–1188, 1999. Molecular Probes, Inc., Eugene, Oregon

Designed to be more photostable than their commonly used spectral analogues

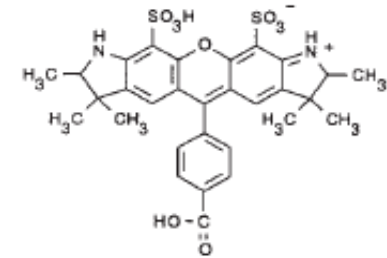
Coumarin-AMCA

Alexa 350 346/442



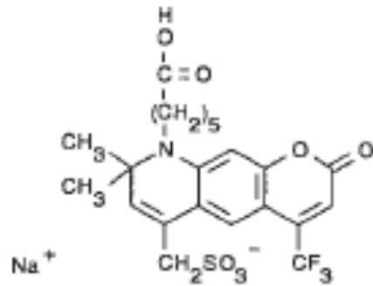
rhodamine 6G

Alexa 532 531/554



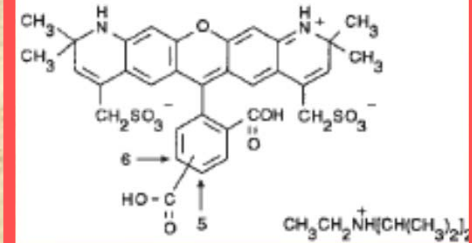
Lucifer Yellow

Alexa 430 434/539



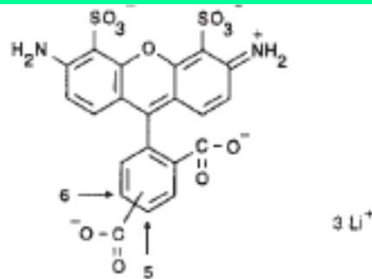
lissamine rhodamine B

Alexa 568 578/603



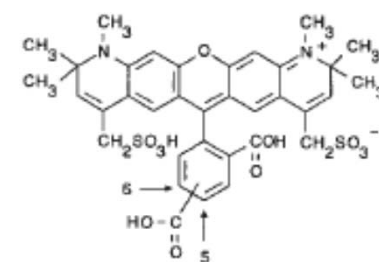
fluorescein

Alexa 488 495/519



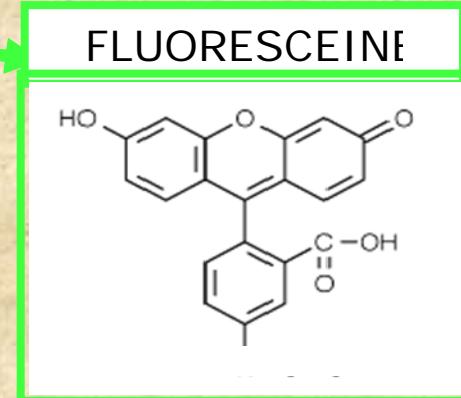
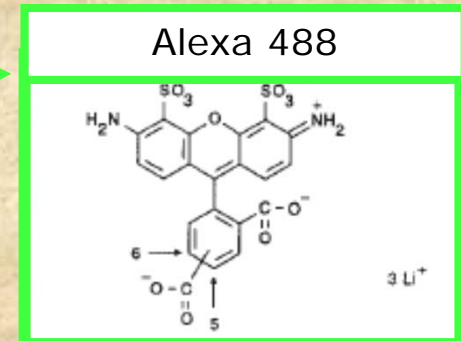
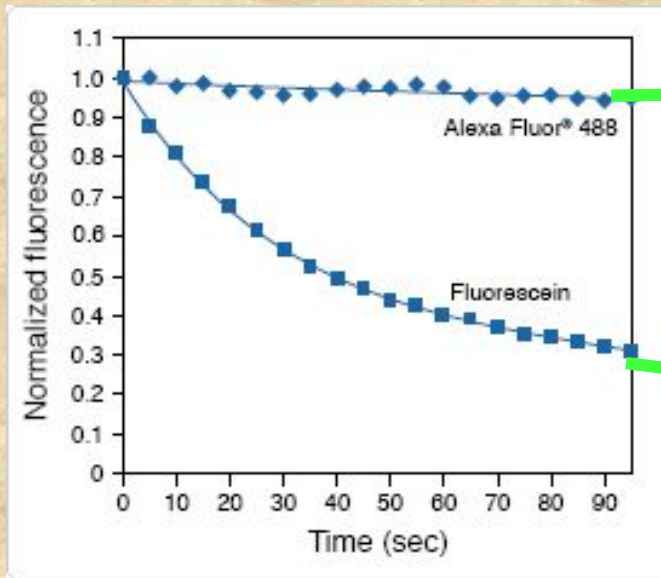
Texas Red

Alexa 594 590/617



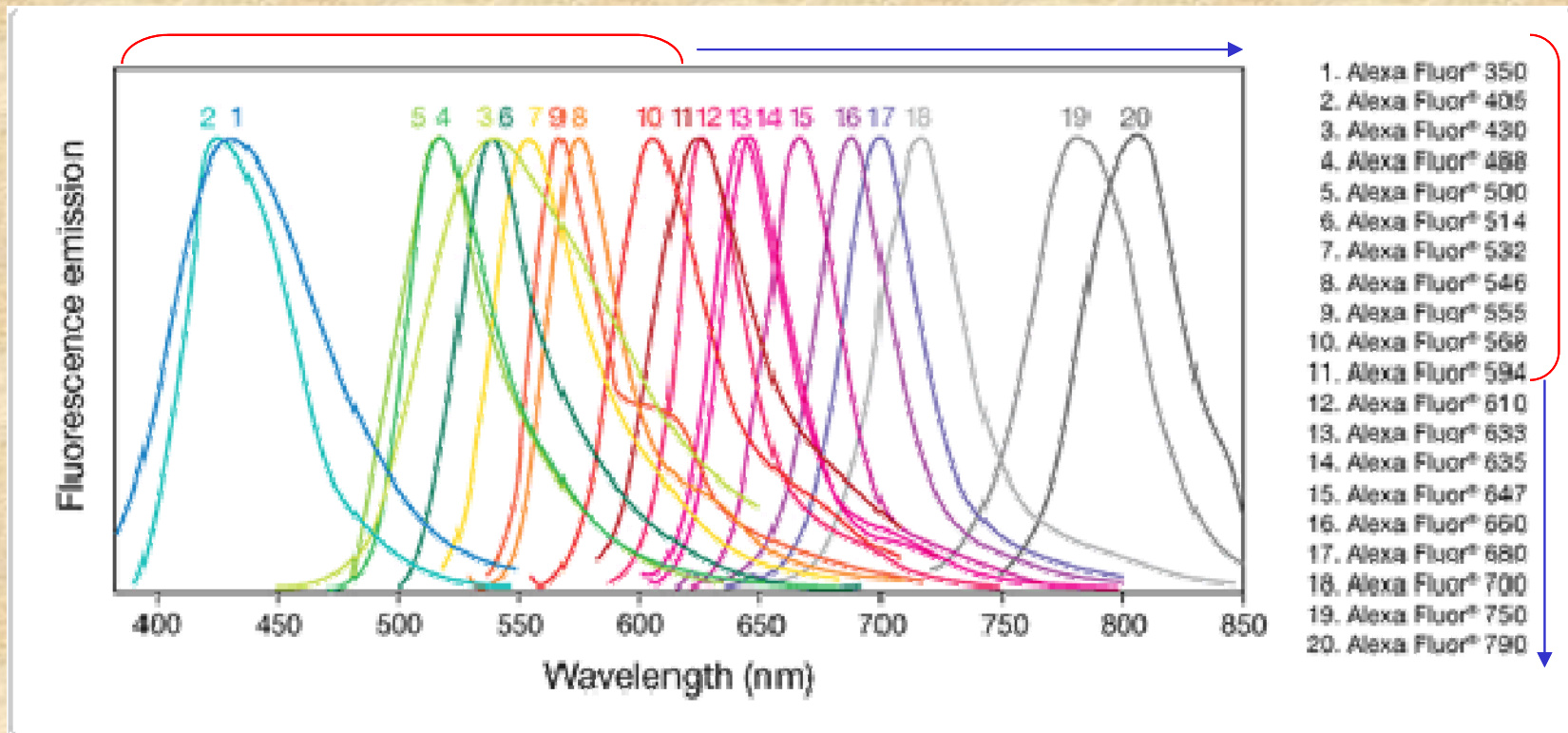
Photostability Alexa Fluor 488 v/s fluorescein

Photo bleaching profile



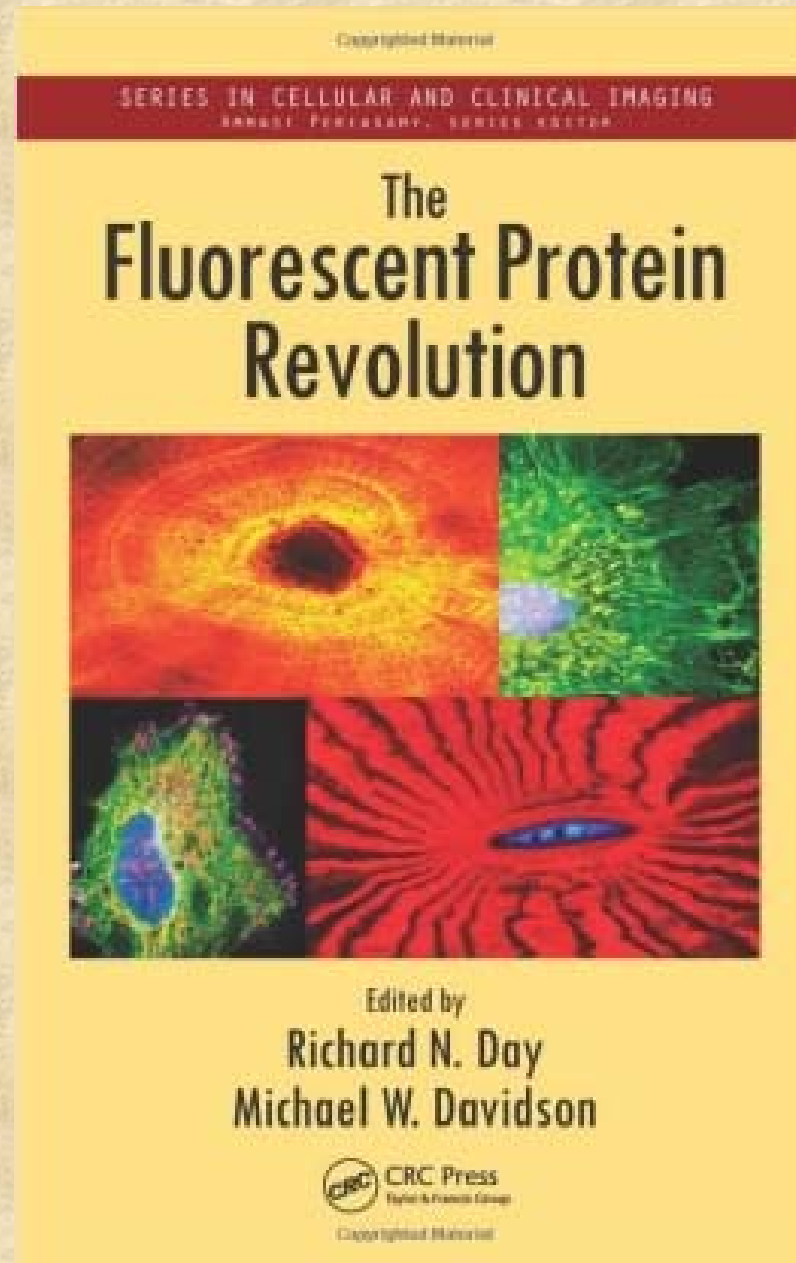
- Cells stained with Alexa Fluor488 or fluorescein conjugates of goat anti–mouse IgG antibody
- Samples were continuously illuminated and images were collected every 5 seconds with a cooled CCD camera.

The Alexa series expanded

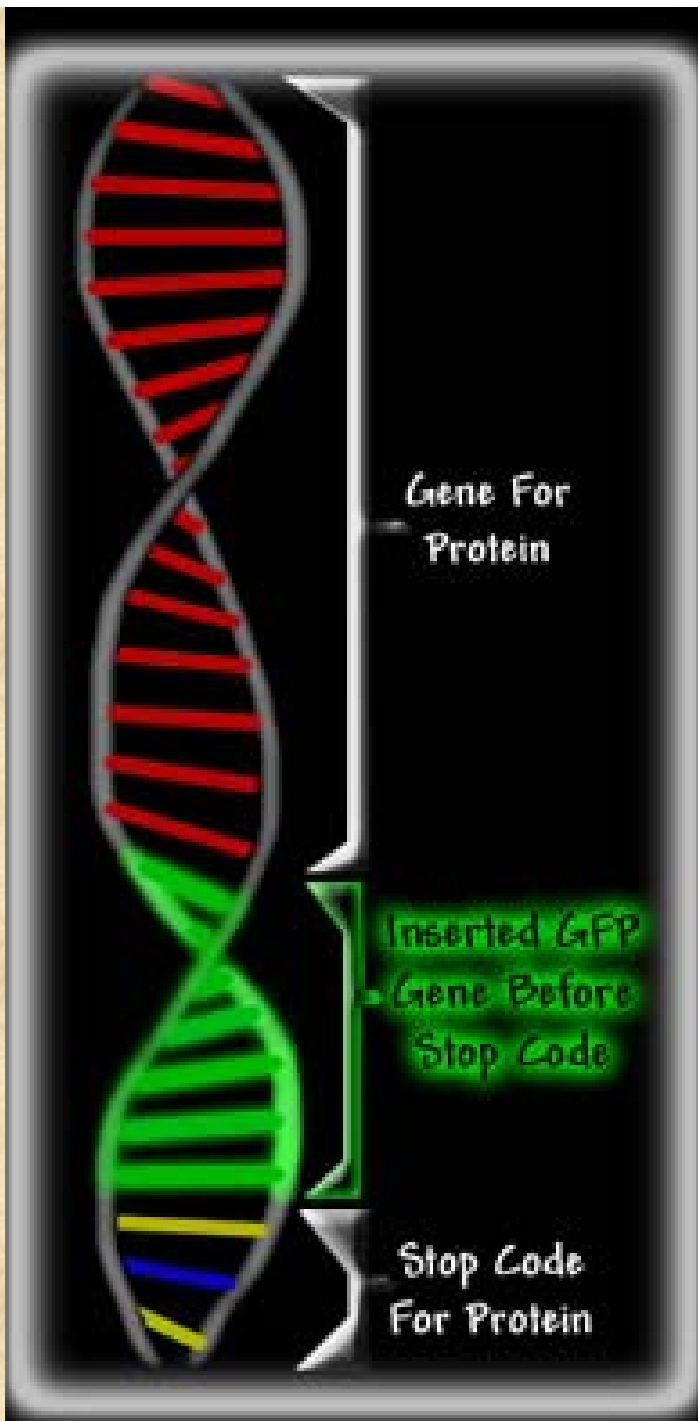


Alexa Fluor dyes are available as amine-reactive succinimidyl esters

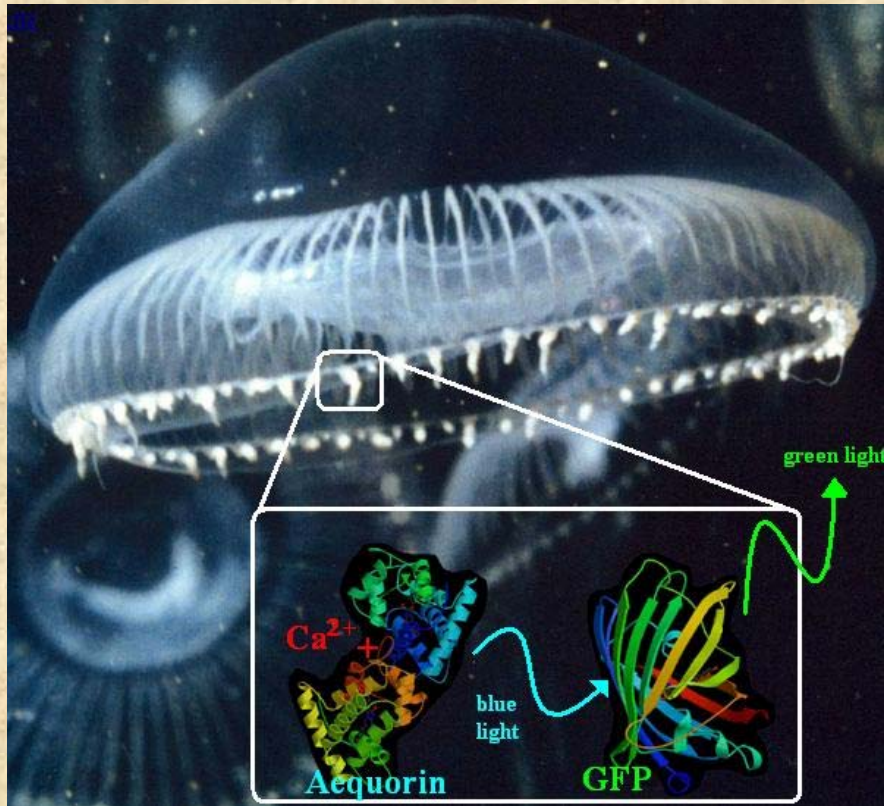
Fluorescent Proteins



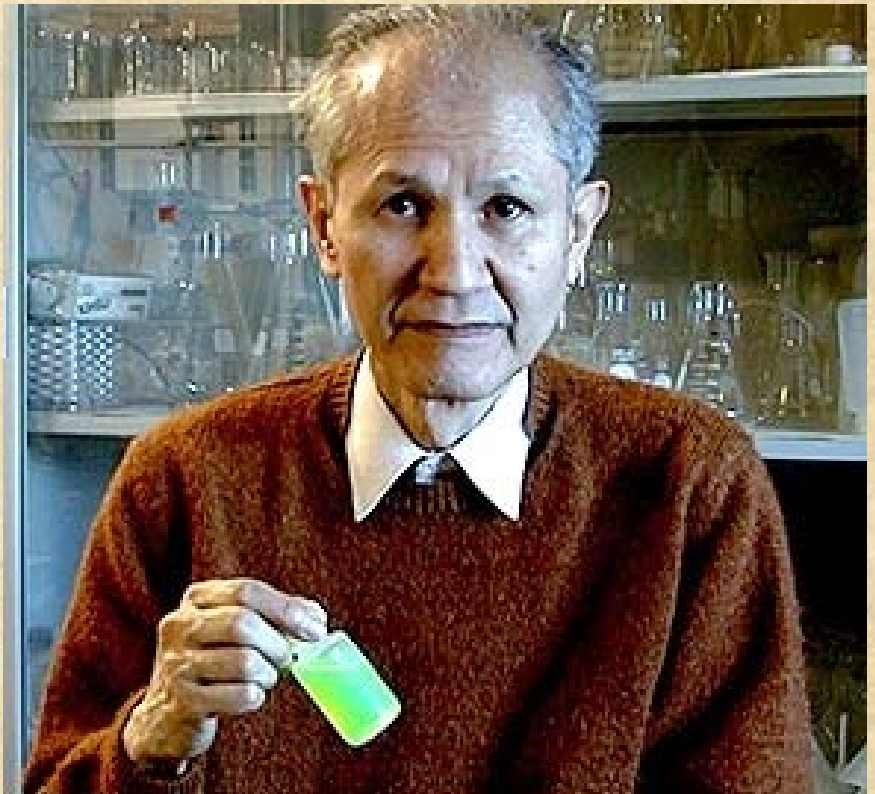
With GFP As Tracer



Green Fluorescent Protein



Aequorea victoria jellyfish



Osamu Shimomura

Shimomura O, Johnson F, Saiga Y (1962). "Extraction, purification and properties of aequorin, a bioluminescent protein from the luminous hydromedusan, *Aequorea*". *J Cell Comp Physiol* 59: 223-39.

Intermolecular Energy Transfer in the Bioluminescent System of *Aequorea*†

Hiroshi Morise, Osamu Shimomura, Frank H. Johnson,* and John Winant

2656 BIOCHEMISTRY, VOL. 13, NO. 12, 1974

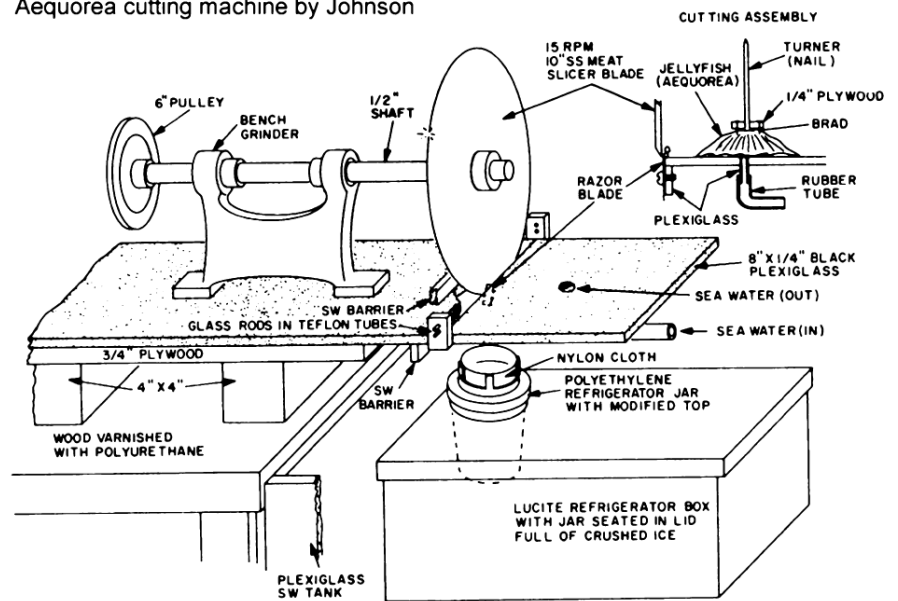
Materials and Methods

Aequorin. The material used in this study was extracted and purified from some 30,000 specimens of *Aequorea*

70 mgs of purified GFP were obtained.
The 30,000 jellyfish weighed about 1.5 tons

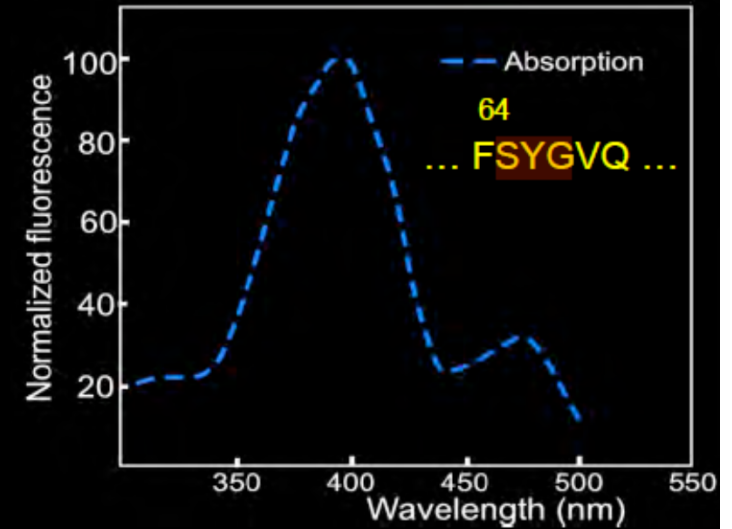
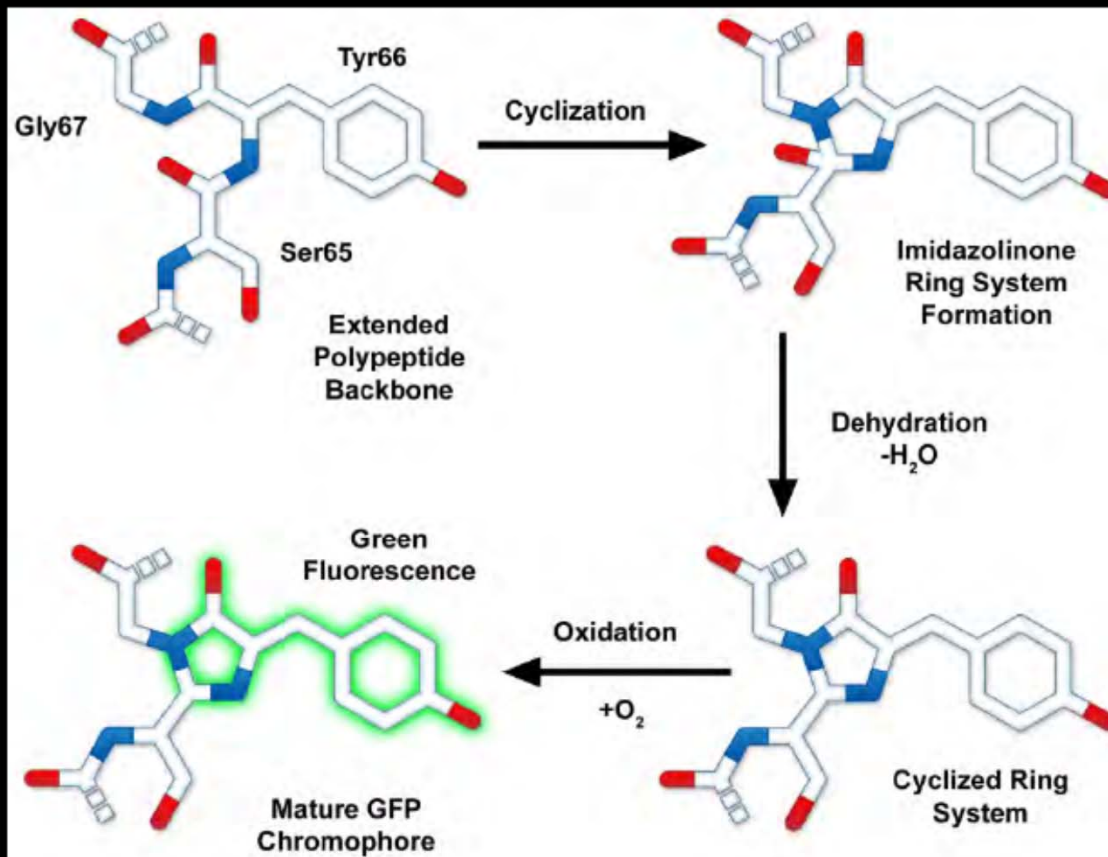
The outer ring of the jellyfish had to be isolated. Initially scissors were used but then a “ring-cutting” machine was built

Aequorea cutting machine by Johnson



General characteristics of GFP

- Using purified GFP, Shimomura showed that a 6 AA fragment was responsible for all light absorption properties.

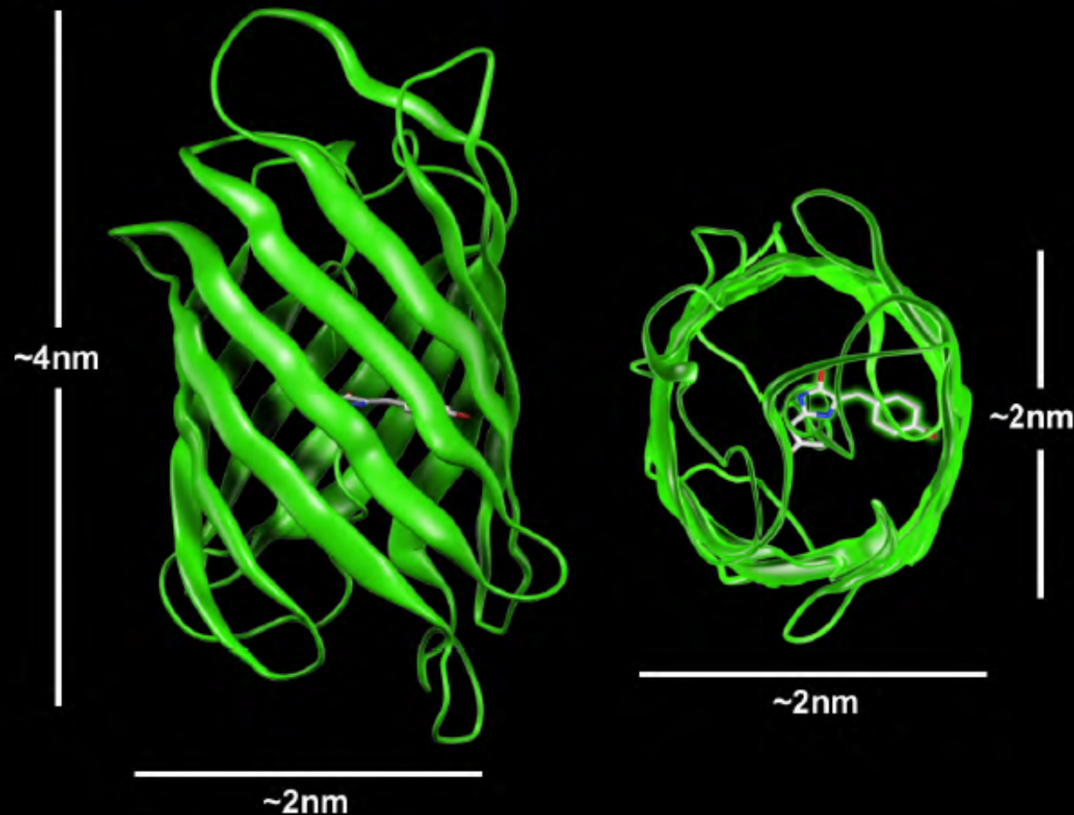


Cody et al. (1993) Biochemistry 32:1212

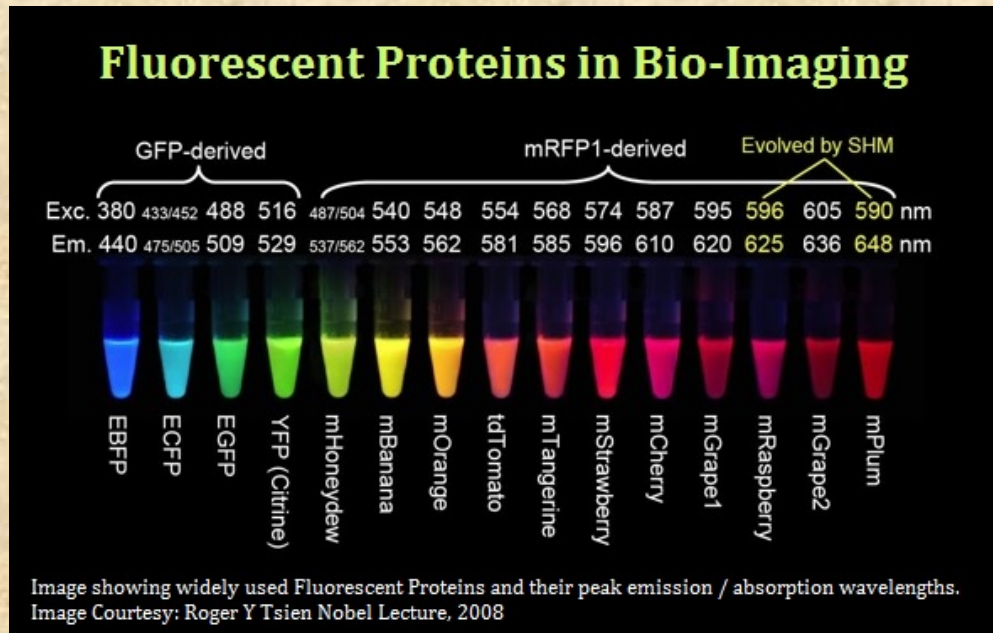
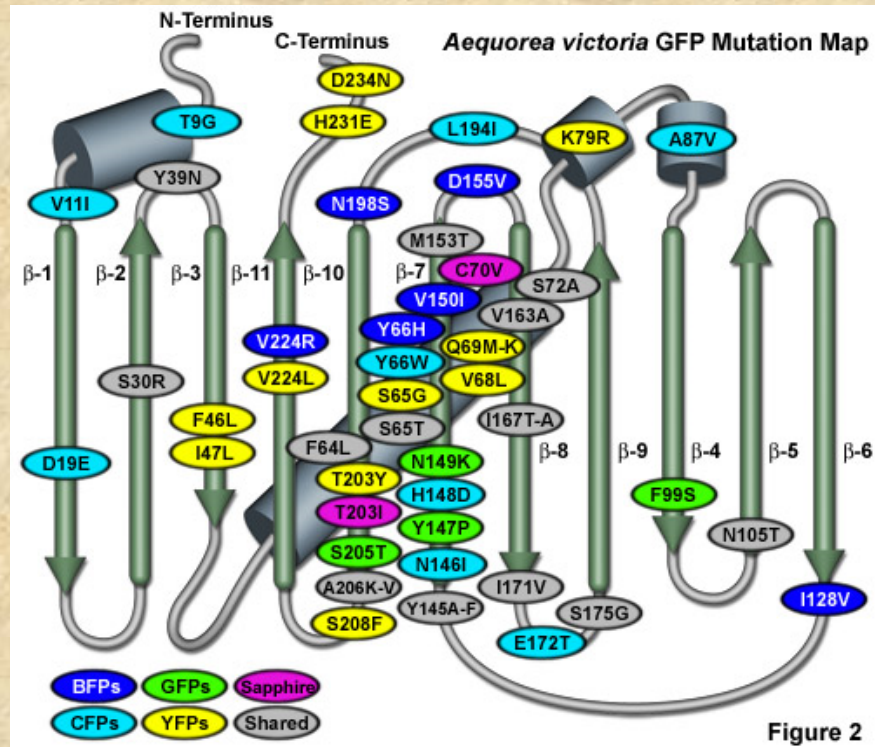
- This led to definition of the chromophore formed by the cyclization of:
-SYG-

General characteristics of GFP

- In 1996, the crystal structure of GFP was solved, showing the cyclic tripeptide buried in the center of an 11-strand β -barrel:



- This explained why the entire protein sequence was required for fluorescence.



Fluorescent Proteins from other marine organisms

14

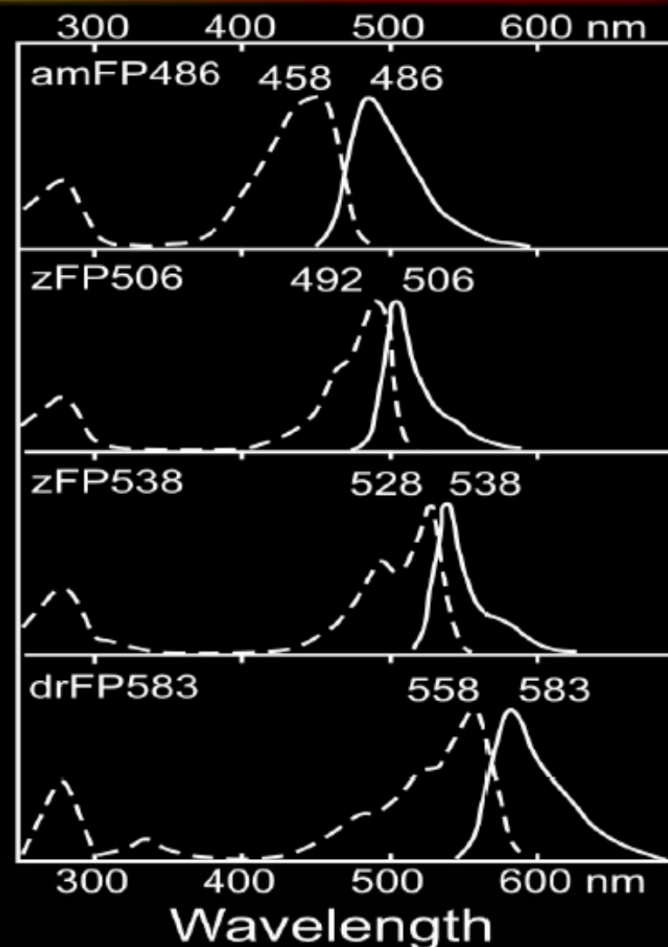
- Most of the colors in reef corals result from GFP-like proteins.



Mushroom anemone *Discosoma striata*

- DsRed from the mushroom anemone was the first of the red FPs, and enabled multicolor imaging in living cells.

Matz et al. (1999) Nat Biotech 17:996



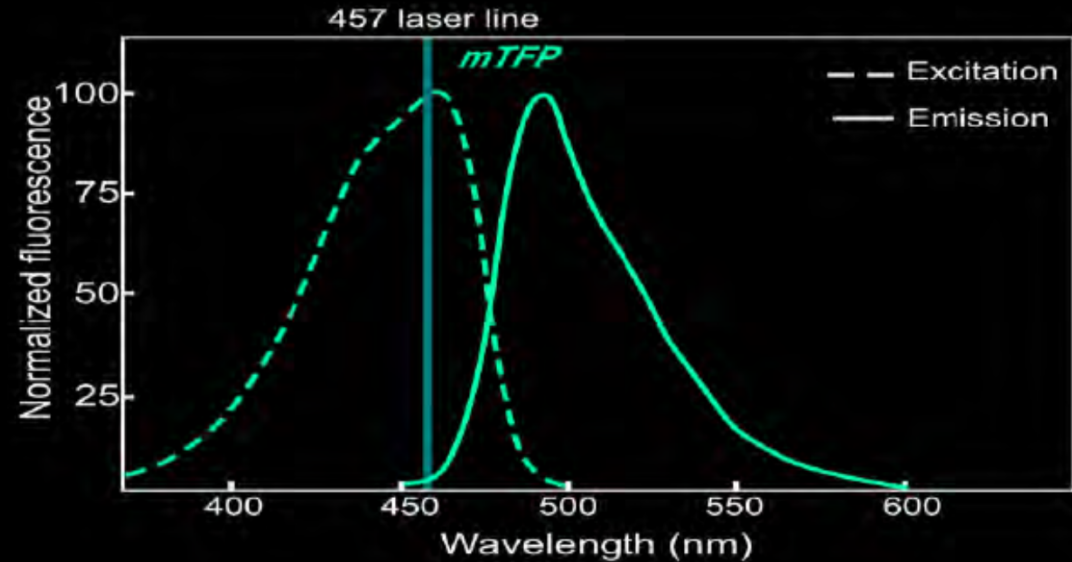
© RNDay_PoFT_2016

The cloning of novel FPs from corals: mTFP1

20



Clavularia sp. "palm coral"



- Directed evolution of cFP484 from *Clavularia* selecting for a bright blue-green (Teal) FP:
- Key mutations mTFP1: Y67; N63T, Q66A, L72F, D125K, M127E, E144D::H163
 - ▶ Ex 462 nm, Em 492 nm, relatively narrow spectra;
 - ▶ intrinsic brightness of 54;
 - ▶ Photostable; acid stable – accumulates in lysosomes.



Ai et al. (2006) *Biochem. J* 400:531

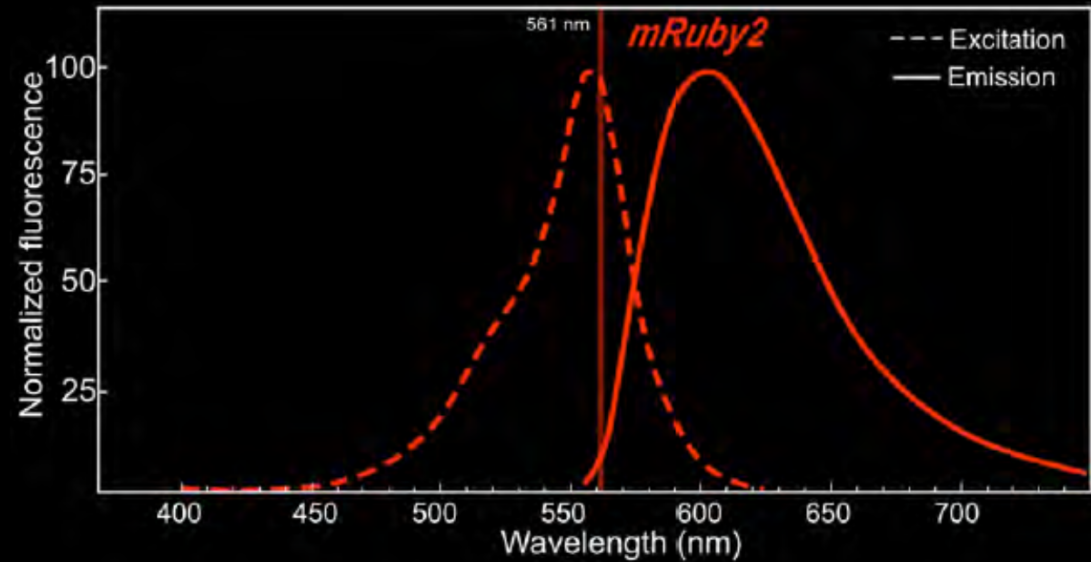
© RNDay_PoFT_2016

The cloning of novel FPs from corals: mRuby2

23



Entacmaea quadricolor anemone



- Directed evolution of the dimeric eqFP611 from *Entacmaea quadricolor* selecting for a bright monomeric Red FP:
- Key mutations: mRuby + L15M, I102V, A119V, A131P
 - Ex 559 nm, Em 600 nm;
 - intrinsic brightness of 43;
 - Maturation 2.5 h, photostable.



Lam et al. (2012) Nat Meth 9:1005

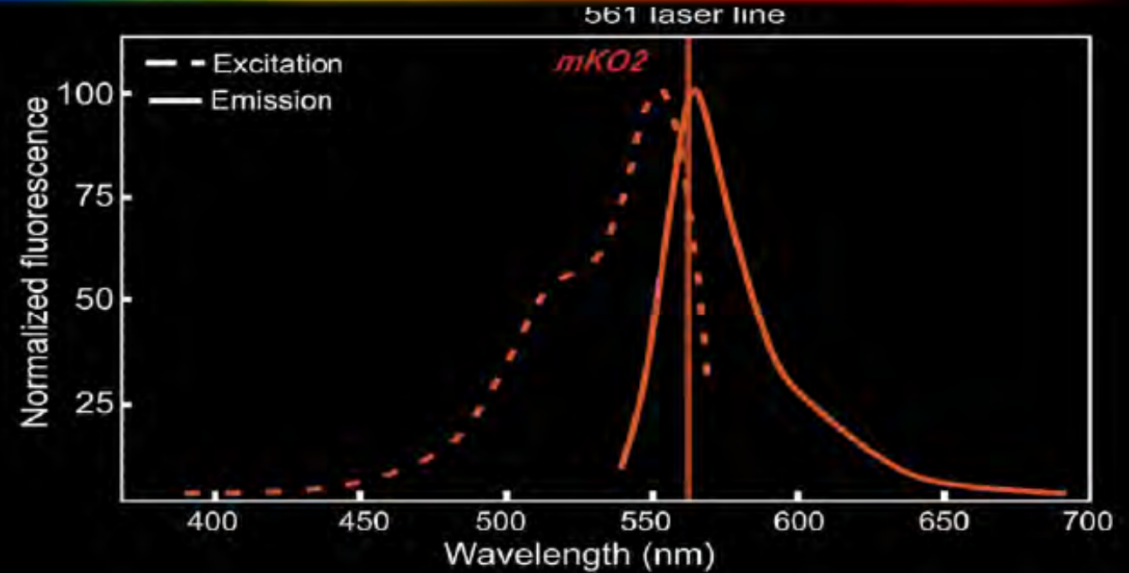
© RNDay_PoFT_2016

The cloning of novel FPs from corals: mKO2

22



Fungia concinna mushroom coral



- Directed evolution of Kusabira orange from *Fungia concinna* selecting for a bright, monomeric orange FP:
- Key mutations: Kusabira + K49E, P70V, F176M, K185E, K188E, S192G, L210Q
 - Ex 551 nm, Em 565 nm;
 - intrinsic brightness of 36;
 - Maturation rapid, photostable - narrow Stokes shift.

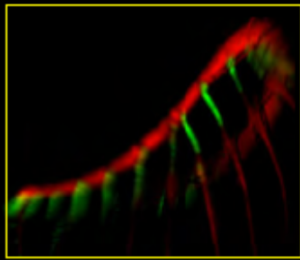


Sakaue-Sawano et al. (2008) Cell 132:487

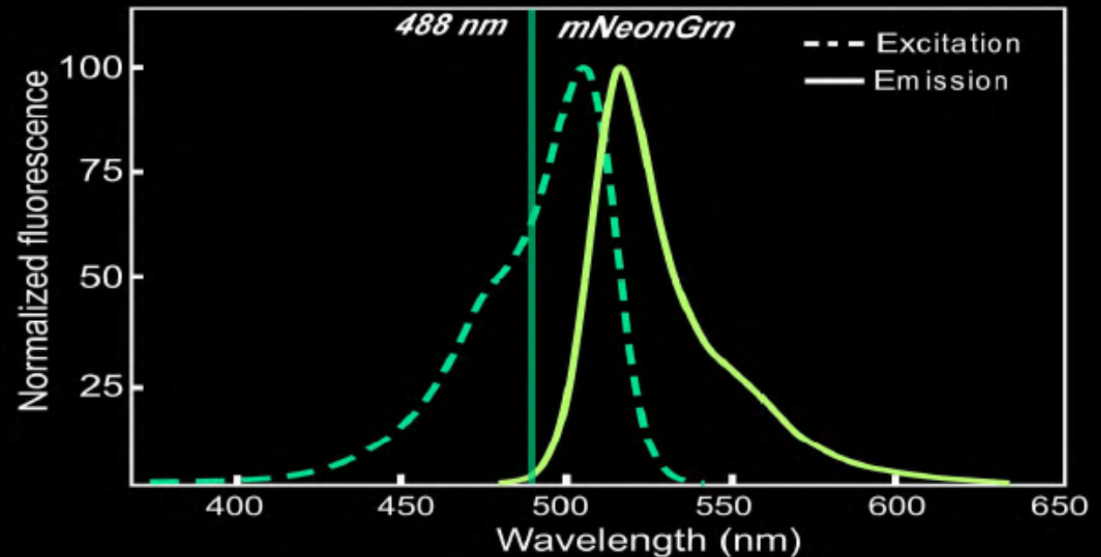
© RNDay_PoFT_2016

The cloning of novel FPs from fish: mNeonGreen

21



Branchiostoma lanceolatum
Lancelet Fish



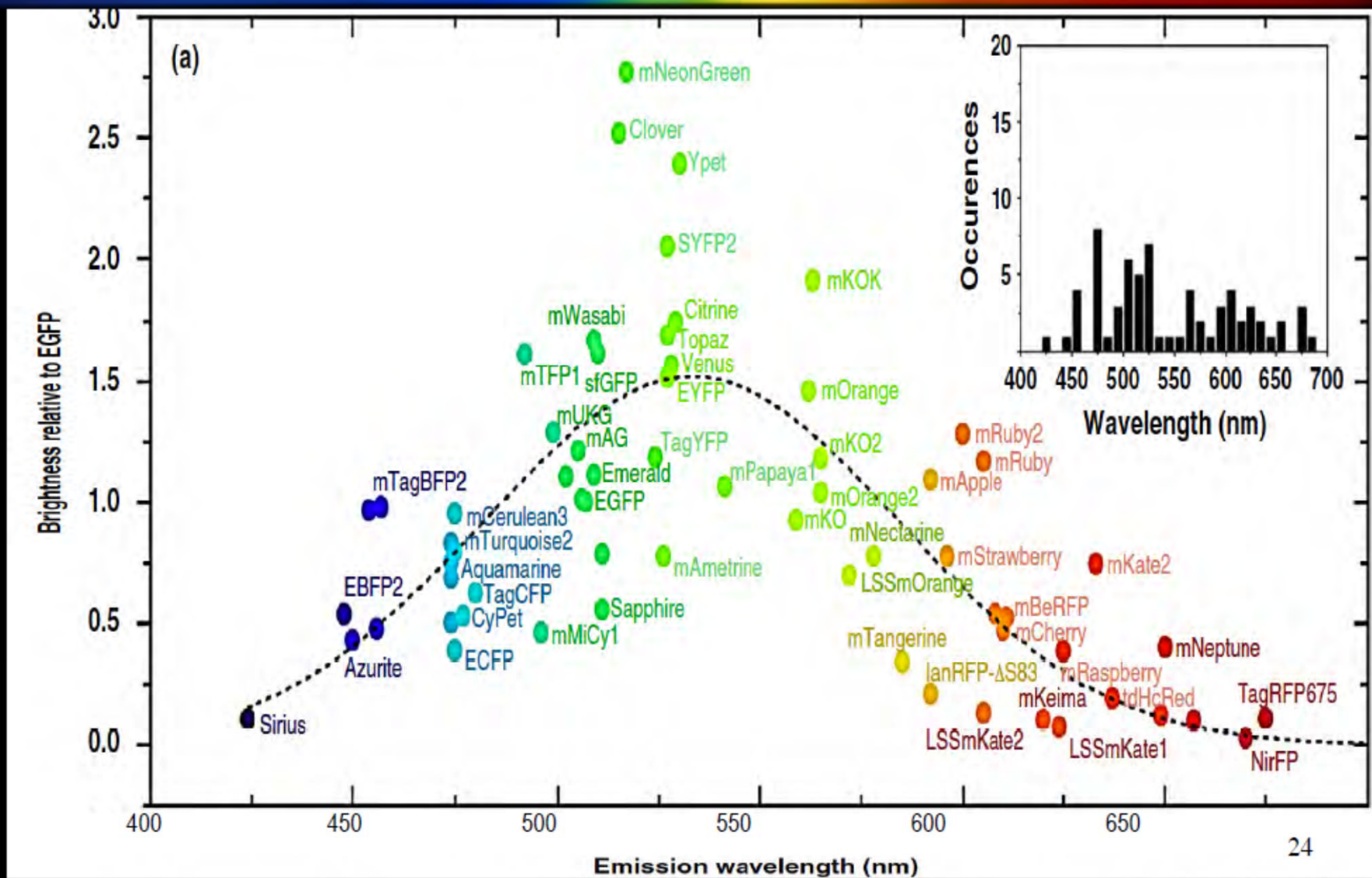
- Directed evolution of dLan YFP from Lancelet fish for a bright, monomeric yellow FP, mNeonGreen:
- Key mutations: Lan YFP + 21 mutations
 - Ex 506 nm, Em 517 nm;
 - intrinsic brightness of **92** ($\epsilon = 115$, QY = 0.80)
 - Maturation rapid, photostable – improvement over Venus.



Baumann et al. (2008) *Bio Direct* 3:28; Shaner et al. (2013) *Nat Meth* 10: 407

© RNDay_PoFT_2016

Summary of the current FPs



Adam et al. (2014) COCB 20:92

© RNDay_PoFT_2016

From Richard Day: ISS Principles of Fluorescence Techniques Course April 2016

How many Fluorescent Proteins are now available?

Hundreds

REVIEW

Open Access

Sea as a color palette: the ecology and evolution of fluorescence



Marie-Lyne Macel, Filomena Ristoratore, Annamaria Locascio, Antonietta Spagnuolo, Paolo Sordino* and Salvatore D'Aniello*

Zoological Letters (2020) 6:9

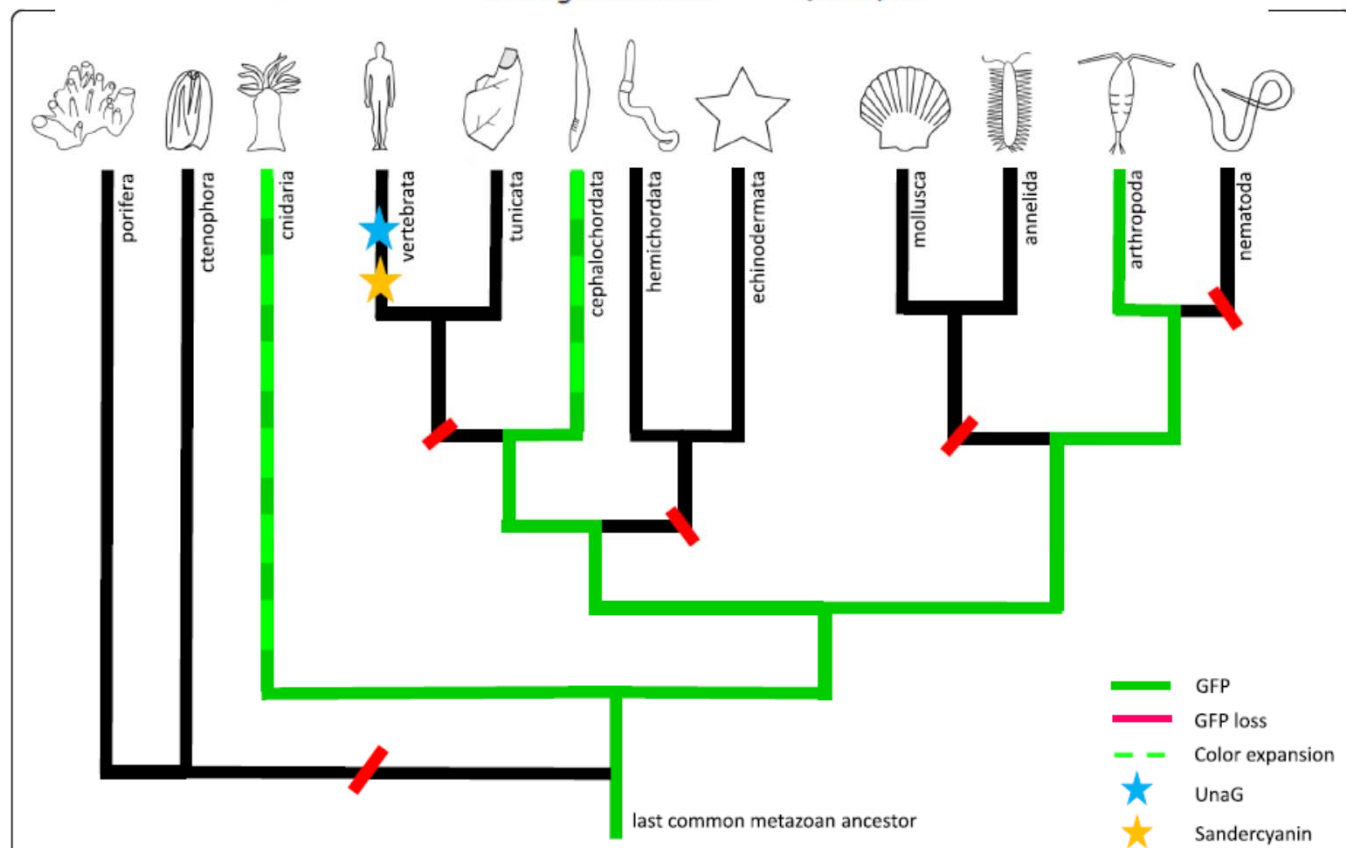


Fig. 2 Distribution of fluorescent proteins in metazoan. Canonical GFPs have been found in cnidarian, arthropods and cephalochordates, supporting the hypothesis of a common metazoan ancestral origin. Color expansion is present in cnidarians and has been recently showed in cephalochordates as well. Furthermore, two other FPs, not related to GFP, have been characterized in vertebrates: UnaG and Sandercyanin

Bimolecular Fluorescence Complementation (BiFC)

Nat Biotechnol. 2003 May ; 21(5): 539–545.

Simultaneous visualization of multiple protein interactions in living cells using multicolor fluorescence complementation analysis

Chang-Deng Hu and Tom K. Kerppola*

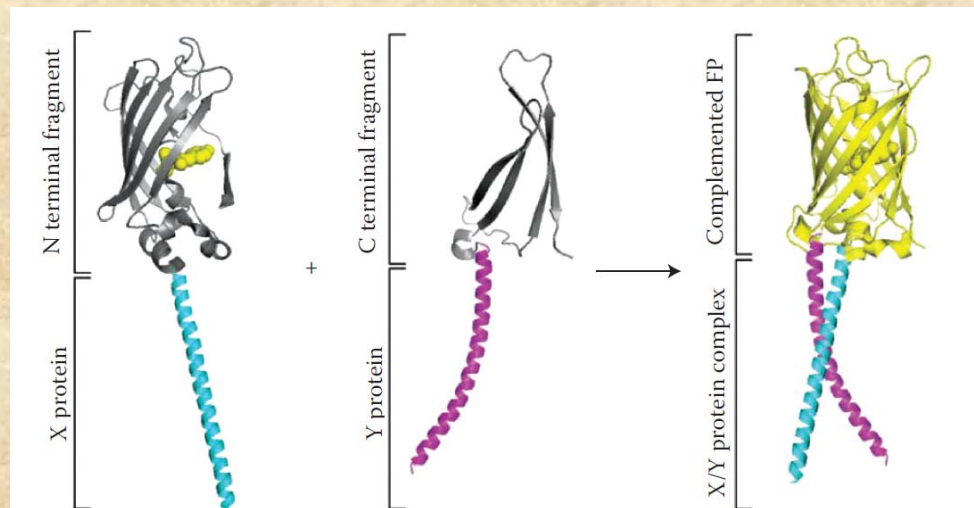
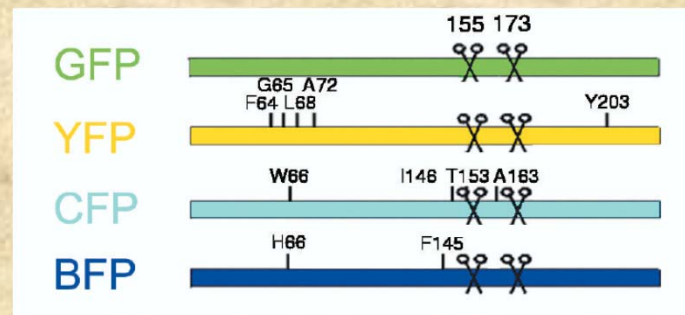


FIGURE 10.62 Illustration of the biomolecular fluorescence complementation method. (From Kodama and Hu (2012) *Biotechniques* 53: 285.)

HALO tags

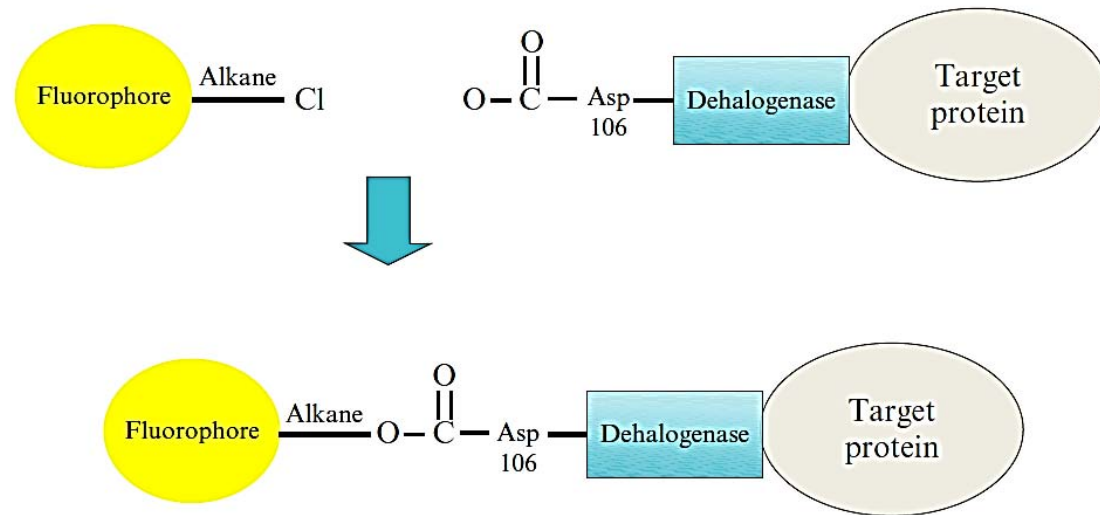


Figure 3.7 Schematic illustrating the principle underlying the HaloTag method. A fluorescent probe is linked to a haloalkane, and the bacterial dehalogenase enzyme is recombinantly fused to the target protein. The fluorescent haloalkane can form a stable covalent linkage with the dehalogenase.

SNAP tags

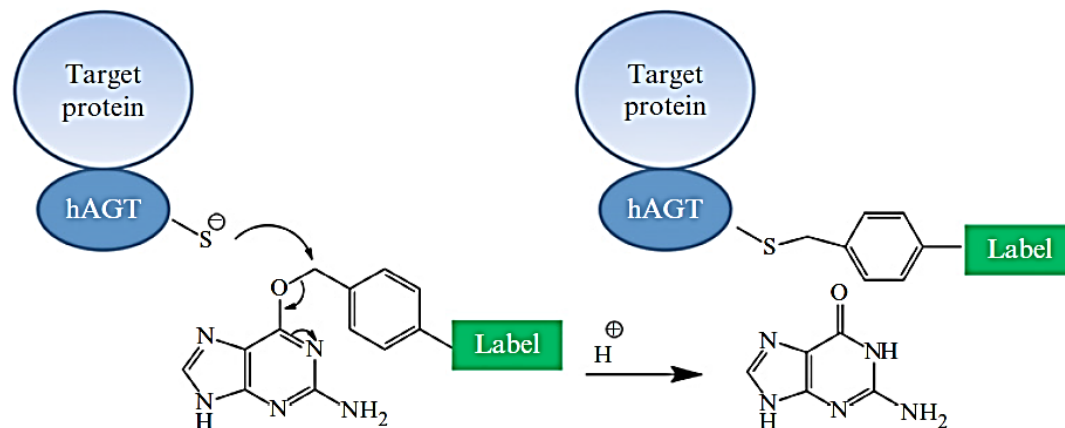
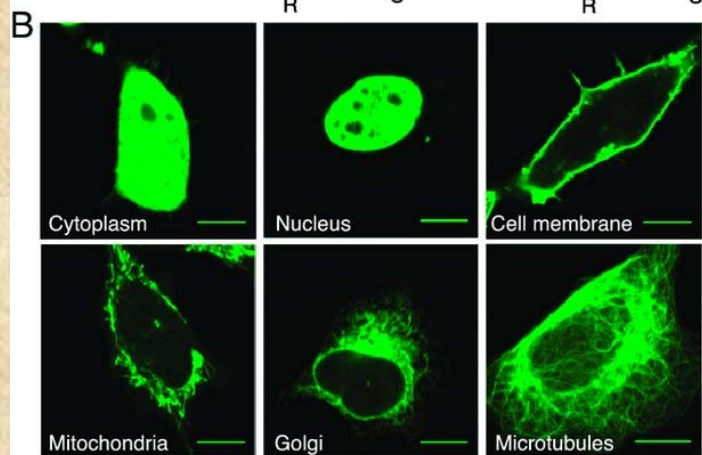
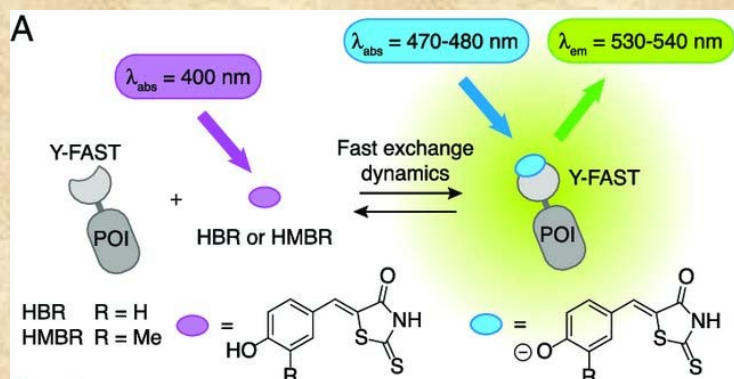


Figure 3.8 Mechanism of covalent labeling of hAGT, which is fused to a target protein, with a fluorescent label linked onto an O⁶-benzylguanine derivative. *Figure modified from Keppler et al. (2003).*

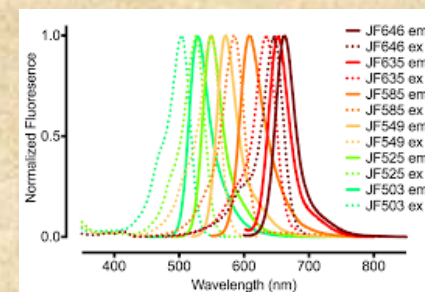
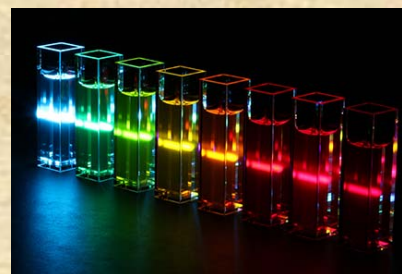
Fluorogen and Janelia Fluor dyes

Arnaud Gautier



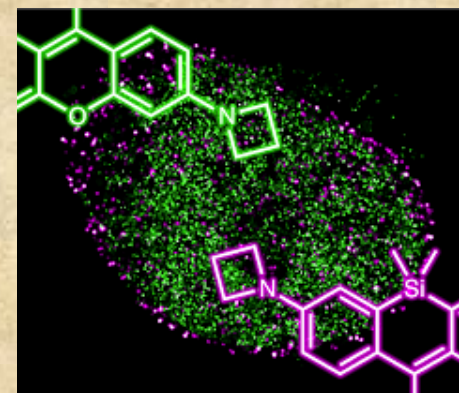
https://www.researchgate.net/publication/288685315_Small_fluorescence-activating_and_absorption-shifting_tag_for_tunable_protein_imaging_in_vivo

Luke Lavis



dye ^a	X	λ_{max} (nm)	ϵ ($M^{-1}cm^{-1}$)	λ_{em} (nm)	ϕ
1, JF ₅₄₉	O	549	101,000	571	0.88
2, JF ₆₄₆	Si(CH ₃) ₂	646	152,000 ^b	664	0.54

^aAll properties taken in 10 mM HEPES, pH 7.3 unless noted
^bMeasurement taken in EtOH containing 0.1% v/v TFA



Protein Labeling

Targeting amino groups

Fluorescent group

Reactive group

+

Reactive group

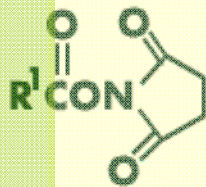
aa



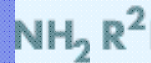
isothiocyanate:



succinimidyl ester:

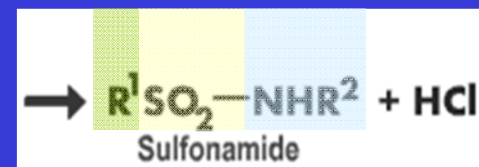
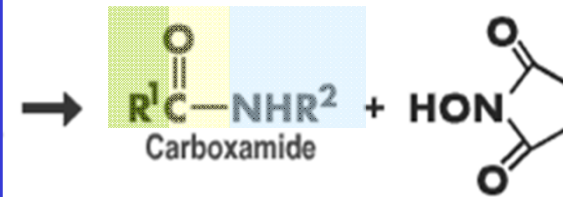
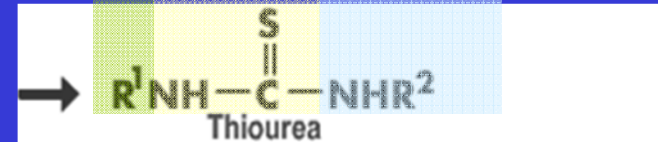


+



Lysine

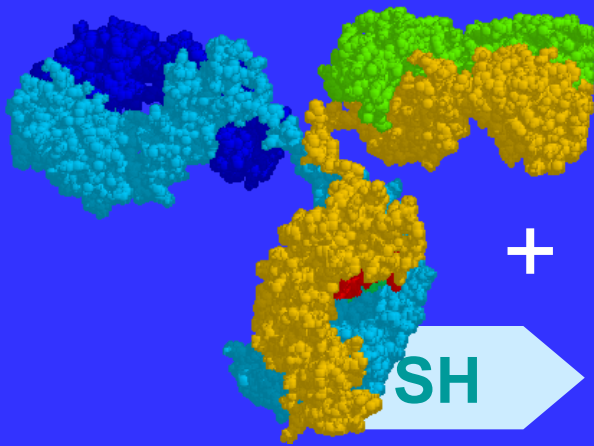
sulfonyl chloride:



Note: To label lysine residues the pH of the solution should be alkaline since the pKa of the amino group is ~9.

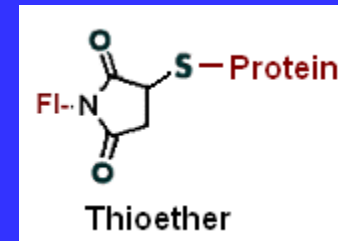
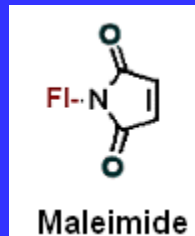
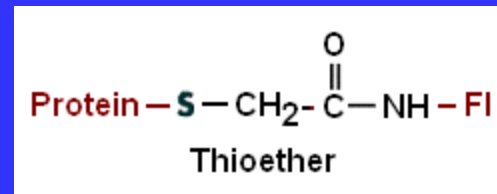
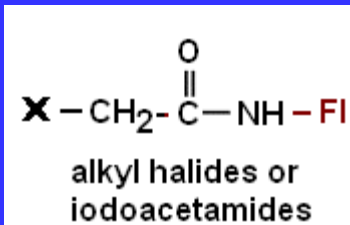
Protein Labeling

Thiol-Modification:



Protein-SH
Cysteine

+



Click Chemistry

In recent years, the method known as “click chemistry,” developed largely by K. Barry Sharpless, has been recognized as an important advance in synthetic organic chemistry, and is now being used in the attachment of fluorophores to target molecules. Click chemistry relies on an azide–alkyne Huisgen cycloaddition reaction, the most popular being a copper (I)-catalyzed azide–alkyne cycloaddition. Basically, an azide and an alkyne react to form a triazole, which forms a stable covalent bond, as illustrated in **Figure 10.21**. Click chemistry “ready” fluorescent reagents are now available commercially (see, e.g., www.setabiomedicals.com, www.jenabioscience.com, and www.activemotif.com).

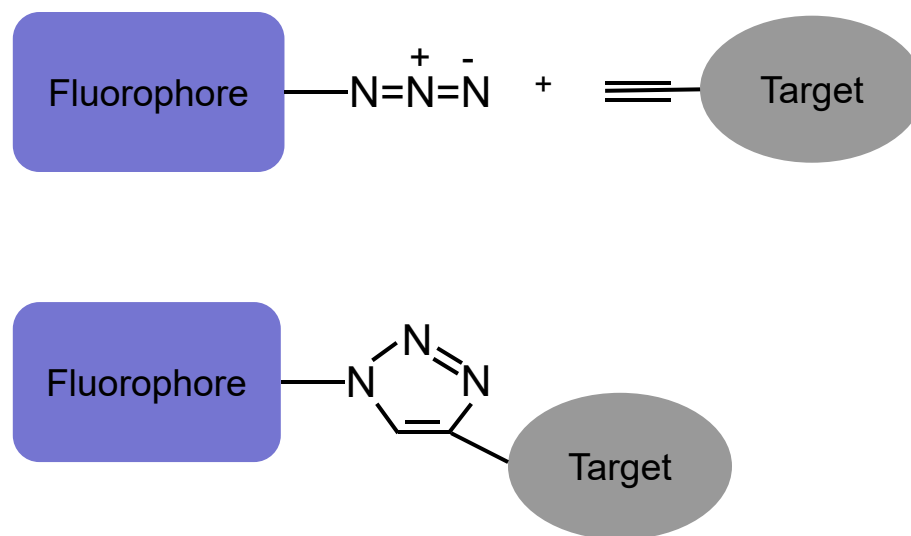


FIGURE 10.21 Example of a click chemistry reaction.

Photoaffinity Labeling

Affinity labels are reagents specifically designed to bind with high affinity to a biomolecule, for example, a protein, nucleic acid, or membrane. They are often analogs of substrates or inhibitors. The photoactivatable moiety is typically an azide group or a benzophenone, although other chemistries are available. A useful design is shown in **Figure 10.22**, which comprises a fluorescent moiety (fluorescein), a photoactivatable moiety (aryldiazirine) and an affinity ligand (a sidechain portion of alyronine A). Such photoaffinity reactions are typically carried out using UV illumination, often from the 366 nm line of a standard UV handlamp.

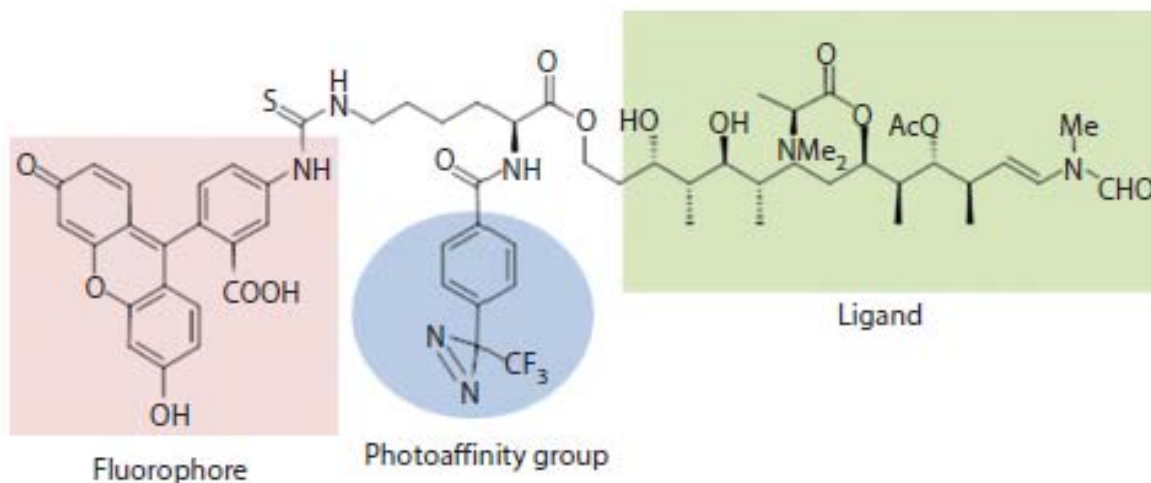
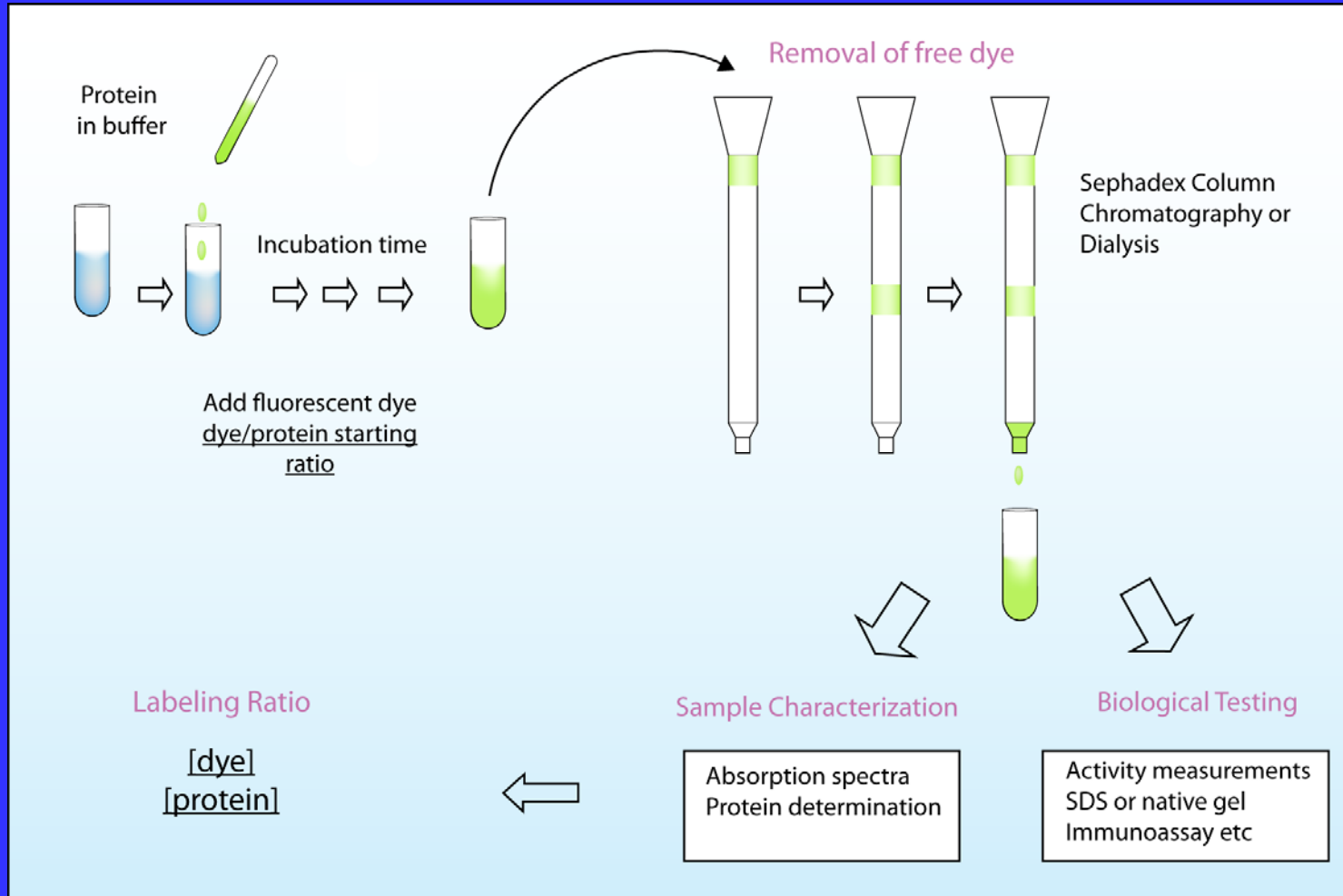
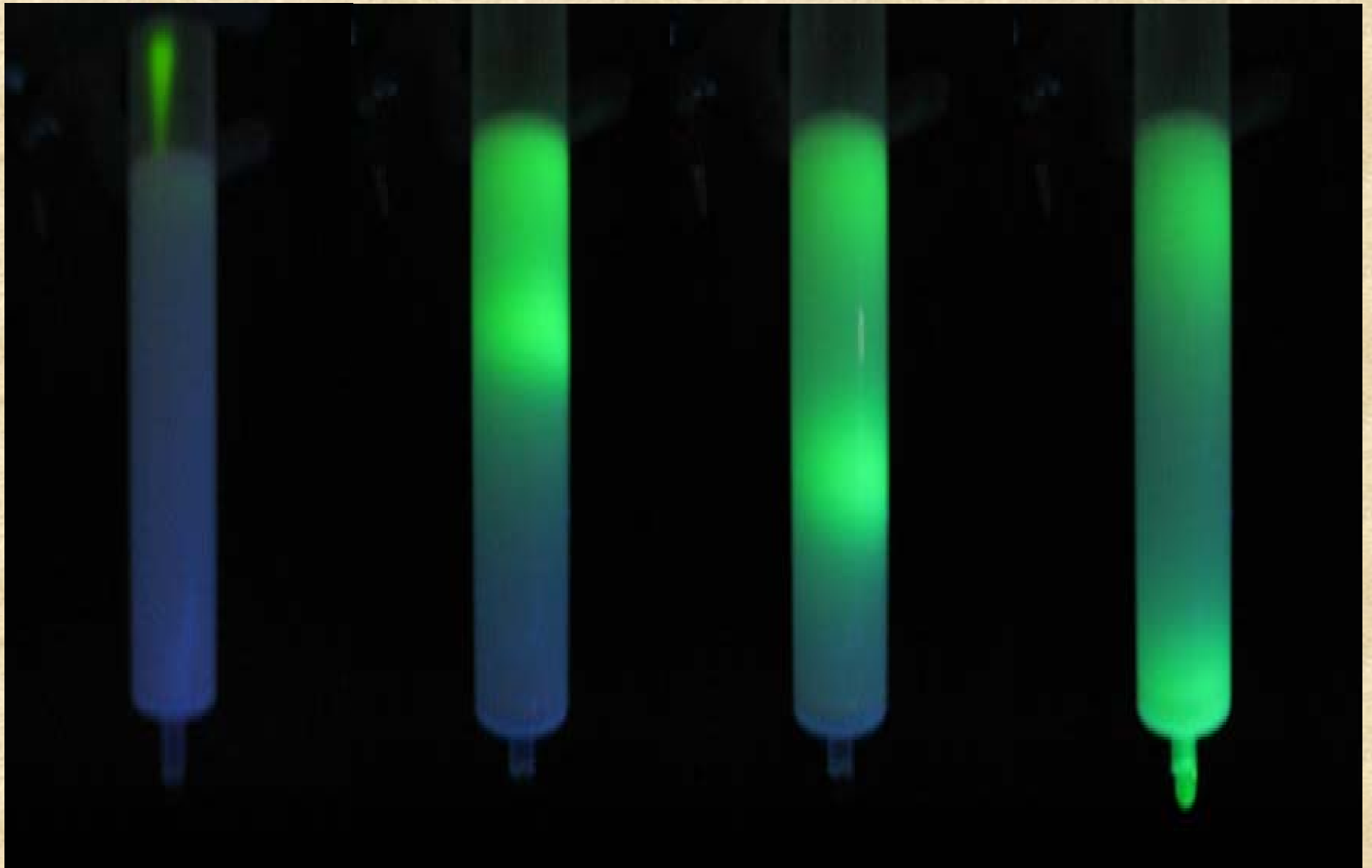


FIGURE 10.22 Example of a photoactivatable probe comprising a fluorescent moiety (fluorescein), a photoactivatable moiety (aryldiazirine) and an affinity ligand (a sidechain portion of alyronine A). (Modified from Kuroda et al., 2006. *Bioconjugate Chem.* 17: 524.)

Labeling Procedure

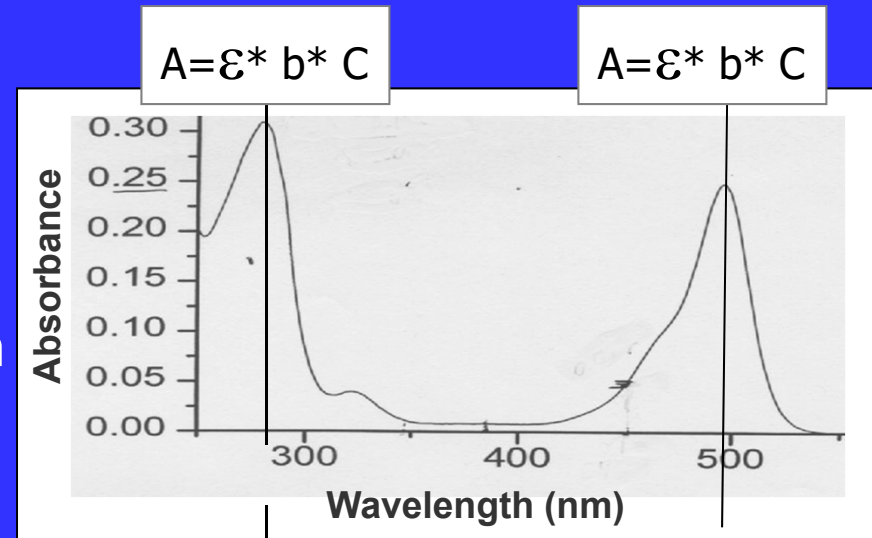




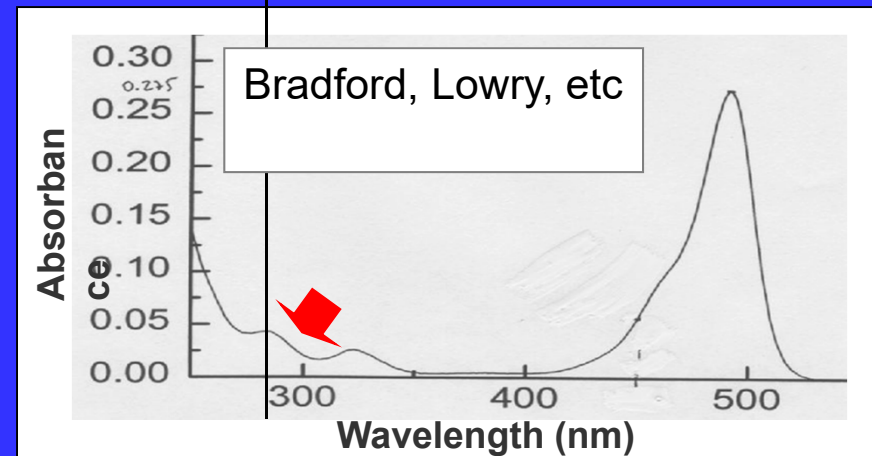
Characterization after the labeling



Protein-
Fluorescein



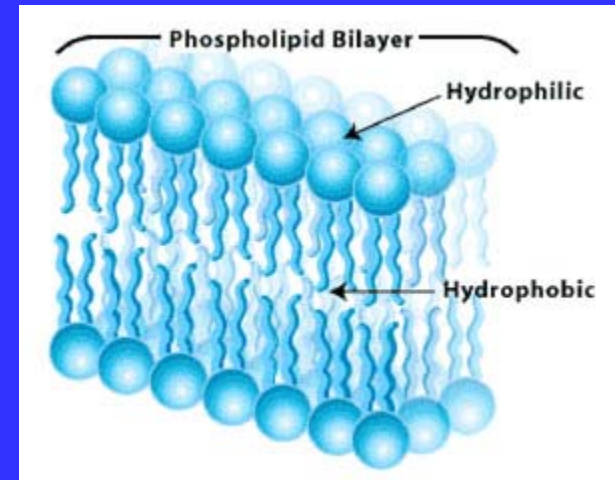
Fluorescein



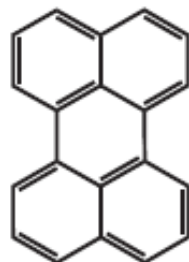
Labeling should not
change the biological
activity of the
protein.

Labeling membranes

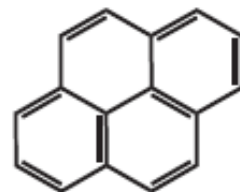
- **Analogs of fatty acids and phospholipids**
- **Di-alkyl-carbocyanine and Di-alkyl-aminostyryl probes.**
- **Other nonpolar and amphiphilic probes.**
DPH, Laurdan, Prodan, Bis ANS



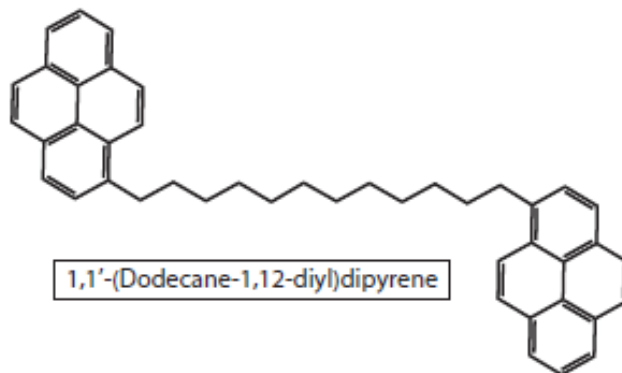
Membrane Probes



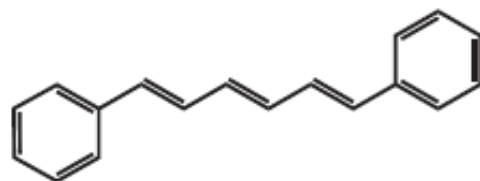
Perylene



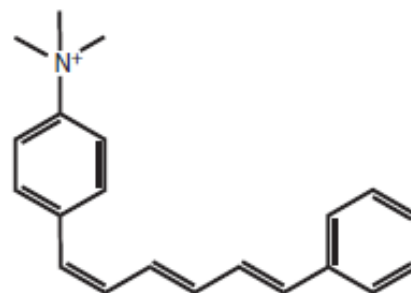
Pyrene



1,1'-(Dodecane-1,12-diyl)dipyrene



DPH



TMA-DPH

FIGURE 10.25 Structures of various membrane probes.

Dynamics of the Hydrocarbon Layer in Liposomes of Lecithin and Sphingomyelin Containing Dicetylphosphate*

(Received for publication, September 12, 1973)

MEIR SHINITZKY AND YECHESKEL BARENHOLZ

From the Department of Biophysics, The Weizmann Institute of Science, Rehovot, Israel, and the Department of Biochemistry, The Hebrew University-Hadassah Medical School, Jerusalem, Israel

SUMMARY

Physical properties of the hydrocarbon region in lipid bilayers were studied in a series of liposomes of lecithin and sphingomyelin containing different concentrations of dicetylphosphate. The technique used was described previously and is based on fluorescence polarization analysis of a specific probe embedded in the analyzed region. The two probes employed in this study were perylene and 1,6-diphenyl-1,3,5-hexatriene, which simulate a rotating disc and a rotating rod, respectively. The determined dynamic properties of the hydrocarbon region in the lecithin liposomes differ markedly from those of the sphingomyelin liposomes. The hydrocarbon region of the lecithin liposomes is of an invariant phase between 0° and 60° characterized by a microviscosity at 25°, $\bar{\eta}$ (25°), of 0.8 ± 0.1 poise and a fusion activation energy, ΔE , of 8 ± 2 Cal per mole. In contradistinction to lecithin, the hydrocarbon region of the sphingomyelin liposomes displays a distinct phase transition at $32^\circ \pm 2^\circ$. The phase at temperatures above the transition point, presumably a liquid crystalline phase, is characterized by $\Delta E = 16 \pm 4$ Cal per mole, whereas the phase below it, presumably a gel state, possesses a ΔE value lower than 3 Cal per mole. In addition to that, the hydrocarbon layer in sphingomyelin liposomes is much more viscous than in lecithin liposomes as shown by $\bar{\eta}$ (25°) = 6 ± 1 poise. All of the above characteristics are only slightly and irregularly affected by the presence of dicetylphosphate, despite the strong effects it exerts on the surface charge potential of the liposomes. This indicates that the forces which dictate the dynamic properties of the hydrocarbon region in lipid bilayers predominantly originate from hydrophobic interactions.

different and specific value for each mammalian species. In some membranes this ratio changes drastically with age (1, 2).

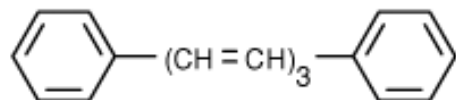
The molecular structure of sphingomyelin and lecithin can be separated into two distinct regions: the hydrophilic region, which contains the phosphorylcholine moiety in both lipids, and the hydrophobic region, which contains the hydrocarbon chains. In addition to the phosphorylcholine group, the polar region of lecithin contains two ester bonds, whereas that of sphingomyelin contains an amide bond, an hydroxyl group, and a *trans* double bond. These groups result in difference in the net dipole moment and in the ability to form hydrogen bonds (3, 4). In the hydrophobic region the average length of the hydrocarbon chains in lecithin is shorter and the degree of unsaturation is greater than in sphingomyelin (1). The special nature of these regions in sphingomyelin and lecithin is therefore expected to exert specific effects on structure and dynamics of lipid layers.

In this study, structure and dynamic properties of sonicated liposomes, made of sphingomyelin or lecithin containing dicetylphosphate, were investigated. The method employed was described previously (5, 6) and is based on determination of fluorescence polarization of a hydrocarbon probe and translating it into microviscosity, $\bar{\eta}$, which is obtained in absolute macroscopic units (*e.g.* poise). From the temperature profile of $\bar{\eta}$ phase transitions were detected and the fusion activation energies, ΔE , of each phase were determined (5, 6).

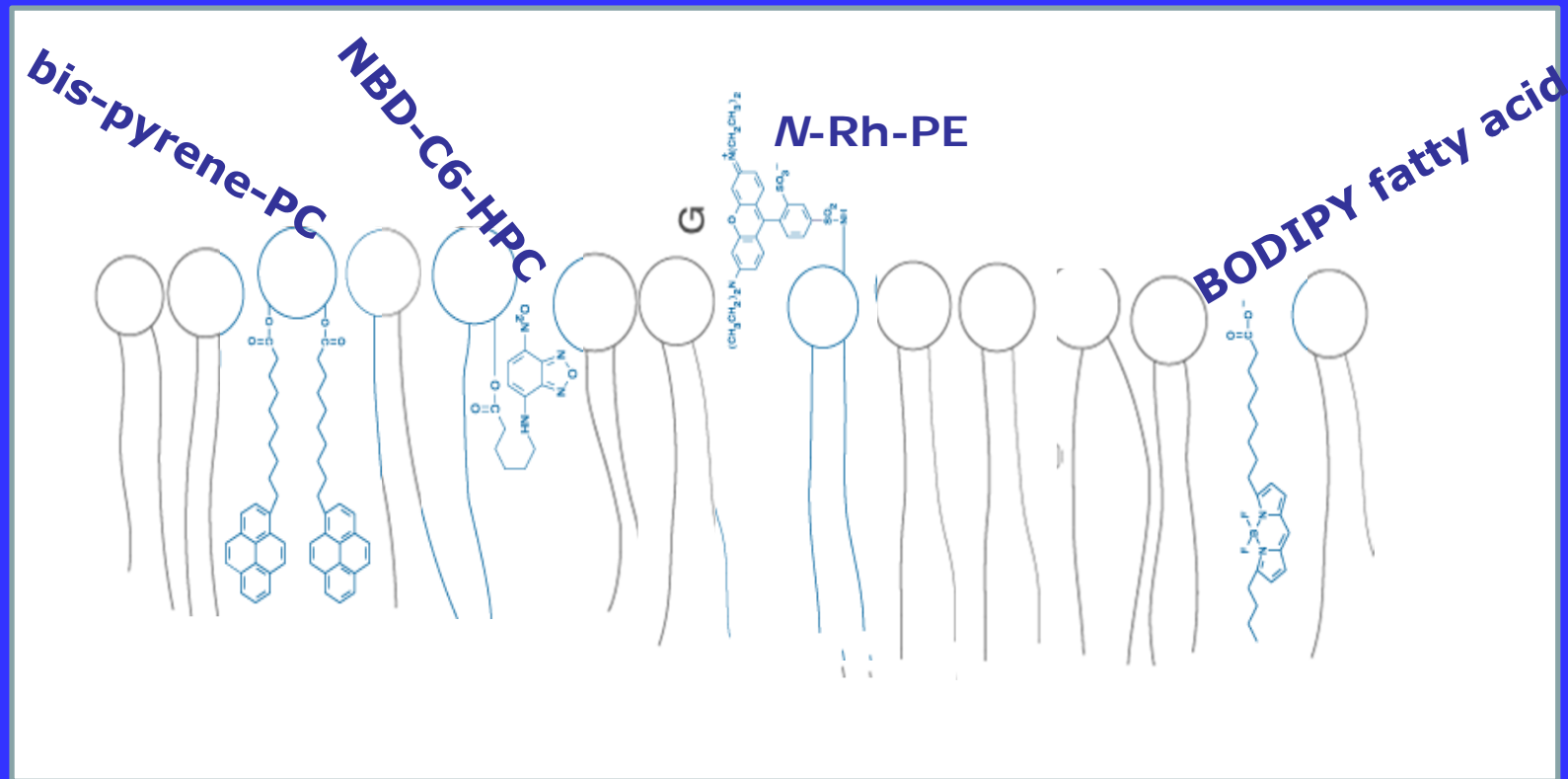
EXPERIMENTAL PROCEDURES

Phospholipids—Lecithin was prepared from egg yolks (7) and purified chromatographically on alumina and silica columns (8). For chemical analysis lecithin was first hydrolyzed by mild alkali (0.4 N KOH in 90% methanol for 2 hours at 37°) and the fatty acids were extracted and methylated with diazomethane. The methyl esters were then analyzed with a Packard gas-liquid chromatograph on 15% ethylene glycol succinate column. The obtained

DPH - diphenylhexatriene



Fatty acids analogs and phospholipids



Pyrene (Figure 10.25) has also been widely used in membrane studies because of its ability to form excited dimers or *excimers*. Formation of an excimer requires that an excited pyrene molecule can form a complex with a ground state pyrene—which, of course, must occur during the lifetime of the excited state. Since pyrene excited states tend to be long (tens or hundreds of nanoseconds depending on the exact probe), the likelihood of such an encounter is reasonable if the concentration of the probe is sufficient and if the medium, in this case a biological membrane, is sufficiently fluid to ensure facile diffusion of the fluorophores. The excimer emission is red-shifted from the monomer emission so one simply has to determine the ratio of excimer to monomer emission to quantify the extent of excimer formation. An example of the use of pyrene excimers is shown in Figure 10.26. In this example, an aptamer probe for platelet-derived growth factor (PDGF) was synthesized with one pyrene molecule at each end. In the absence of the target protein, the aptamer adopts an open conformation such that each pyrene molecule is free to emit as a monomer (emission in the 350–440 nm range). When bound to the PDGF, however, the two pyrenes come into proximity and are able to emit as an excimer (emission above 440 nm). The increase in the excimer to monomer emission allows one to track the formation of the aptamer–PDGF complex. One can also use pyrene probes which contain two pyrene molecules connected by a linker. These types of dual probes have the advantage that both potential excimer partners are in the same molecule—hence, eliminating the requirement for the high probe concentrations necessary to ensure diffusional contact during the fluorescent lifetime.

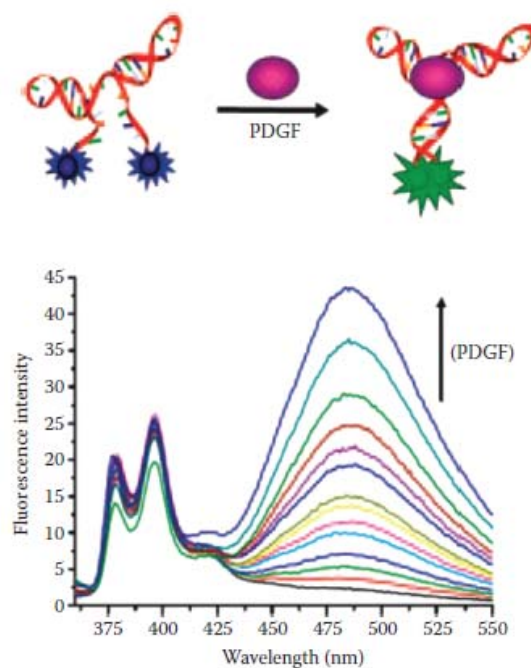
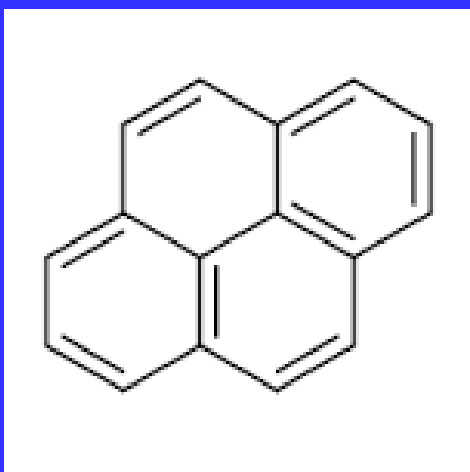
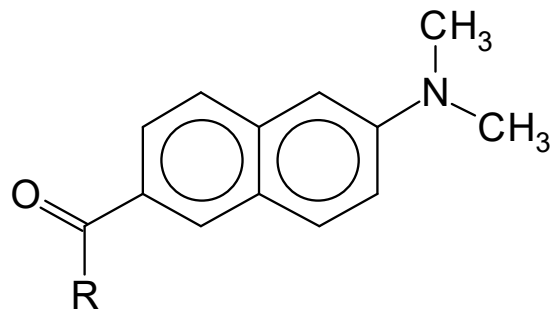


FIGURE 10.26 Example of the use of pyrene excimers. (Adapted from Yang et al., 2005. *Proc. Natl. Acad. Sci. USA* 102: 17278.) An aptamer probe for platelet-derived growth factor (PDGF) has one pyrene molecule at each end. In the absence of the target protein, the aptamer adopts an open conformation such that each pyrene molecule is free to emit as a monomer (emission in the 350–440 nm range). When bound to the PDGF, however, the two pyrenes come into proximity and are able to emit as an excimer (emission above 440 nm).

Nonpolar probes


Environment-sensitive spectral shifts

Weber, G. and Farris, F. *J. Biochemistry*, 18, 3075-3078 (1979).



LAURDAN R = $-(\text{CH}_2)_{10}\text{CH}_3$

PRODAN R = $-\text{CH}_2\text{CH}_3$

DANCA R = 

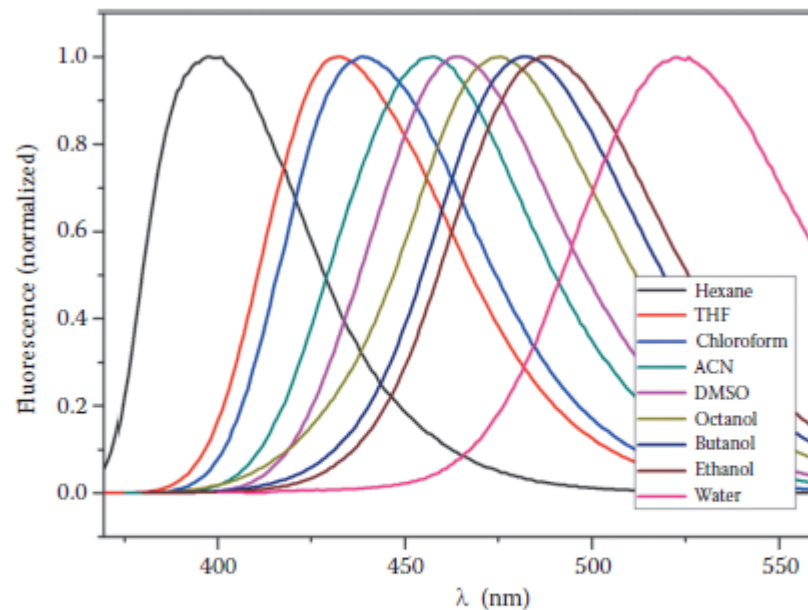


FIGURE 10.29 Emission spectra for Prodan in a series of solvents. The author would like to thank Leonel Malacrida for these spectra.

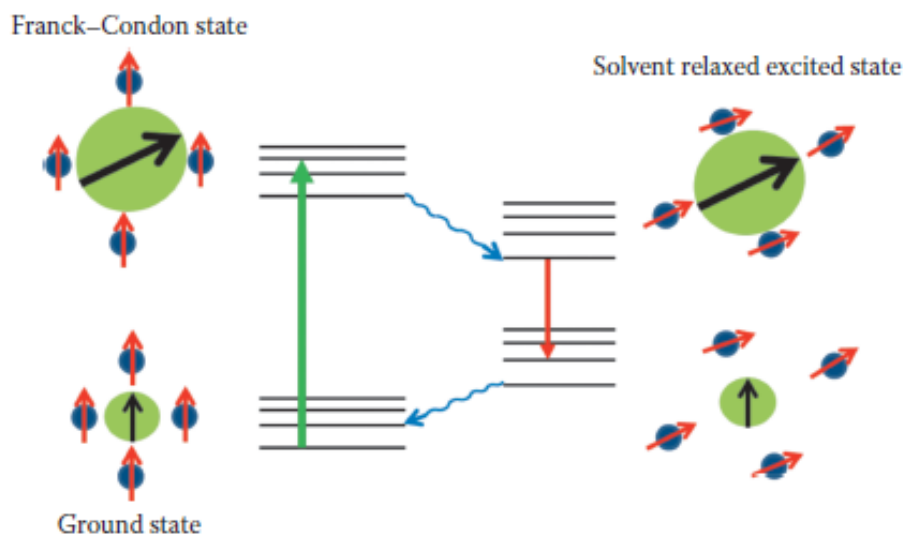


FIGURE 10.27 Depiction of excited state solvent reorientation (dipolar relaxation).

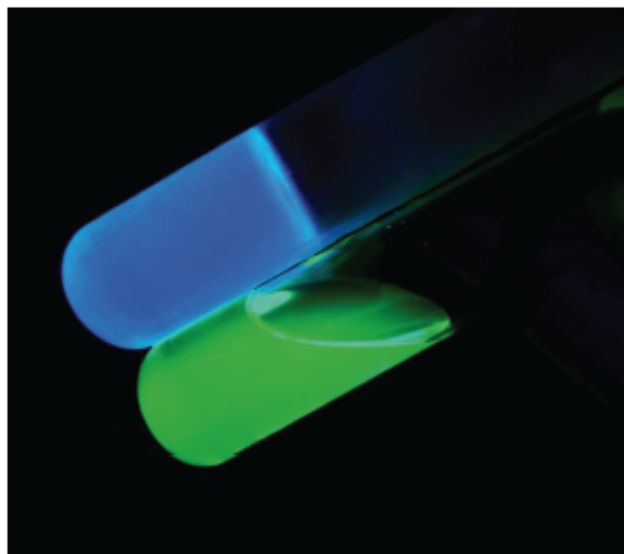
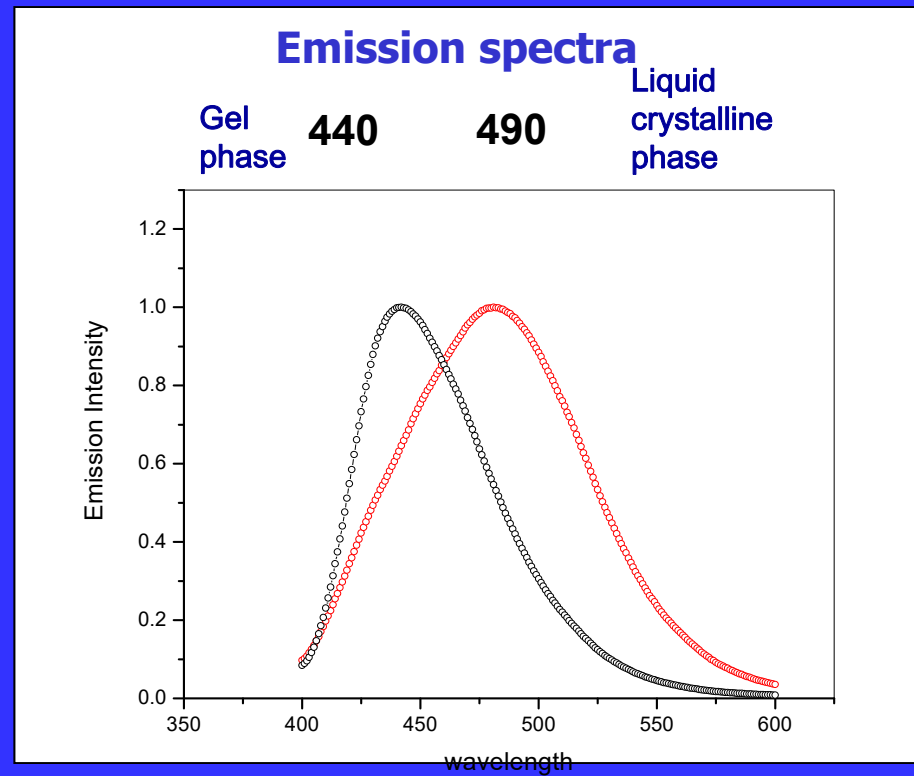
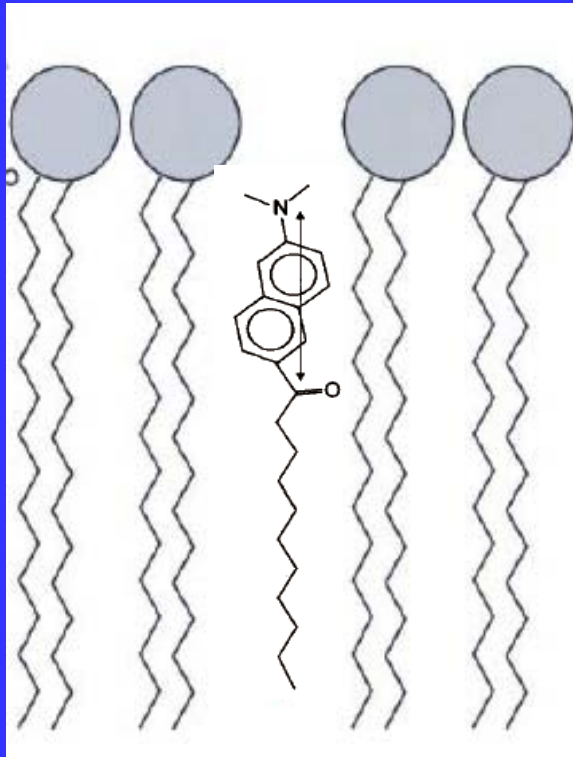


FIGURE 10.28 Prodan in glycerol at -80°C (top blue tube) and $+60^{\circ}\text{C}$ (bottom green tube) illuminated using a UV handlamp.

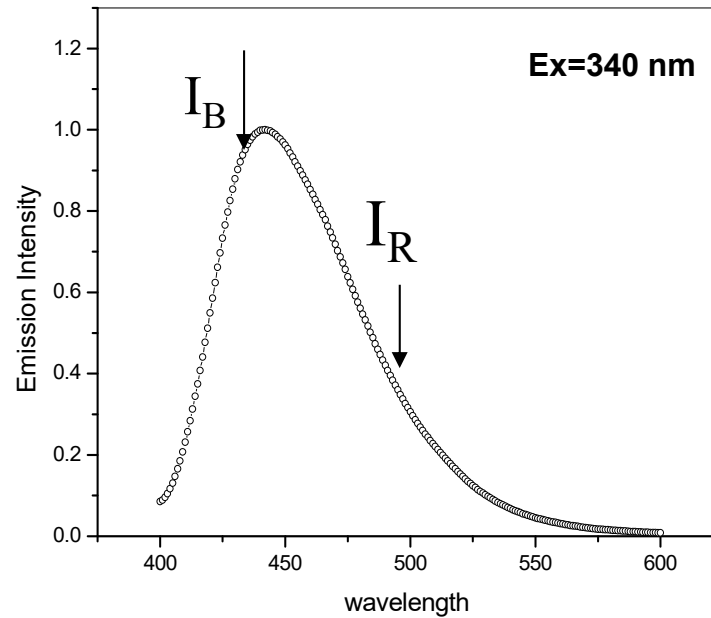
Nonpolar probes (continued)

example: *Laurdan*.



Laurdan Generalized Polarization (GP)

Emission spectra



$$GP_{ex} = \frac{I_B - I_R}{I_B + I_R}$$

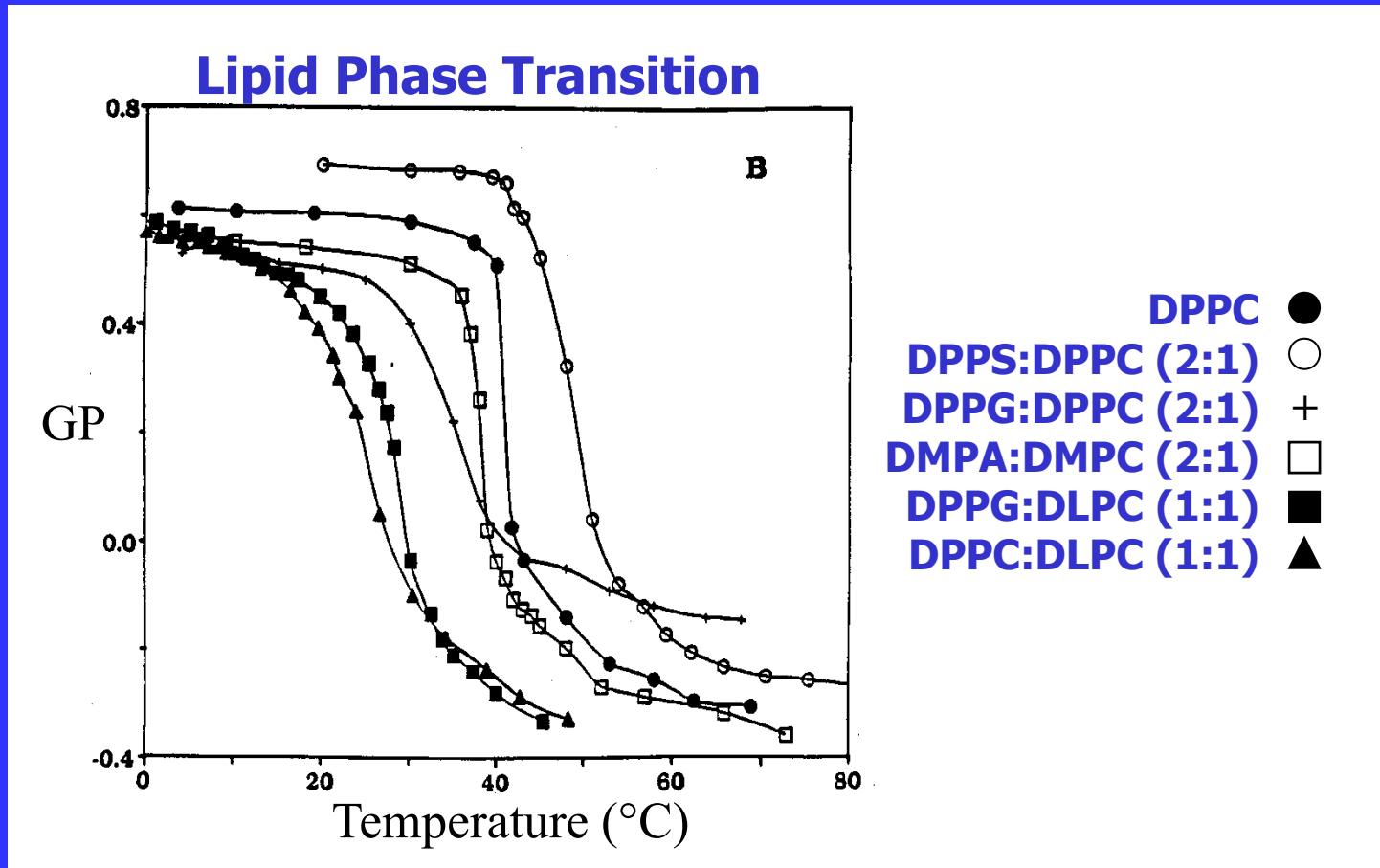
-0.2
loose lipid
packing



0.6
tight lipid
packing

GP in the cuvette

MLVs, SUVs, LUVs



Parassassi et al. Biophys. J. 60, 179 (1991)

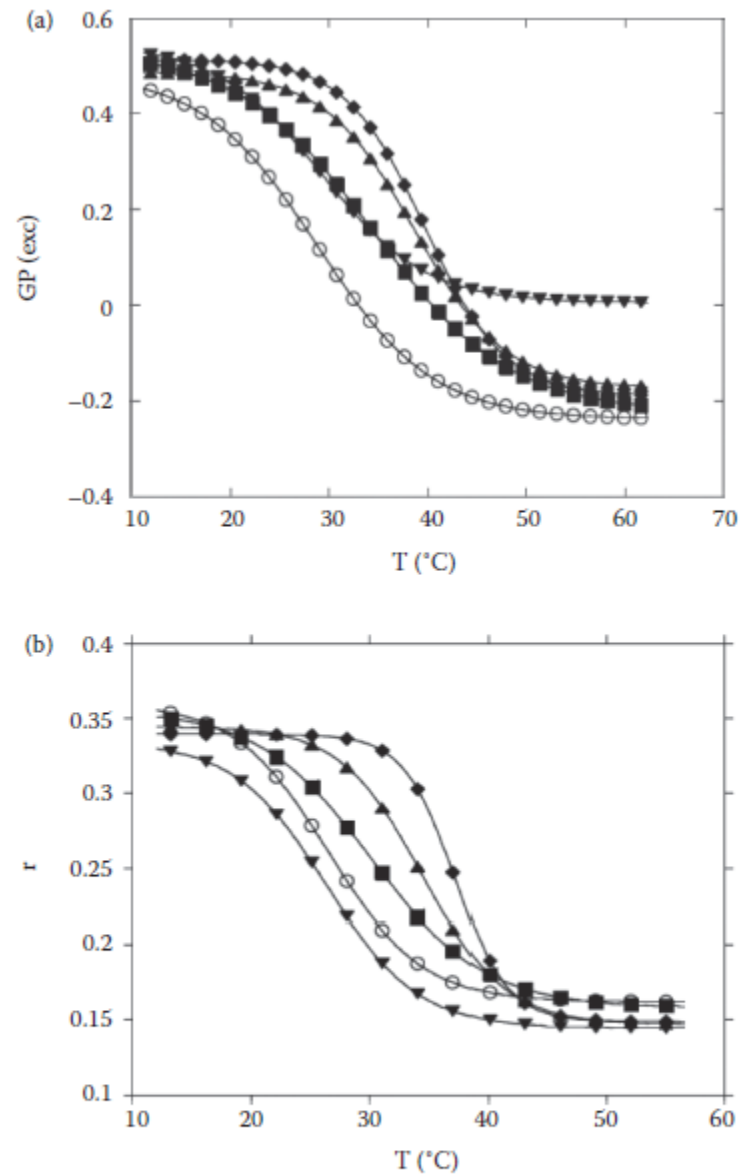
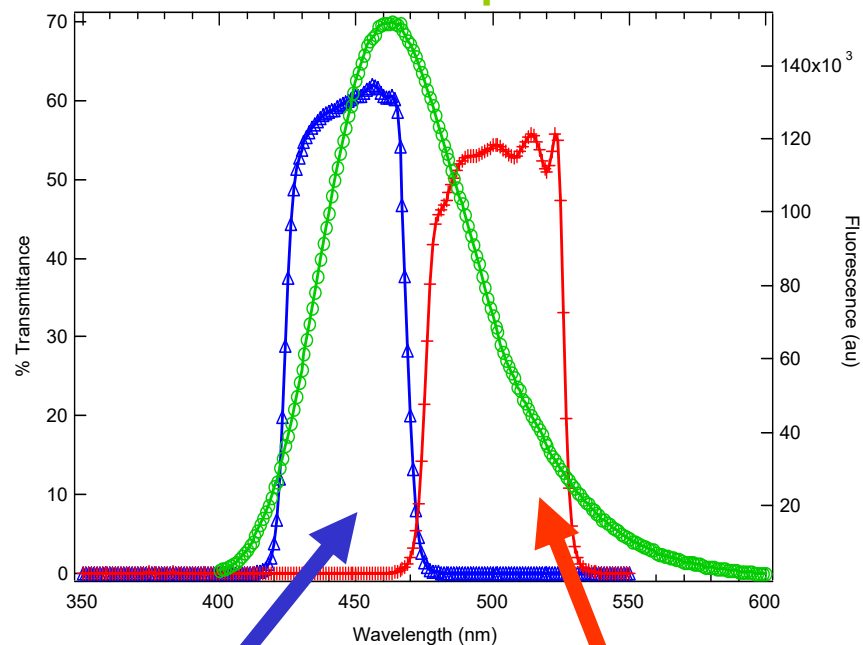


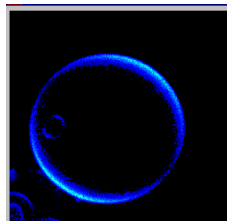
FIGURE 10.33 Example of the use of Laurdan's GP values to monitor phase transitions in a model membrane system. The figure, from Deleu et al., 2013. (*Biochim. Biophys. Acta* 1828: 801), presents a comparison of (a) Laurdan GP with (b) DPH anisotropy in the same system, specifically, DOPC:DPPC large unilamellar vesicles with increasing concentrations of surfactin.

GP in the microscope (2-photon excitation)

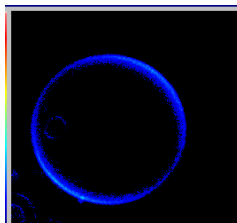
LAURDAN emission spectra



Ch1: Blue filter

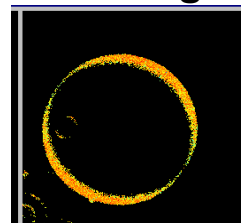


Ch2: Red filter

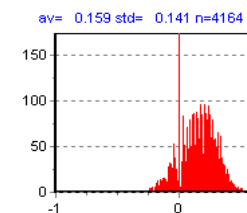


SimFCS software

GP image



GP histogram

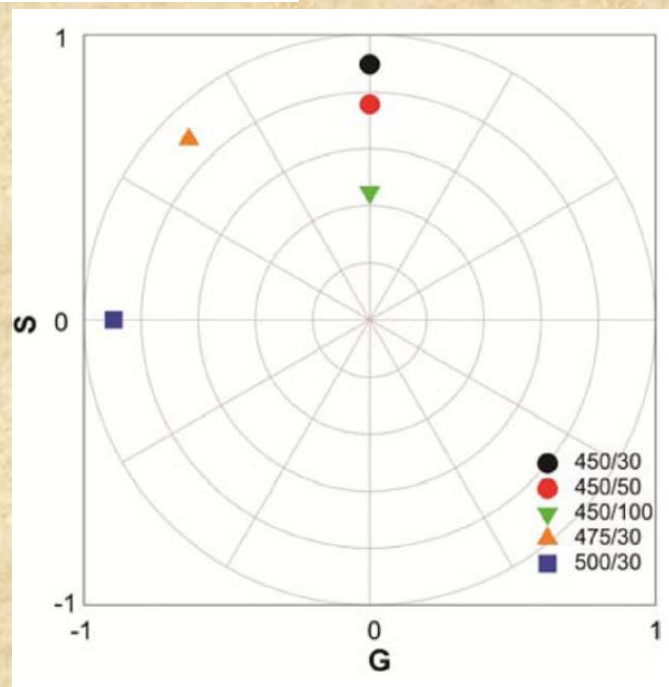
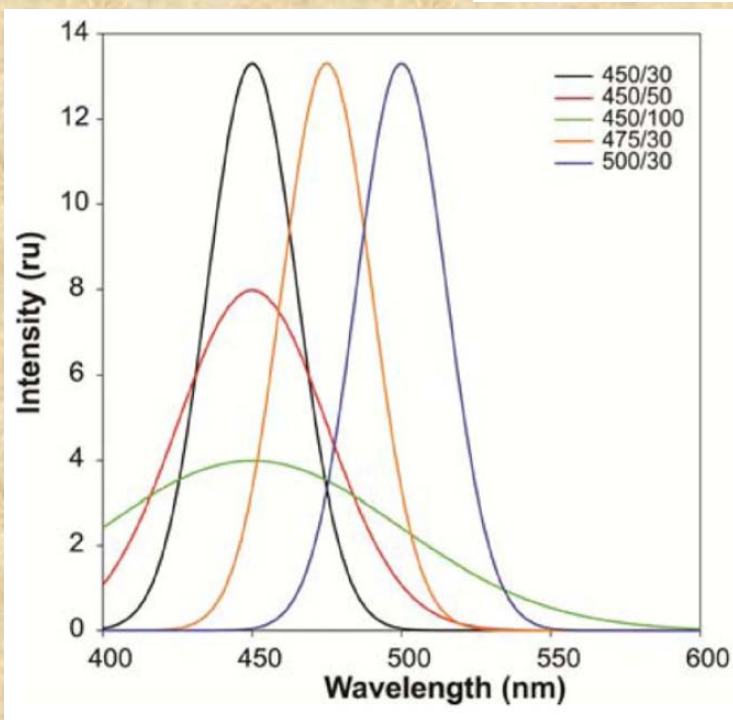


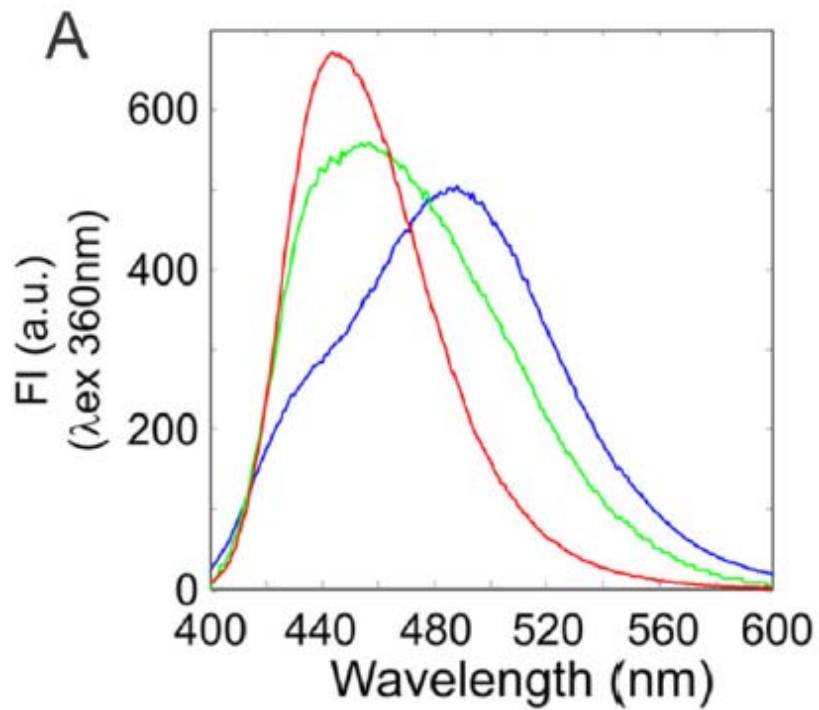
Spectral Phasors

The emission spectrum of a sample, recorded on a spectrofluorimeter or in an image from a spectral confocal microscope, is used to calculate the real and imaginary components (the amplitude and phase, respectively) for the first harmonic Fourier transformed spectrum (X and Y , called G and S , respectively). The data are then plotted in a phasor scatter plot, termed the spectral phasor plot.

$$x \text{ coordinates} = G = \frac{\sum_{\lambda} I(\lambda) \cos(2\pi n/L)}{\sum_{\lambda} I(\lambda)}$$

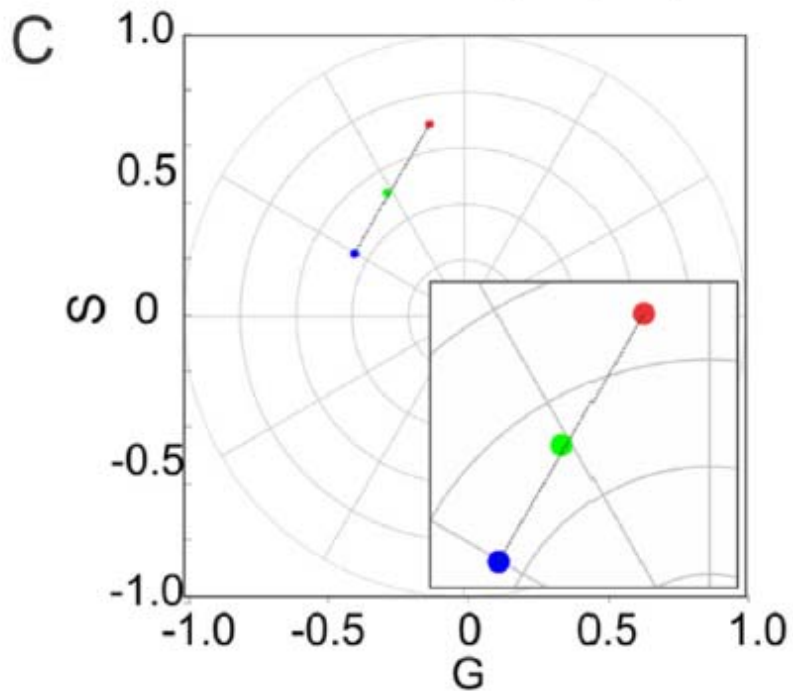
$$y \text{ coordinates} = S = \frac{\sum_{\lambda} I(\lambda) \sin(2\pi n/L)}{\sum_{\lambda} I(\lambda)}$$



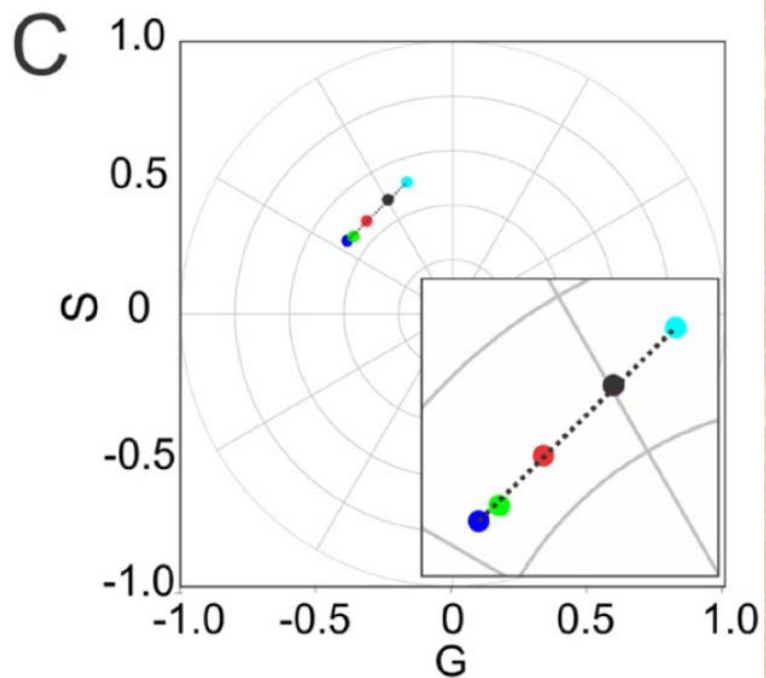
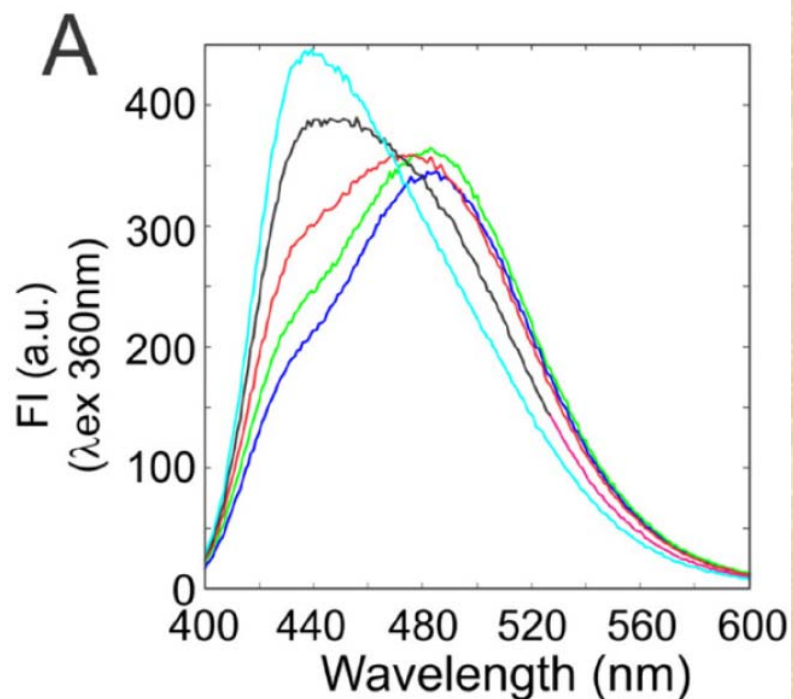


Example of the identification of linear combination in the emission of LAURDAN in a binary mixture of fluid and gel membrane with spectral phasor.

(a) Spectra recorded of the MLVs of DOPC (blue), DPPC (red) and a mixture 1 : 1 mol of DOPC:DPPC (green) at 25 °C.



(c) Spectral phasor position of each sample



Example of the effects of the cholesterol in a membrane with coexisting fluid/gel phases studied using spectral phasors.

(a) Spectra recorded of the MLVs of a mixture 1:1 mol of DOPC:DPPC with the addition of cholesterol (0%—green, 5%—blue, 10%—red, 20%—pink and 50%—cyan) at 25 °C.

(c) Spectral phasor position of each sample

Model-free methods to study membrane environmental probes: a comparison of the spectral phasor and generalized polarization Approaches

Leonel Malacrida, Enrico Gratton and David M Jameson

Methods Appl. Fluoresc. **3** (2015) 047001

Fluorescent Ion-Probes

Fluorescence probes have been developed for a wide range of ions:

Cations:

H^+ , Ca^{2+} , Li^+ , Na^+ , K^+ , Mg^{2+} , Zn^{2+} , Pb^{2+} *and others*

Anions:

Cl^- , PO_4^{2-} , Citrate, ATP, *and others*

Probes For Calcium determination

UV

FURA

(Fura-2, Fura-4F, Fura-5F, Fura-6F, Fura-FF)

INDO

(Indo-1, Indo 5F)

Ratiometric

VISIBLE

FLUO

(Fluo-3, Fluo-4, Fluo5F, Fluo-5N, Fluo-4N)

RHOD (Rhod-2, Rhod-FF, Rhod-5N)

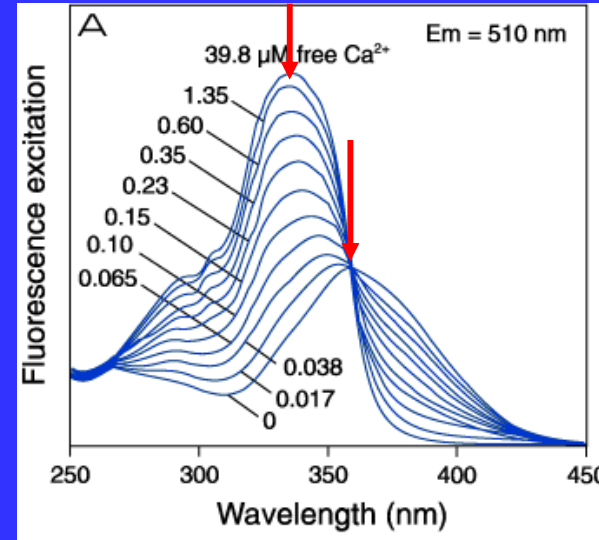
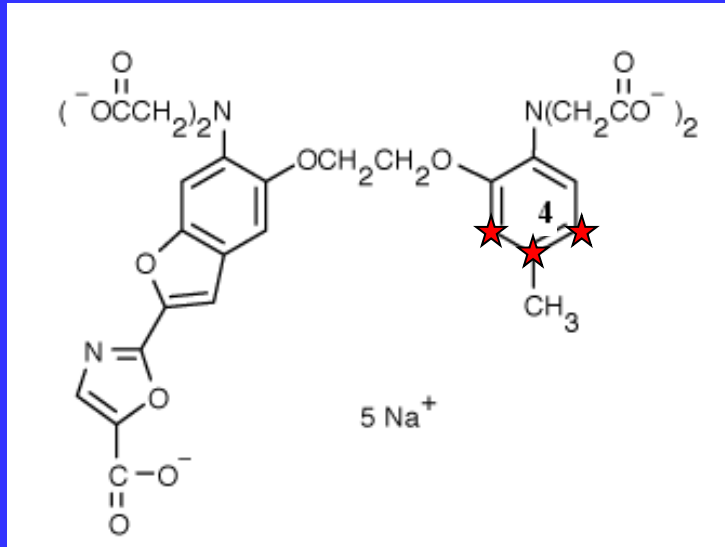
CALCIUM GREEN (CG-1, CG-5N,CG-2)

OREGON GREEN 488-BAPTA

**Non
Ratiometric**

Ratiometric: 2 excitation/1 emission

FURA-2



Indicator	K _d (Ca ²⁺)
Fura-2	0.14 μM
Fura-5F	0.40 μM
Fura-4F	0.77 μM
Fura-6F	5.30 μM
Fura-FF (5,6)	35 μM

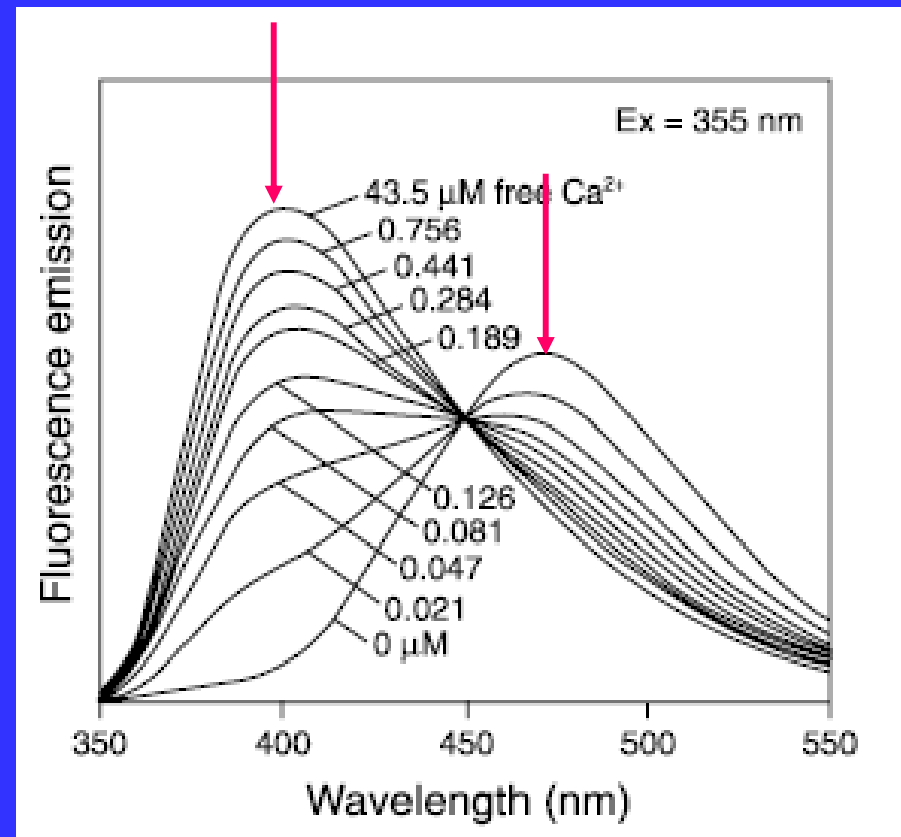
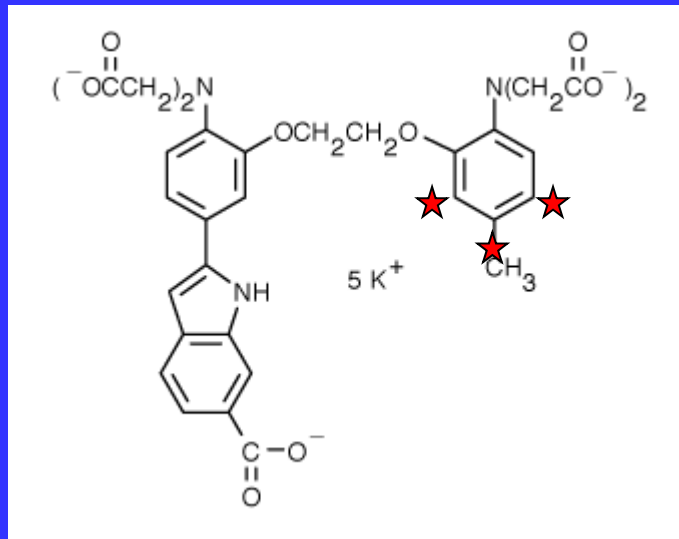
Most used in microscopic imaging

Good excitation shift with Ca²⁺

Ratiometric between 340/350 and 380/385 nm

Ratiometric: 1excitation / 2emission

Indo-1



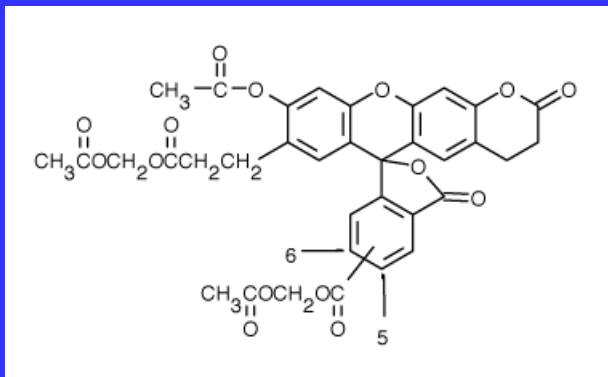
Indicator	K _d (Ca ²⁺) (μM)
indo-1	0.23
indo-5F	0.47

pH-Probes

Probe	pH Range	Measurement Mode
SNARF indicators	6.0-8.0	Em. ratio 580/640 nm
HPTS (pyranine)	7.0-8.0	Exc. ratio 450/405 nm
BCECF	6.5-7.5	Exc. ratio 490/440 nm
Fluoresceins and Carboxyfluoresceins	6.0-7.2	Exc. ratio 490/450 nm
Oregon Green dyes	4.2-5.7	Exc. ratio 510/450 nm
LysoSensor Yellow/Blue DND-160	3.5-6.0	Em. ratio 450/510 nm

Molecular Probes' pH indicator families, in order of decreasing pK_a

BCECF

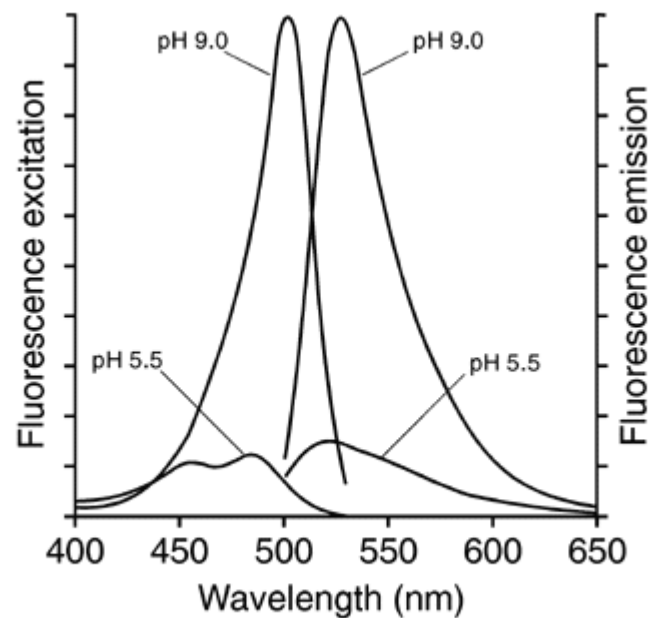


R. Tsien 1982

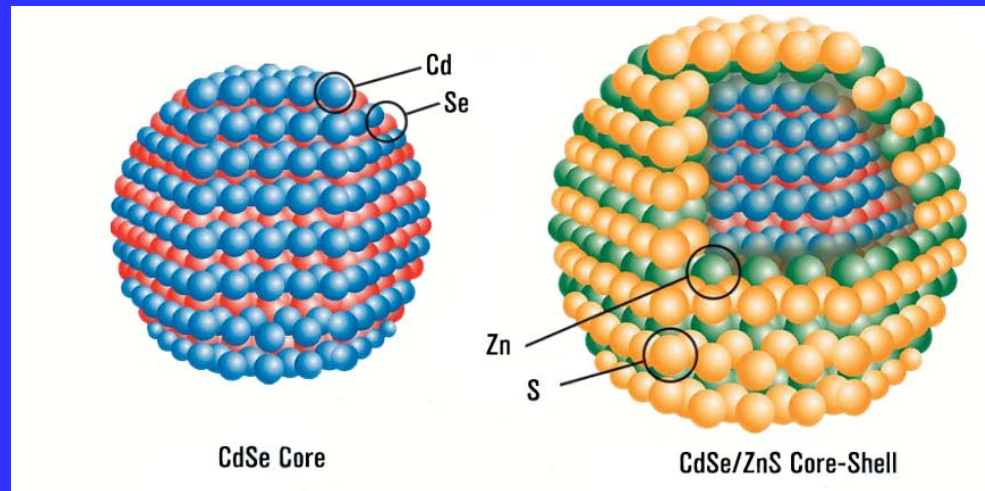
Most widely used fluorescent indicator for intercellular pH

Membrane-permeant AM: pKa ~ 6.98 is ideal for intracellular pH measurements

Excitation-ratiometric probe with λ_p at 439 nm, which is used as the reference point



Quantum Dots



Quantum Dots

Nanometer-Scale Atom Clusters

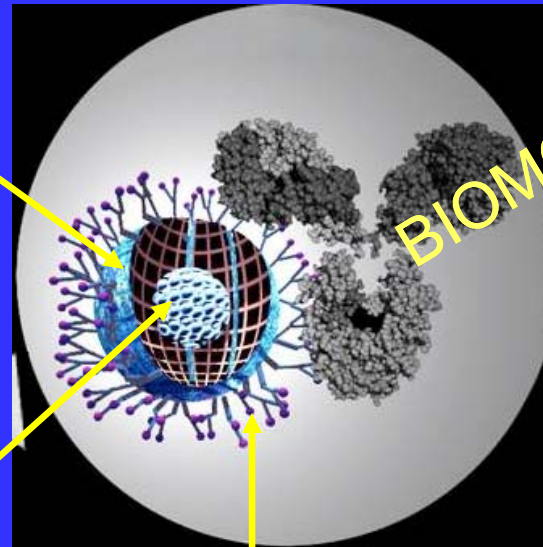
CORE

Cadmium selenide (**CdSe**), or
Cadmium telluride (**CdTe**)
few hundred – few thousand atoms

The semiconductor material is chosen
based upon the emission wavelength,
however it is the **size** of the particles
that **tunes the emission
wavelength**.

SHELL

In the core emission is typically weak
and always unstable.
The shell material (**ZnS**) has been
selected to be almost entirely
unreactive and completely insulating
for the core.



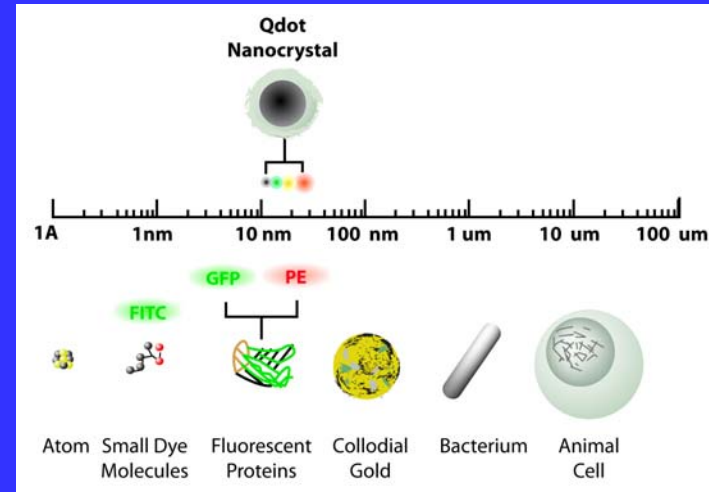
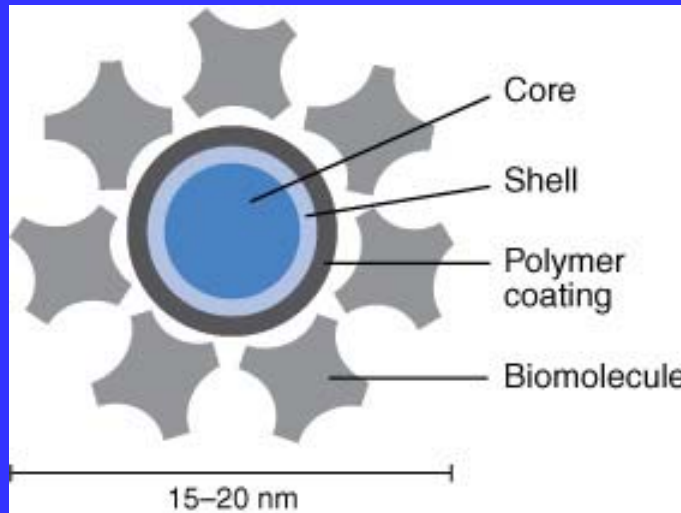
BIOMOLECULE

COATING

A layer of organic ligands covalently attached to the surface
of the shell. This coating provides a **surface for
conjugation** to biological (antibodies, streptavidin, lectins,
nucleic acids) and nonbiological species and makes them
“water-soluble”

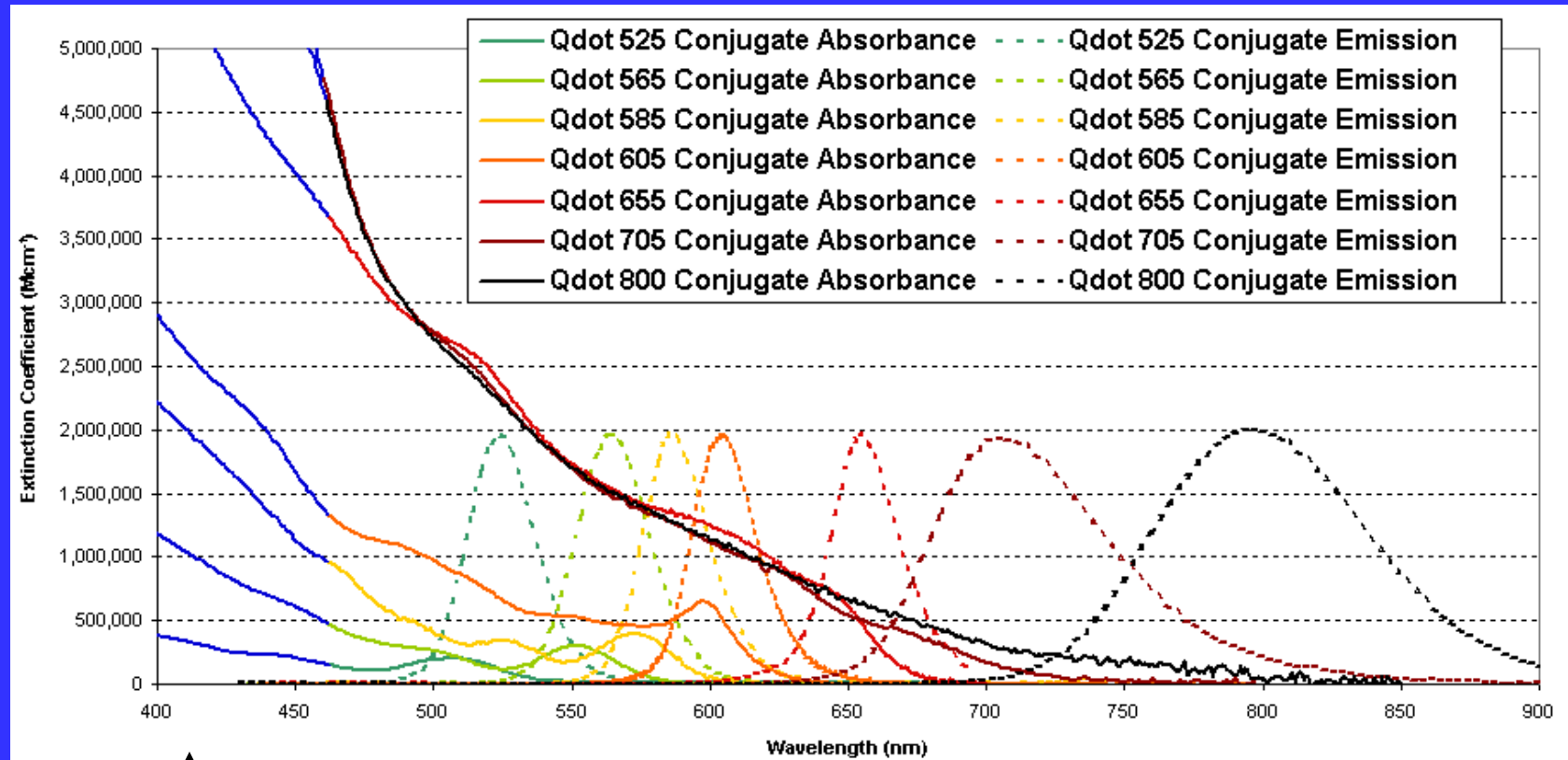
Quantum Dots

Nanometer-Scale Atom Clusters



Quantum Dot Material System	Emission Range	Quantum Dot Diameter Range	Quantum Dot Type	Standard Solvents	Example Applications
CdSe	465nm - 640nm	1.9nm - 6.7nm	Core	Toluene	Research, Solar Cells, LEDs
CdSe/ZnS	490nm - 620nm	2.9nm - 6.1nm	Core-Shell	Toluene	VisibleFluorescence Applications, Electroluminescence, LEDs
CdTe/CdS	620nm - 680nm	3.7nm - 4.8nm	Core-Shell	Toluene	Deep Red Fluorescence Apps.

Qdot Optical Spectra



↑
Violet
excitation

Absorbance × Quantum Yield = Brightness
photons in fraction converted photons out

←—————→
Broad range of emissions

High absorbance means increased brightness

Single-color excitation, multicolor emission for easy multiplexing

Courtesy of Invitrogen

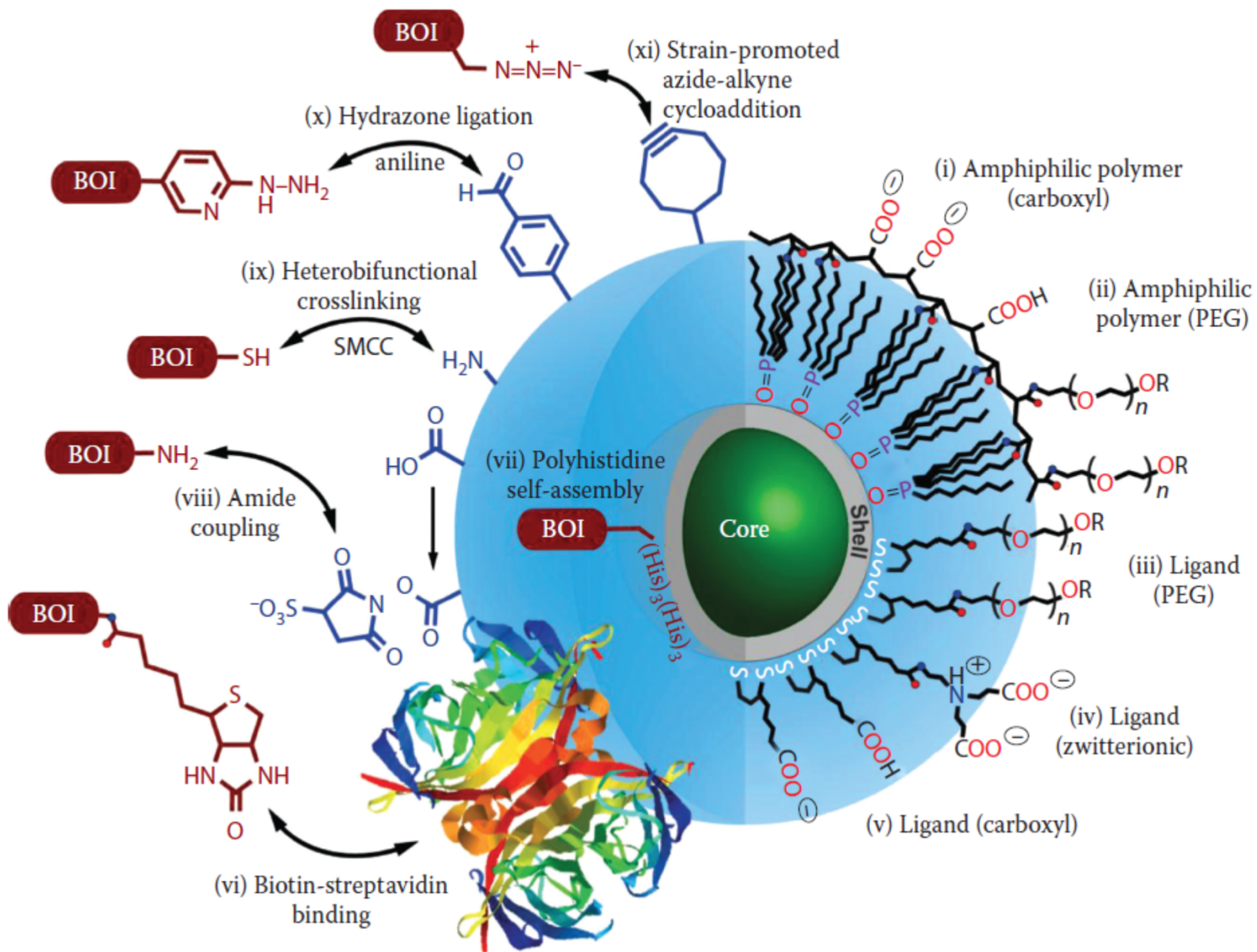
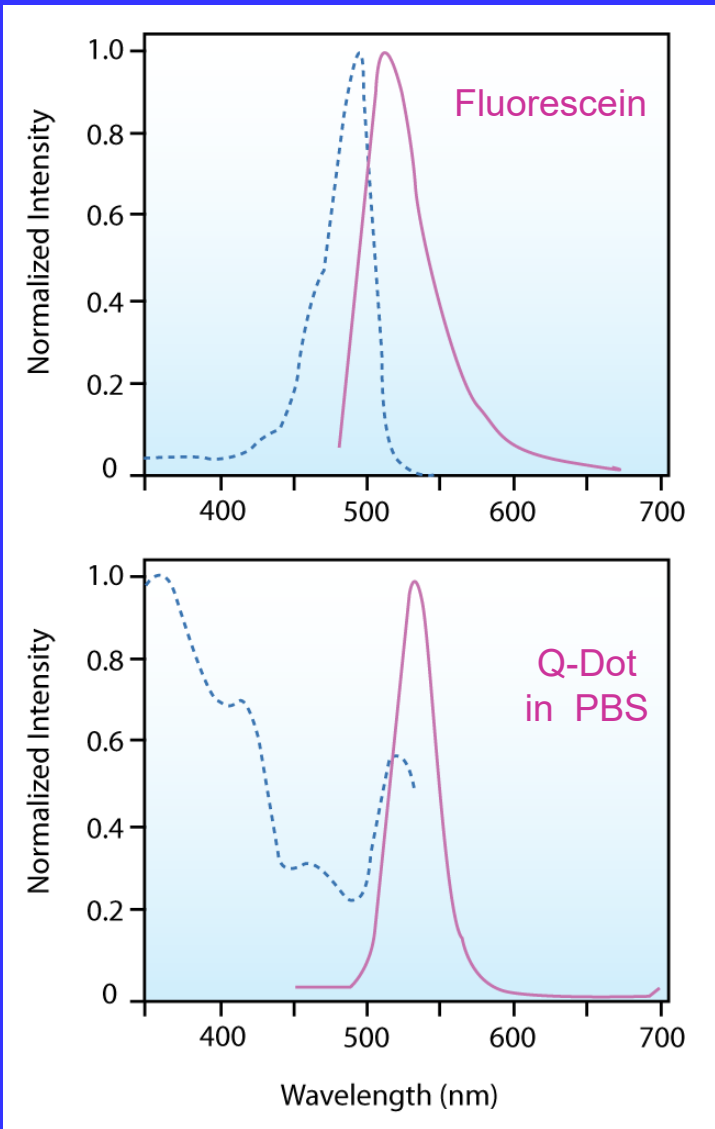


FIGURE 10.57 Illustration of functionalization strategies for Q-dots. (From Petryayeva et al., 2013 *Appl. Spectros.* 67: 215.)

Qdot Summary



Advantages:

Broad absorption spectra, making it possible to excite all colors of QDs simultaneously with a single light source - **Multiplexing**

Narrow and symmetrical emission spectra

Emission tunable with size and material composition

Exhibit excellent **photo-stability**

Disadvantages:

Large size and high mass limit their use in applications requiring high diffusional mobility

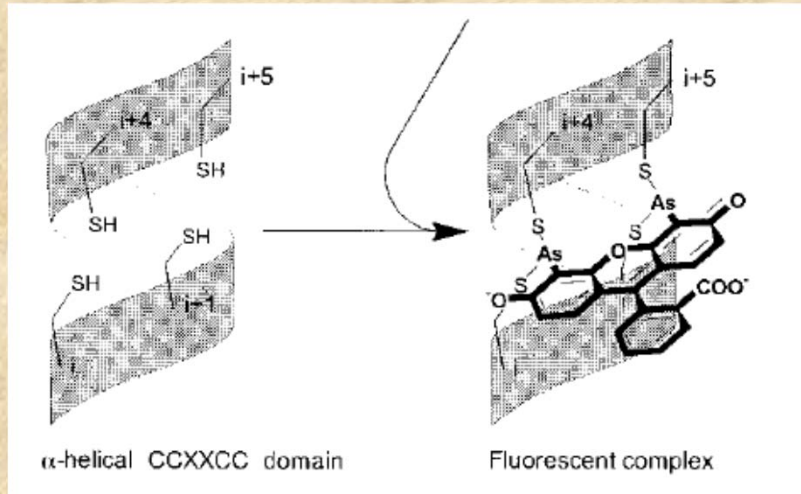
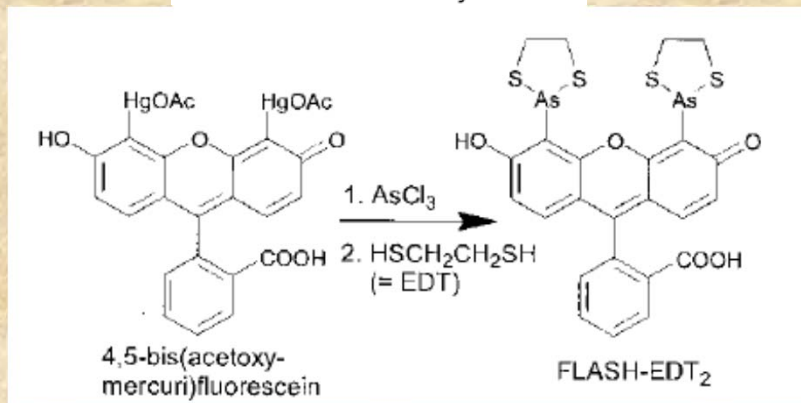
QDot	$\lambda_{\max}(\text{abs})$ [nm]	$\lambda_{\max}(\text{em})$ [nm]	ϵ ($\text{M}^{-1}\text{cm}^{-1}$)	Q.Y.
655	350	655	9,000,000	~0.5
705	350	705	13,000,000	~0.5
800	350	800	13,000,000	~0.5

FIAsh-EDT2 labeling (FIAsh tag)

Specific Covalent Labeling of Recombinant Protein Molecules Inside Live Cells

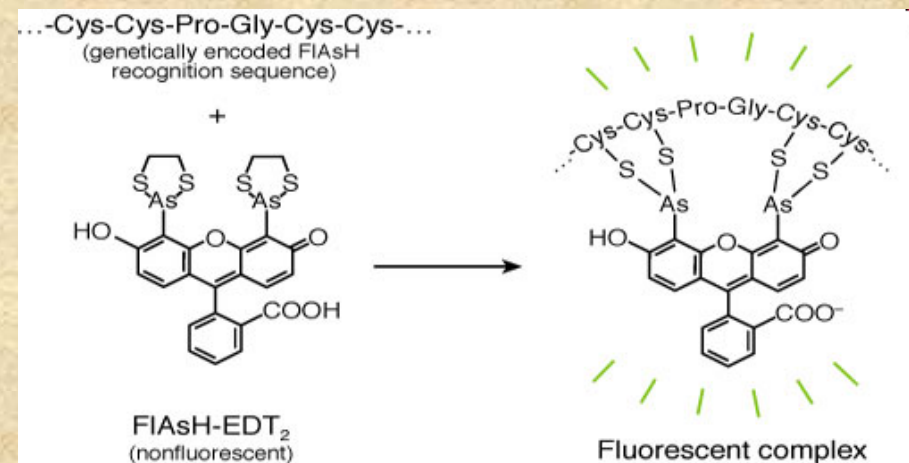
B. Albert Griffin,* Stephen R. Adams, Roger Y. Tsien†

SCIENCE VOL 281 10 JULY 1998



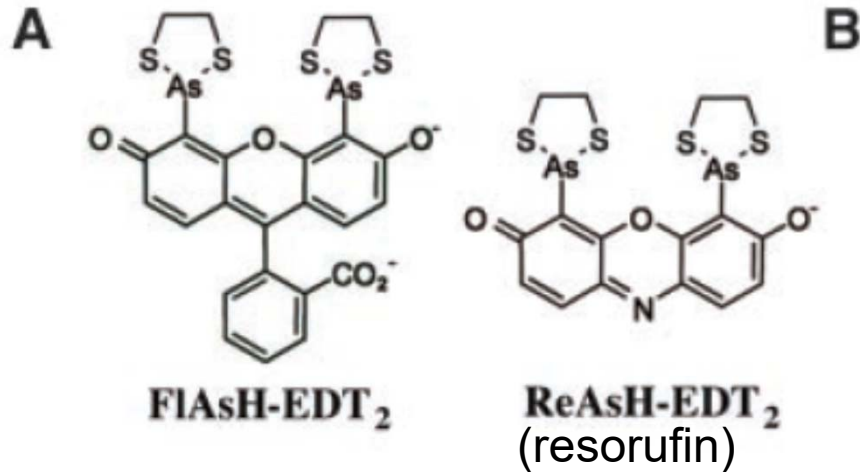
The original motif “CCXXCC” often gave rise to significant nonspecific background.

The use of the “CCPGCC” motif led to reduced background



New motifs include “HRWCCPGCCKTF” and “FLNCCPGCCMEP”

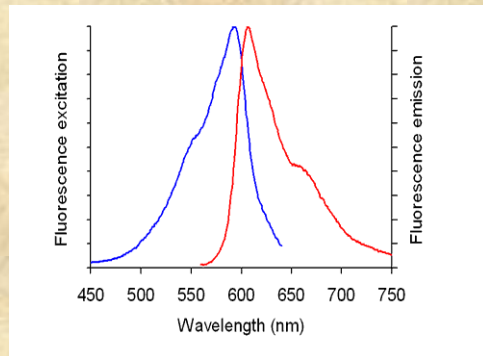
ReAsH



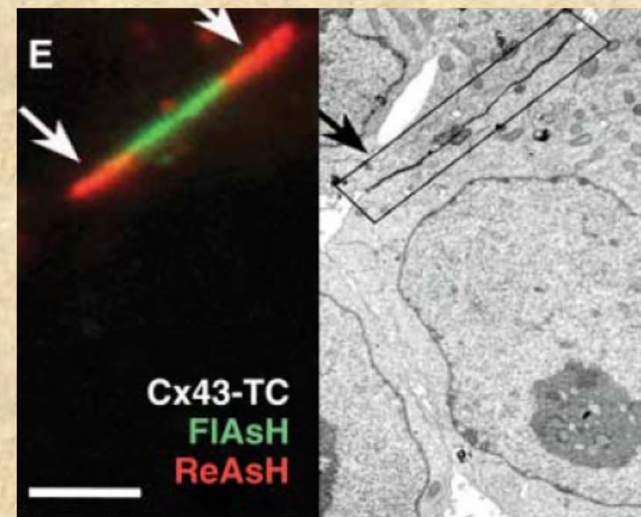
Multicolor and Electron Microscopic Imaging of Connexin Trafficking

Guido Gaietta,¹ Thomas J. Deerinck,¹ Stephen R. Adams,²
James Bouwer,¹ Oded Tour,^{2*} Dale W. Laird,³ Gina E. Sosinsky,¹
Roger Y. Tsien,^{2*} Mark H. Ellisman^{1†}

SCIENCE VOL 296 19 APRIL 2002



Tetracysteines on connexin43 were pulse-labeled with FIAsh (green) and subsequently ReAsH (red), thus distinguishing old from new connexins, respectively. ReAsH is also visualized in EM using photooxidation (E) (right).



Bimolecular Fluorescence Complementation (BiFC)

Nat Biotechnol. 2003 May ; 21(5): 539–545.

Simultaneous visualization of multiple protein interactions in living cells using multicolor fluorescence complementation analysis

Chang-Deng Hu and Tom K. Kerppola*

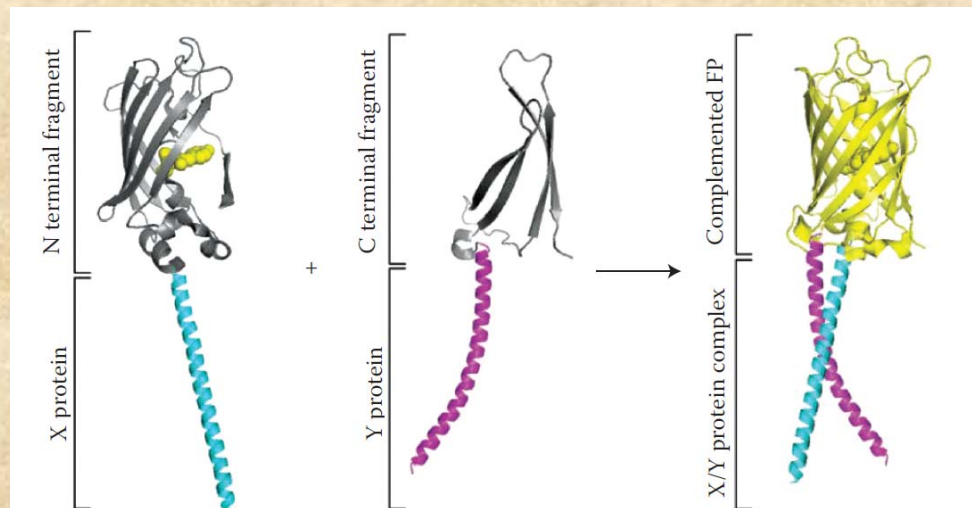
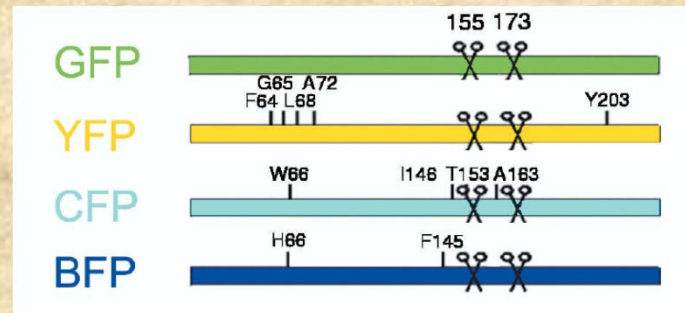
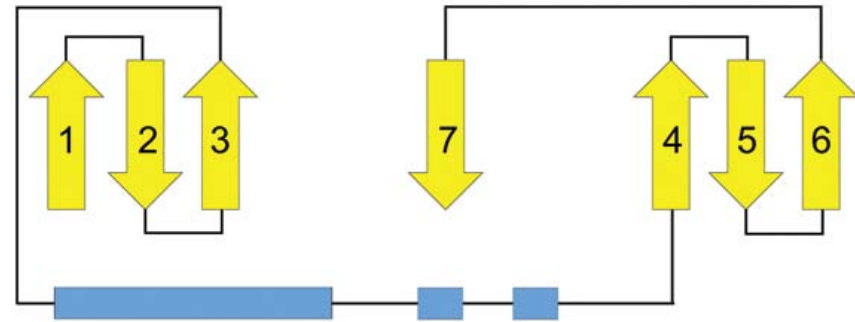
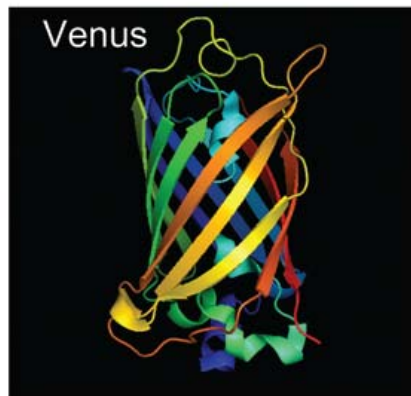
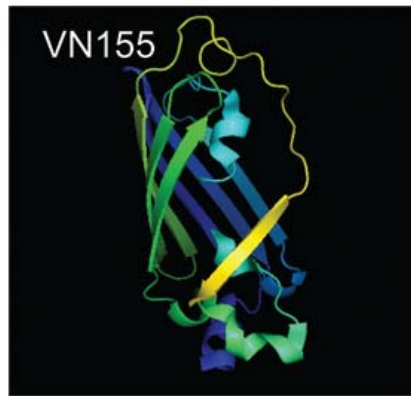
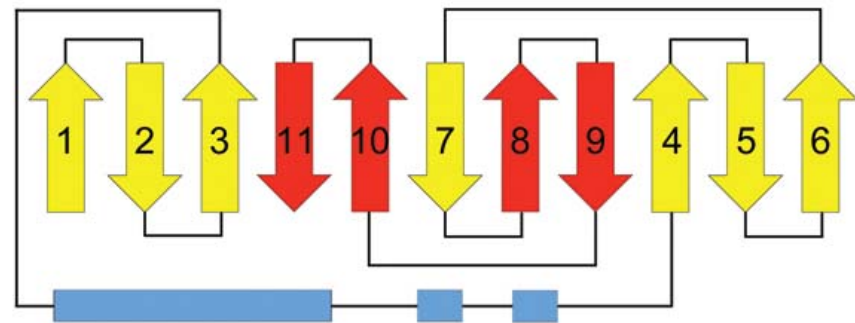
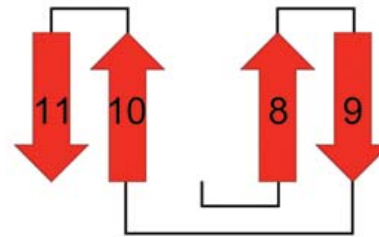
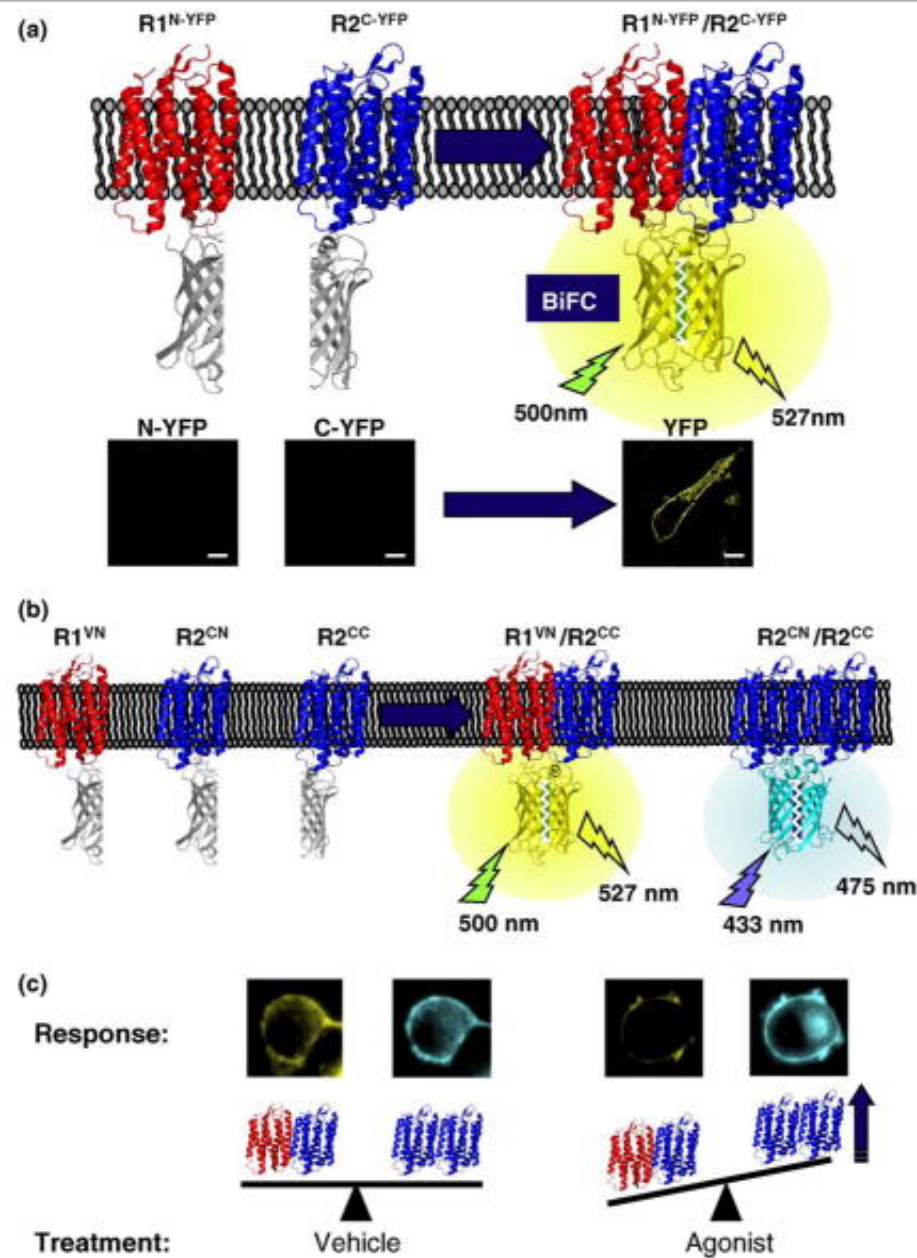


FIGURE 10.62 Illustration of the biomolecular fluorescence complementation method. (From Kodama and Hu (2012) *Biotechniques* 53: 285.)



+





Trends Biotechnol. 2010 August ; 28(8): 407–415.

Francisco Ciruela¹, Jean-Pierre Vilaradaga^{2,3}, and Víctor Fernández-Dueñas¹